DOKUZ EYLÜL UNIVERSITY

GRADUATE SCHOOL OF NATURAL AND APPLIED SCIENCES

AN INVESTIGATION ON THE CONTRIBUTION OF JET GROUT STRUTTING TO THE STABILITY OF DEEP RETAINING SYSTEMS BY FINITE ELEMENT METHOD

by

Ejder SÖNMEZ

July, 2010

İZMİR

AN INVESTIGATION ON THE CONTRIBUTION OF JET GROUT STRUTTING TO THE STABILITY OF DEEP RETAINING SYSTEMS BY FINITE ELEMENT METHOD

A Thesis Submitted to the

Graduate School of Natural and Applied Sciences of Dokuz Eylül University

In Partial Fulfillment of the Requirements for the Degree of Master of Science

in Civil Engineering, Geotechnics Program

by

Ejder SÖNMEZ

July, 2010

İZMİR

M. Sc. THESIS EXAMINATION RESULT FORM

We have read the thesis entitled **"AN INVESTIGATION ON THE CONTRIBUTION OF JET GROUT STRUTTING TO THE STABILITY OF DEEP RETAINING SYSTEMS BY FINITE ELEMENT METHOD"** completed by **EJDER SÖNMEZ** under supervision of **PROF. DR. ARİF ŞENGÜN KAYALAR** and we certify that in our opinion it is fully adequate, in scope and in quality, as a thesis for the degree of Master of Science.

.....

PROF. DR. ARİF ŞENGÜN KAYALAR

Supervisor

.....	.....
PROF. DR. M. YALÇIN KOCA	**DOÇ. DR. GÜRKAN ÖZDEN**
(Jury Member)	(Jury Member)

Prof.Dr. Mustafa SABUNCU

Director

Graduate School of Natural and Applied Sciences

ACKNOWLEDGMENTS

The author is grateful to the advisor of this thesis, Prof. Dr. Arif Şengün KAYALAR for his invaluable guide, helps and advises, at all stages of this thesis study.

Also, the author would like to thank to Prof. Dr. M. Yalçın KOCA and Associate Prof. Dr. Gürkan ÖZDEN for their help.

He also thanks to his family for their endless supports.

The author hopes that the thesis will be useful for professional engineers and researchers.

EJDER SÖNMEZ

AN INVESTIGATION ON THE CONTRIBUTION OF JET GROUT STRUTTING TO THE STABILITY OF DEEP RETAINING SYSTEMS BY FINITE ELEMENT METHOD

ABSTRACT

Jet grouting columns are used to enhance stability of deep retaining systems, to improve safety of excavations and to constitute stable structures. Depending on properties, lateral resistance of the soil below excavation level can sometimes be insufficient. The need of improvement of the lateral stability of deep retaining walls ongoing subway structures is a current problem. In order to eliminate this problem economically, horizontal support systems can be formed below the level of excavation by the application of jet grout columns.

In this thesis, the contribution of jet grout strutting to the stability of deep retaining system is studied by finite elements analyses. For this purpose, engineering properties of jet grout columns are investigated and structural uses are mentioned. The geometry of the problem used in the analyses has been inspired by İzmir Karşıyaka Subway Tunnel Construction Project.

Combinations of analyses are formed by changing strength characteristics, treated soil area ratios, patterns and location types of jet grouted columns. Analyses are made for sandy and clayey soil profiles seperately. Plaxis 2D and 3D finite element programs are employed in the analyses. The results of analyses in terms of displacements and moments of diaphragm wall are presented comparatively. Also vertical soil displacements at both natural ground surface and excavation level are presented.

Keywords: jet grouting struts, diaphragm wall, finite element analyses, moments and displacements diagrams.

JET GROUT DESTEKLEMENİN DERİN DAYANMA YAPILARI STABİLİTESİNE KATKISININ SONLU ELEMANLAR YÖNTEMİYLE ARAŞTIRILMASI

ÖZ

Jet grout kolonlar derin dayanma yapılarının stabilitesine katkı sağlamak, kazı güvenliğini arttırmak ve kalıcı yapı oluşturmak amacıyla kullanılmaktadır. Kazı seviyesinin altındaki mevcut zeminin yanal direnci zemin özelliklerine bağlı olarak yetersiz kalabilmektedir. Ülkemizde inşaatları devam eden metro inşaatlarındaki derin dayanma yapılarında yanal stabiliteyi arttırma ihtiyacı güncel bir sorun olarak ortaya çıkmaktadır. Bu sorunun ortadan kaldırılması amacıyla pahalı çözümler yerine jet grout kolonlarla kazı seviyesinin altında yatay destek sistemleri oluşturularak ekonomik çözümler elde edilebilmektedir.

Bu tez kapsamında, jet grout desteklemenin derin dayanma yapısı stabilitesine katkısı sonlu elemanlar metodu kullanılarak yapılan analizlerle araştırılmıştır. Bu amaçla öncelikle jet grout kolonların mühendislik özellikleri araştırılmış ve yapısal kullanım türlerine değinilmiştir. Analizlerde kullanılacak problemin geometrisini belirlemek amacıyla halen inşaatı devam etmekte olan "İzmir Metrosu Karşıyaka Tünel Projesi" örnek alınmıştır. Jet grout kolon mukavemeti özellikleri, iyileştirilmiş zemin alan oranları, paternleri ve yerleşim tipleri değiştirilerek analiz kombinasyonları oluşturulmuştur. Analizler kumlu ve killi zemin profilleri için ayrı ayrı yapılmıştır. Analizlerde Plaxis 2D ve 3D sonlu elemanlar programları kullanılmıştır. Analizler sonucunda elde edilen diyafram duvar deplasmanları ve momentleri karşılaştırılmalı olarak sunulmuştur. Doğal zemin yüzeyi ve kazı seviyesindeki zemin düşey deplasmanları da tez kapsamında sunulmuştur.

Anahtar Kelimeler: jet-grout destekleme, diyafram duvar, sonlu eleman analizleri, moment ve deplasman dağılımları.

CONTENTS

CHAPTER ONE

INTRODUCTION

Jet grouting technique is used mostly to improve the soil properties and to transfer the loads to hard soil layers. However, it is also used to provide the slope stability, to prevent liquefaction, as base plugs to prevent excess water movements at the base of excavation level and to create impermeable curtain wall. Jet grouting uses a high pressure jet to cut the natural soil in order to mix and partially replace it with the grout. This creates a "soilcrete" body whose strength and/or permeability characteristics are independent of the original soil fabric.

In this thesis, contribution of the jet grouting struts to the stability of the deep retaining systems has been investigated. Relevant literature research has been done. Selected papers including jet gout strutting, inclinometer readings and finite element analysis are Wang et al. (1999), Hsiung et al. (2000), Wong & Poh (2000), Hsieh et al. (2003), Shirlaw (2003) and Ayoubian & Nasri (2004).

Wang et al. (1999) presented a case study to compare the effects of two different methods of jet grout installation (triple-tube jet grouting and the Superjet) for a two level basement structure in soft clay. Inclinometer readings and finite element analyses had been carried out. They have concluded that Super jet is more suitable for large area improvement. Hsiung et al. (2000) observed the behavior of well-instrumented deep excavations during the construction of the Taipei Rapid Transit Systems. Jet grouting slabs and in-situ cross-walls were used inside these excavations to reduce the lateral displacements of the retaining walls. Wong & Poh (2000) evaluated the performance of the production of jet grouting during the basement construction for Singapore Post Center to study the effects grouting on the diaphragm walls, adjacent soils and nearby structures. Hsieh et al. (2003) described the design and implementation of a soil improvement scheme to reduce diaphragm wall displacement of a six-level basement excavation. Soil improvement carried out to increase the passive resistance of soil and inclinometer readings were studied. The results showed that the jet grouting affects on reducing the diaphragm wall

displacements. Shirlaw (2003) reported that jet grouting had been cased to reduce related ground movements, to improve the stability of tunnels and deep excavations in soft clay in Singapore.

Ayoubian & Nasri (2004) presented the results of a finite element analysis of a proposed approach structure of a rail road tunnel in Quenens, New York City which includes a combination of diaphragm walls and jet grout plugs for base stability and groundwater control of the excavation. The plugs were made of overlapping jet grout columns. The study had been carried out to understand the interaction between jet grout columns, glacial till and slurry walls and aid the design of jet grout plugs. Vertical movements and horizontal stresses generated at the top of jet grouting plug according to various unconfined compressive strengths (UCS) and thicknesses of the jet grouting plug have been presented.

Engineering properties of jet grouted soilcrete vary according to existing soil properties, jet grouting methods and procedures. There is no fixed method to determine mechanical properties of treated soil. There are various empirical relations from the experimental studies made by various investigators. But they are not valid for all soil conditions. Empirical relations are mainly based on unconfined compressive strength (UCS) of jet grouted soilcrete. Hence, engineering properties of jet grouted soilcrete such as modulus of elasticity, cohesion intercept and friction angle are determined in terms of UCS.

In this study, the contribution of jet grout strutting to the stability of deep retaining systems has been investigated through analyses made by finite element method. A deep retaining system has been analyzed. Deep retaining system is a part of a cut and cover tunnel. The geometric model of the tunnel is inspired by Karşıyaka Subway Tunnel construction project. The geometric properties of the cut and cover tunnel such as depth of the excavation, span of the excavation and the length of the retaining wall have been taken from this project. Two different soil profiles have been considered. One is composed of sand and the other one is composed of clay. Soil parameters are selected as average values for medium dense sand and medium plastic clay. Retaining system was considered as a diaphragm wall with two level steel struts.

Various jet strut configurations were formed and analyzed. These include variations in pattern type, soilcrete location, treated soil area ratio and soilcrete stiffness.

Geometric properties of the problem, soilcrete patterns types, construction stages and material properties (diaphragm wall, steel strut, jet struts and soils) used in finite element analyses (Plaxis 2D and Plaxis 3D) have been explained in detail.

Analyses have been performed basically with Mohr-Coulomb model both for the sand and the clay profiles. Finite element analyses with Hardening-Soil model have also been performed for representative cases and obtained results have been compared with the solutions of Mohr-Coulomb model.

Moment and lateral displacement curves of the diaphragm wall have been presented comparatively with respect to analyses combinations. Vertical soil displacement curves at the excavation level and at the ground surface have been plotted according to the analyses combinations and presented.

Economical and applicable solutions have been suggested according to finite element analyses results for both sandy and clayey soils.

In chapter two, jet grouting structures and mechanical properties of jet grouted soilcrete have been presented. Definition of the problem and finite element parameters of the materials have been given in chapter three. In chapter four, finite element analyses have been done. Results and conclusions have been given in chapter five.

CHAPTER TWO

JET GROUTING STRUCTURES AND MECHANICAL PROPERTIES OF JET GROUTED SOILCRETE

2.1 Jet Grouting Structures

Jet grouting can be used for different purposes. Case records are available on the successful use of the jet grouting. Examples are listed as below.

a) Soil improvement below the wide foundations as bearing elements to provide base stability and the settlement criteria,
b) Retaining walls and supporting structures,
c) Impervious cut off walls to create low permeability barriers,
d) Stabilization of soil slopes,
e) Excavation bottom plugs against the seepage and reduction of the wall displacements and wall internal forces,
f) Soil stabilization for temporary support of the excavated tunnels,
g) Cofferdams,
h) Restoring the existing foundations.

Jet grouted element is a volume of soil treated through a single drilled hole. The most common types of jet grouted elements are jet grouted column that is a cylindrical jet grouted element and jet grouted panel, which is a plane jet grouted element. Examples of these elements are shown in Fig. 2. 1.

The jet grouted elements can be created in a fresh in fresh sequence or in a primary-secondary sequence as illustrated in Fig. 2. 2. With the fresh in fresh sequence of work the jet grouting elements are constructed without waiting for grout to harden in the overlapping elements. With the primary-secondary sequence of work, the execution of an overlapping element cannot commence before a specified hardening time has elapsed or before a pre-determined strength of the adjacent previously constructed elements has been achieved (Stoel, 2001).

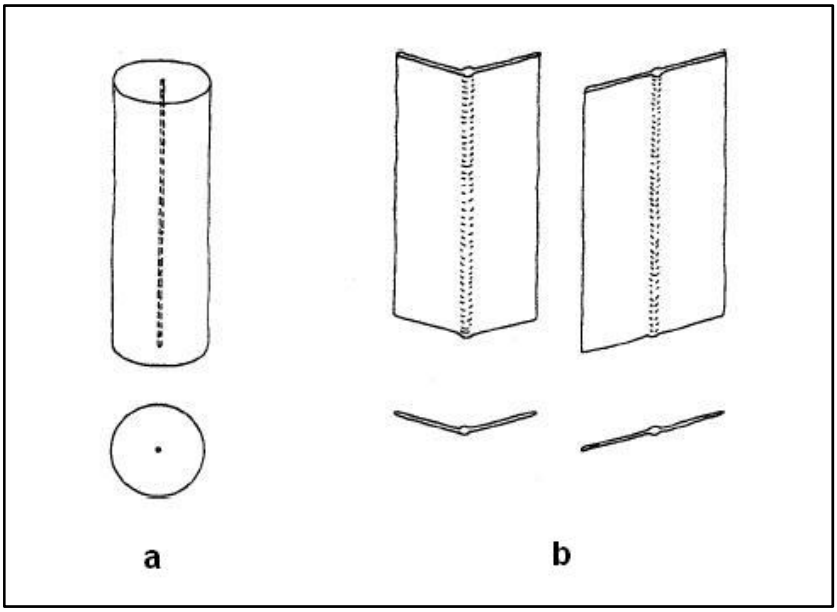

Figure 2. 1 Jet grouted elements: (a) jet grouted column, (b) jet grouted panels

(British Standard, 2001)

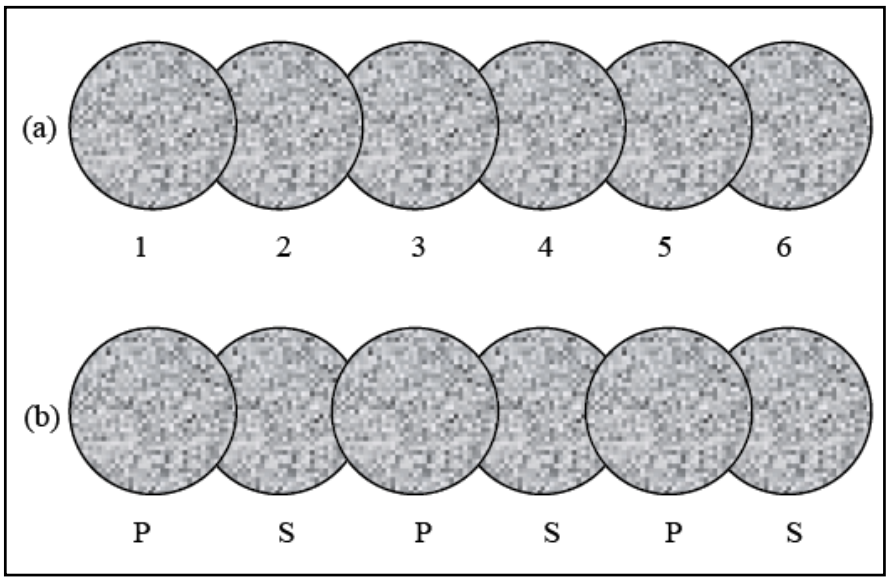

Figure 2. 2. Jet grouting sequences; fresh in fresh (a) and primary-secondary (b)

Jet grouted structures can be created from different arrangements of jet grouted elements. The most common jet grouted structures are listed below.

1. Diaphragm: It is a wall obtained by making interlocked elements.
2. Slab: It is a horizontal structure formed by interlocked elements.

3. Canopy: It is an arch formed by interlocked horizontal or sub-horizontal elements.
4. Block: It is a three dimensional structure formed by interlocked elements.

The jet grouted structures 1, 2 and 3 are presented in Fig. 2. 3. Interlocking can be full or partial. When jet grouting is used to create stability, partial interlocking is often sufficient. If jet grouting is used to create a low permeability barrier, the jet grouted elements must interlock completely.

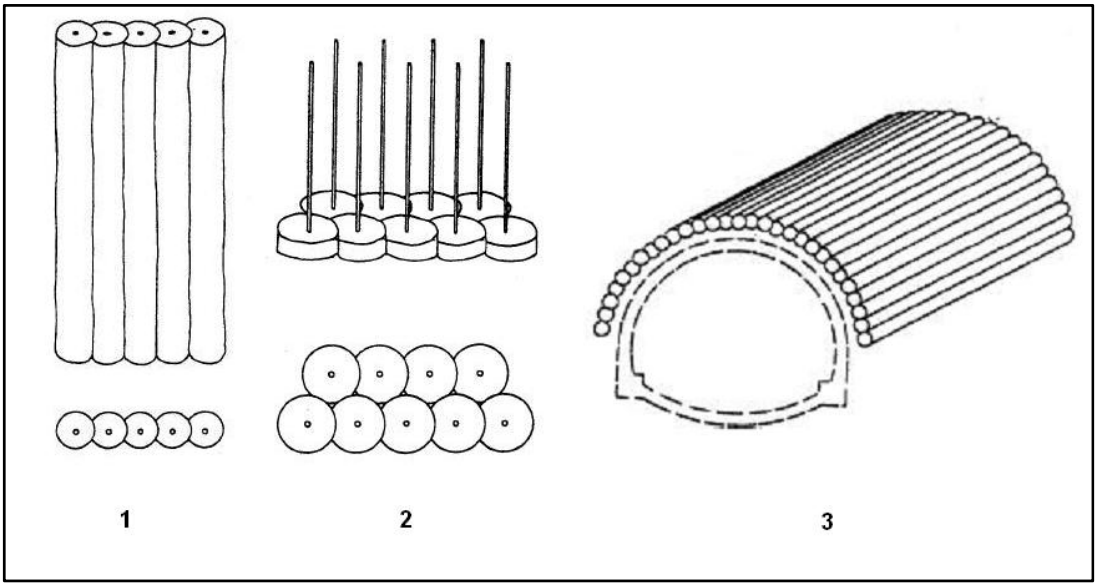

Figure 2. 3. Jet grouting structures; diaphragm wall (1), slab (2) and canopy (3). (TS EN 12716)

2.2 Jet Grouting

Jet grouting is a technique that is used to create grouted soil for soil stabilization, reduction of settlement and permeability of soil in the underground. Soil improvement by jet grouting method affects the soils in two different ways that are direct and indirect effects. The direct effect increases the mechanical characteristics as shear strength, modulus of elasticity and compression strength in the treated soils. The indirect effect produces the compression on the adjacent soils and changes volumes of the soil (Melegari & Garassino, 1997).

The new formation of the jet grouted soil is called as “soilcrete”. It has better strength, stiffness and permeability properties than the original soil. To investigate the mechanical properties of jet grouted soilcrete, unconfined compression strength

tests and Brazilian tests might be performed simply in the soil mechanics laboratories. Unconfined compression strength, modulus of elasticity, tensile strength can be determined by those tests. However, to understand the indirect effect of the compression to the adjacent soils by jet grouting, other methods like standard penetration test (SPT), cone penetration tests (CPT) and pressuremeter tests must be carried out in situ before and after treating process. Also, integrity tests should be performed to determine the integrity of the soilcrete column pile.

Jet grouting technique makes use of high-velocity jet streams to cut, replace and then mix the native soil with a cementing agent. Presently there are three main process of jet grouting. These processes are single fluid system (grout), double fluid system (air and grout) and triple fluid system (air, water and grout). Jet grouting processes are not covered in this study.

Some factors affect the mechanical properties of jet grouted soilcrete. The strength of jet grouted soilcrete by single fluid system has greater values than by double system because of much cement consumption in the treated soil. Double fluid system injects lower amount of cement to treated soil thereby the strength of soilcrete has lower values than by single fluid system.

The cement dosage in per meter treated soil is also effective on strength of soilcrete. The strength of jet grouted soilcrete increase with increasing cement dosage in per meter in treated soil.

On the other side, water cement ratio, injection parameters such as injection pressure, flow rates, nozzle sizes, number of nozzles, rods rotation speed, rods lifting time per step and soil type are also effective on the strength of the jet grouted soilcrete. Injection parameters are commonly selected according to soil type and design value of the project. Before the process of jet grouting, trial columns are produced and checked for controlling the design values.

2.3 An Overview of Mechanical Properties of Jet Grouted Soilcrete

Engineering properties of jet grouted soilcrete such as unconfined compression strength, modulus of elasticity, tensile strength and Poisson ratio had been

investigated by Yohiro et al. (1975; 1982), Miki (1985), Bertero et al. (1988), Fang et al. (1994; 1994), Wong & Hwang (1997), Stoel & Ree (2000), Stoel (2001), Poh & Wong (2001), Shibazaki (2003), Ökmen (2004), Coulter & Martin (2006). These investigators carried out some tests on soilcrete and reported mechanical properties of soilcrete and suggested design values for engineers. In this study, the papers of these investigators are summarized.

Unconfined compression strength is determined according to the unconfined compression tests. By these tests, modulus of elasticity can also be determined. It can be calculated as the tangent modulus of elasticity at 40% or 50% of unconfined compressive strength or can be calculated as the slope of the straight portion of the stress-strain curve.

It is mentioned in the previous section that unconfined compressive strength (UCS) of soilcrete changes according to the soil type. Unconfined compressive strength ranges for different soil types according to various investigators are presented in Table 2.1.

Table 2. 1 Unconfined compressive strength ranges of soilcrete for different soil types according to various investigators

	Unconfined Compressive Strength (UCS) of Soilcrete, MPa						
Soil Type	Miki (1985)	Bell (1993)	Fang et al. (1994)	Melegari & Garassino (1997)	Stoel & Ree (2000)	Shibazaki (2003)	Ökmen (2004)
Clay	<5	0.5 ~ 8	2 ~ 10	1.8 ~ 3	3 ~ 14	10	1 ~ 5
Silt		4 ~18		3 ~ 4.5			
Sand	5 ~ 10	5 ~ 25	5 ~ 21	6 ~ 9	3 ~ 33	30	5 ~ 23
Gravel		5 ~ 30		10			

It is clear to realize that unconfined compression strength of soilcrete is lower for cohesive soils than cohesionless soils. Granular soils have higher strength values than silty and clayey soils.

Ballarin & Forti (1998) reported that the UCS of soilcrete changes between 1.2 and 4 MPa for clays and clayey silts. The values of the strength of soilcrete are

between 3 and 12 MPa in silts and sands. For sands and gravels it changes between 6 and 12 MPa.

Stoel (2001) have investigated to examine the use of grouting methods for pile foundation improvement in Amsterdam. One of the methods was jet grouting. Treatment performed in sandy and clayey layers. Unconfined compressive strength and elasticity modulus were determined according to unconfined compression test. The ratios of water/cement 0.8, 1.0 and 1.2 had been used for the tests.

Stoel (2001) produced some empirical equations between tensile strength, compressive strength and modulus of elasticity of the soilcrete according to the test results. The empirical equations are presented in Table 2. 2 below. They are both for sandy layers and clayey layers.

Table 2. 2. Empirical equations for relation between various grout parameters.

Relation	**Grouted Sand Layers**	**Grouted Clay Layers**
Tensile Strength ($f_{ct,sp}$) and UCS (f_c)	$f_{ct,sp} = 0.3\ (f_c)^{3/5}$	$f_{ct,sp} = 0.4\ (f_c)^{3/10}$
Young Modulus (E_{cm}) and UCS (f_c)	$E_{cm} = 800\ (f_c)^{1/2}$	$E_{cm} = 500\ (f_c)^{2/3}$
UCS (f_c) and Water Cement Ratio (wcr)*	$f_c = 7 + 8.1\ (wcr)^2$	$f_c = 2 + 3.6\ (wcr)^2$

*Applicable for $0.6 < wcr < 1.4$

Stoel (2001) had also performed Cone Penetration Tests before and after jet grouting for a selected column. Stoel reported that, it was not possible to deduce an unambiguous relation for the change of cone resistance due to jet grouting.

Fang et al. (1994) investigated the strength characteristics of soilcrete from the construction sites at Taipei Mass Rapid Transit (MRT) and Hsinchu Science-based Industrial Park (SIP). Jumbo Jet Special Grout (JSG) Method that belongs to double injection category had been discussed and an empirical failure criterion was established for soilcrete.

Treated soils were gray silty sand (SM) and red brown clay with high plasticity (CH). The composition for each cubic meter of JSG included 760 kg of Portland cement and 750 liters of water. Water-cement ratio was 1.0. The soil composition included silty sand and clay formations.

Unconfined compressive strengths were found between 5.4 MPa and 24.3 MPa and modulus of elasticities varied from 1.1 GPa to 4.2 GPa.

The test results were in good agreement with range $E_{50} = 100q_u \sim 300q_u$ suggested by JSG Association (1986). Experimental Poisson's ratios ranged between 0.12 and 0.22 which are closer to that for concrete than that for native soils.

Trevi (1994) obtained deformability of soilcrete in high degree of variability. The results obtained on various sites in silty or sandy silty formation are shown in Fig 2. 4. Modulus of elasticity varied from 100 MPa to 1500 MPa. Compressive strength varied from 0.6 MPa to 4.5 MPa.

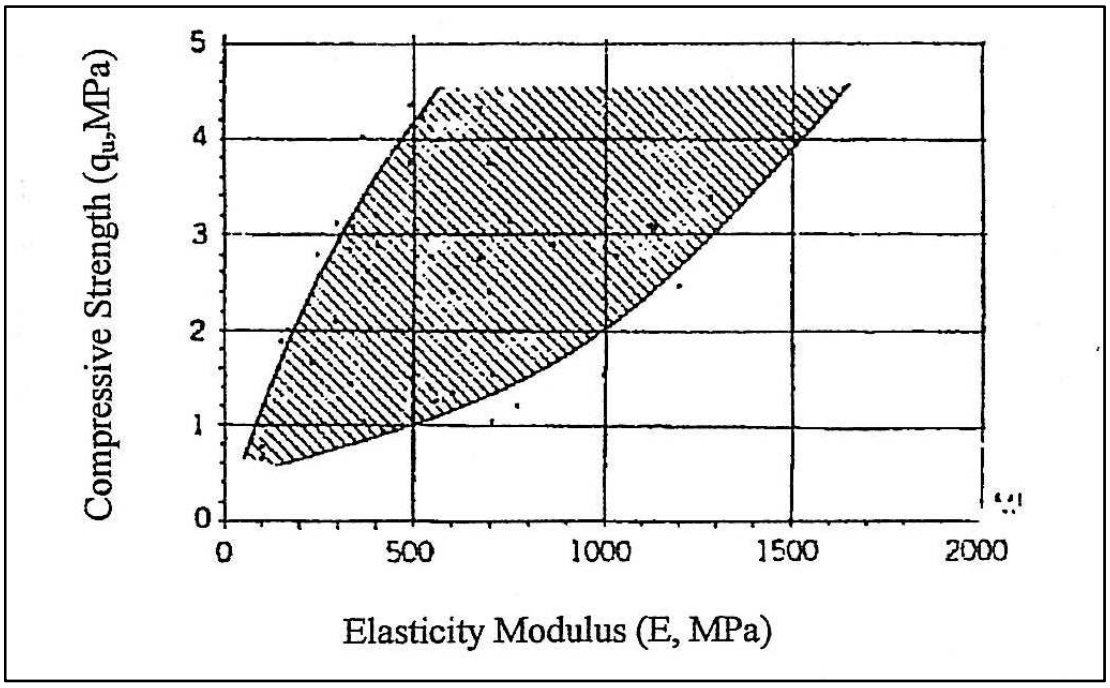

Figure 2. 4 Values of the tangential elasticity modulus in relation to the values of unconfined compressive strength. Treatments in silty or silty-sandy soils. (Trevi, 1990)

Kauschinger et al. (1992) investigated the mechanical properties of the Boston blue clay soilcretes that were artificial. The cement percent used varied from 12% to 45%. Cement percent was the ratio of weight of cement to total weight of mixture. Different water cement ratios were used. The compressive strength of the soilcrete noted as decreased as the water cement ratio increased. The relationship between water cement ratio and compressive strength is shown in Fig. 2. 5.

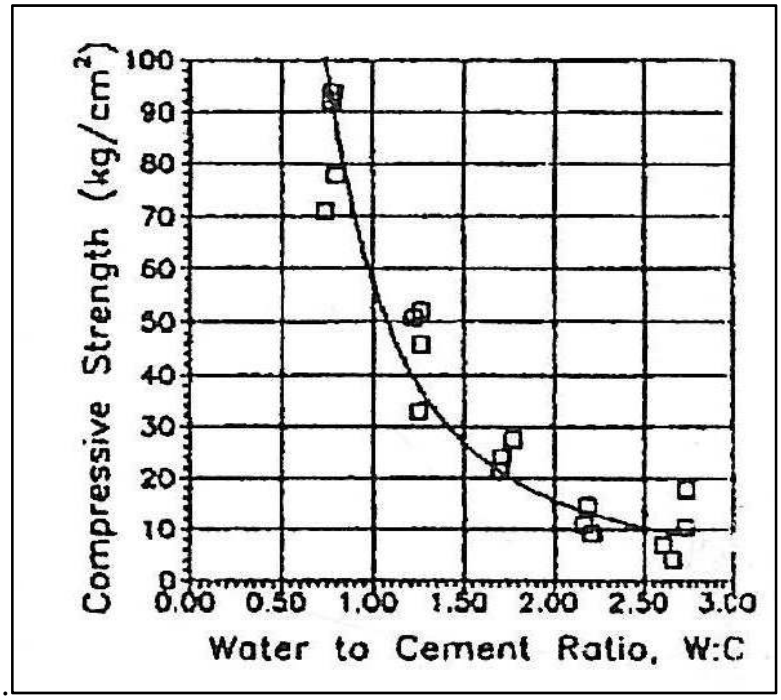

Figure 2. 5 Relationship between water cement ratio and compressive strength (Kauschinger et al., 1992).

The relationship of modulus of elasticity versus unconfined compressive strength is shown in Fig. 2. 6.

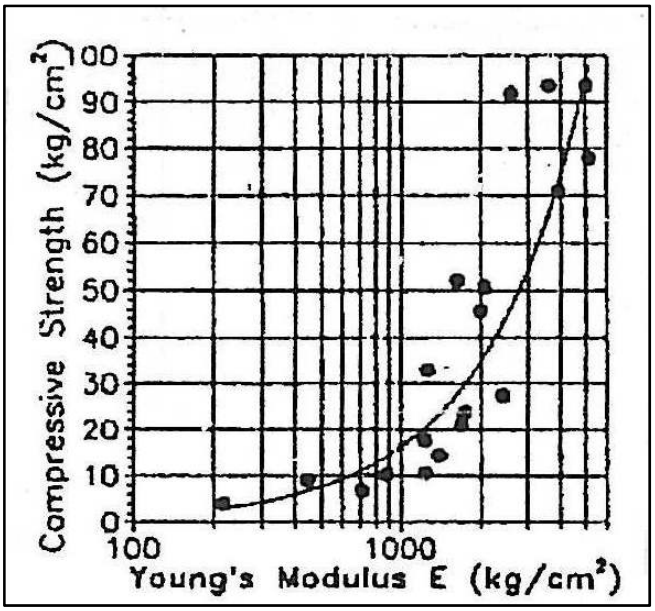

Figure 2. 6 Relationship between Young's modulus and compressive strength (Kauschinger et al., 1992).

The modulus of elasticity increased as the unconfined compressive strength increased. Unconfined compressive strength varied from 0.5 MPa to 9.5 MPa and modulus of elasticity varied from 20 MPa to 500 MPa for Boston blue clay.

Ökmen (2003) had an experimental study to investigate the characteristic properties of the soilcrete that water cement ratios varied from 0.75 to 2.75. Unconfined compressive strength obtained as between 5 MPa and 23 MPa for sandy soil whereas the unconfined compressive strength obtained as between 1 MPa and 5 MPa for clayey soil. The modulus of elasticity varied from 300 MPa to 1200 MPa for sandy soils, whereas the modulus of elasticity varied from 100 MPa to 350 MPa for clayey soil.

The ratio of the modulus of elasticity to unconfined compressive strength varied over a range from 45 to 75 and from 70 to 85 for sandy and clayey soilcrete samples, respectively.

Following relationships between modulus of elasticity and unconfined compressive strength were derived for sandy and clayey soilcretes (Ökmen, 2003).

$$\text{for sandy soils, } E = 150\ (q_u)^{0.6} \tag{1}$$

$$\text{for clayey soils, } E = 75(q_u) \tag{2}$$

Wong & Hwang (1997) evaluated undrained shear strength and modulus of elasticity of treated soil by unconfined compression tests, cone penetration tests and pressuremeter tests. Ground improvement by jet grouting is conducted in clayey soils on construction site in Taipei Rapid Transit System.

The $E_{50}/s_{u(UC)}$ values varied from 70 to 200 and the average value of E_{50} expressed as (Wong, 1997)

$$E_{50} = 114\ s_{u(UC)} \tag{3}$$

According to pressuremeter test (PMT) relationship between modulus of elasticity E and undrained shear strength $s_{u(PMT)}$ is expressed as (Wong & Hwang, 1997)

$$E = 108\ s_{u(PMT)} \tag{4}$$

Fang et al. (1994) also reported mechanical properties of jet grouted soilcrete by uniaxial compression tests, Brazilian test and ultrasonic tests. The tests were conducted on silty sand and silty clay soils from construction site of Taipei Mass Rapid Transit (MRT). It was found that the uniaxial compressive strength, modulus of elasticity, failure strain, tensile strength and P-wave velocity of soilcrete increase with increasing dry density.

Variations of uniaxial compressive strengths obtained as a function of depth are shown in Fig. 2. 7.

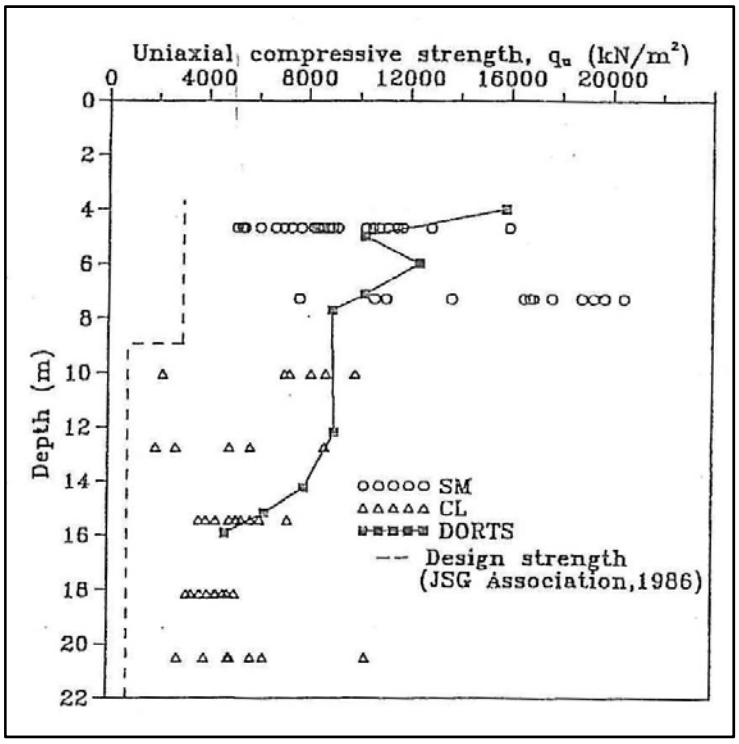

Figure 2. 7 Variation of uniaxial compressive strength with depth (Fang et al., 1994).

The relationship between uniaxial compressive strength and dry density is shown Fig. 2. 8. From these data, it may be seen that the strength of soilcrete increases with increasing dry density. For the soilcrete formed in silty sand, the maximum q_u obtained as 20600 kN/m^2 was similar to that of concrete.

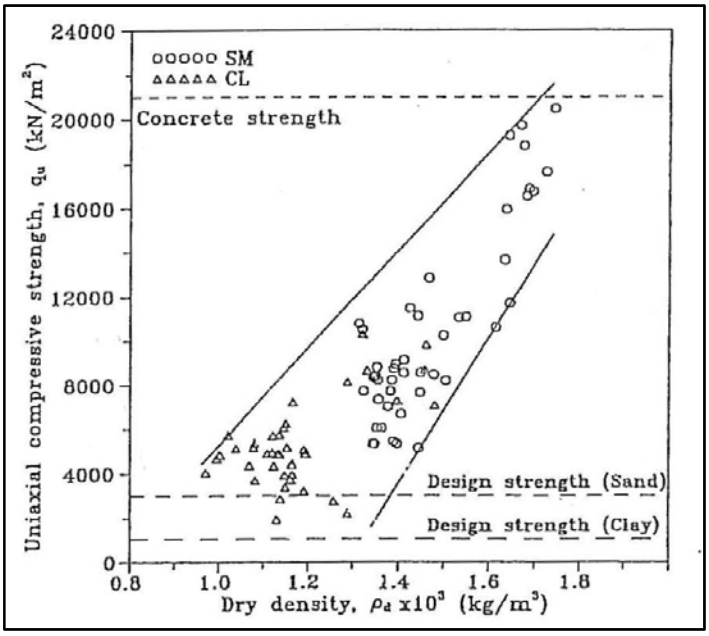

Figure 2. 8 Relationship between uniaxial compressive strength and dry density (Fang et al., 1994).

Tensile strengths are determined from Brazilian tests. As with compressive strength, the tensile strengths for sandy soilcrete are greater than those for clayey soilcrete. Based on the data shown in Fig. 2. 9, an empirical correlation is suggested as below;

$$\sigma_{t,B} = \frac{q_u}{10} \; to \frac{q_u}{30} \tag{5}$$

Where $\sigma_{t,B}$ is the tensile strength and q_u is unconfined compressive strenght.

Based on the Fang's experimental test results for jet grouted soilcrete, the uniaxial compressive strength, modulus of elasticity, failure strain, tensile strength of soilcrete are increased with increasing dry density. The dry density should be an important criterion fort he quality control of jet grouting.

The Brazilian indirect tensile strength of soilcrete varied between 1/10 and 1/30 of its uniaxial compressive strength.

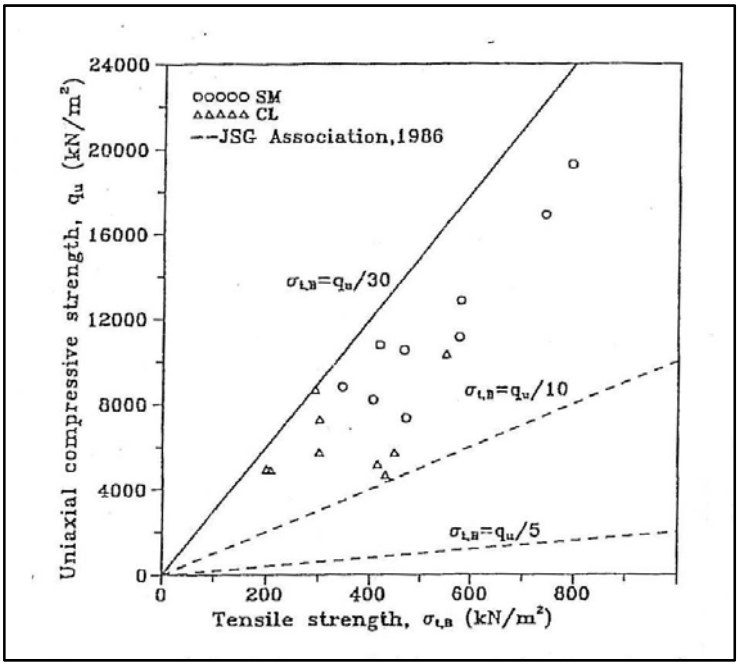

Figure 2. 9 Correlation between uniaxial compressive strength and tensile strength (Fang et al., 1994).

2.4 Comparisons of Uniaxial Compressive Strengths (UCS) of Soilcretes in Literature

Comparison of the uniaxial compressive strength values of clayey and sandy soilcrete samples according to literature is presented in Fig. 2. 10 and Fig. 2. 11, respectively.

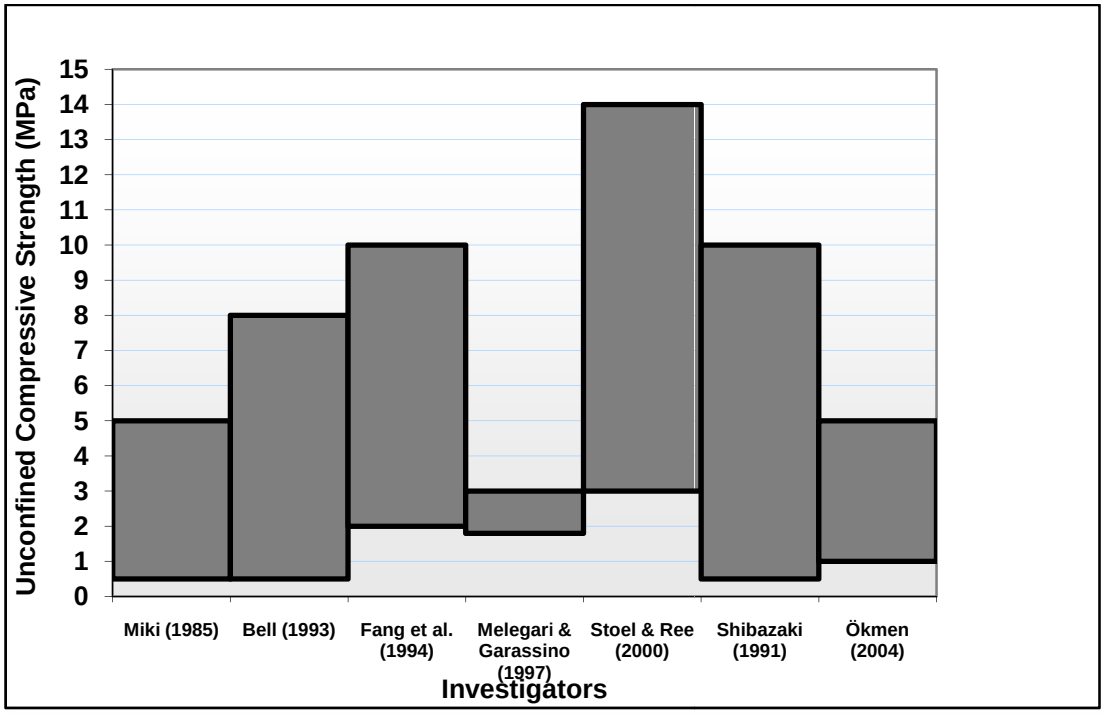

Figure 2. 10 Comparison of the unconfined compressive strength (UCS) values of clayey soilcrete according to literature.

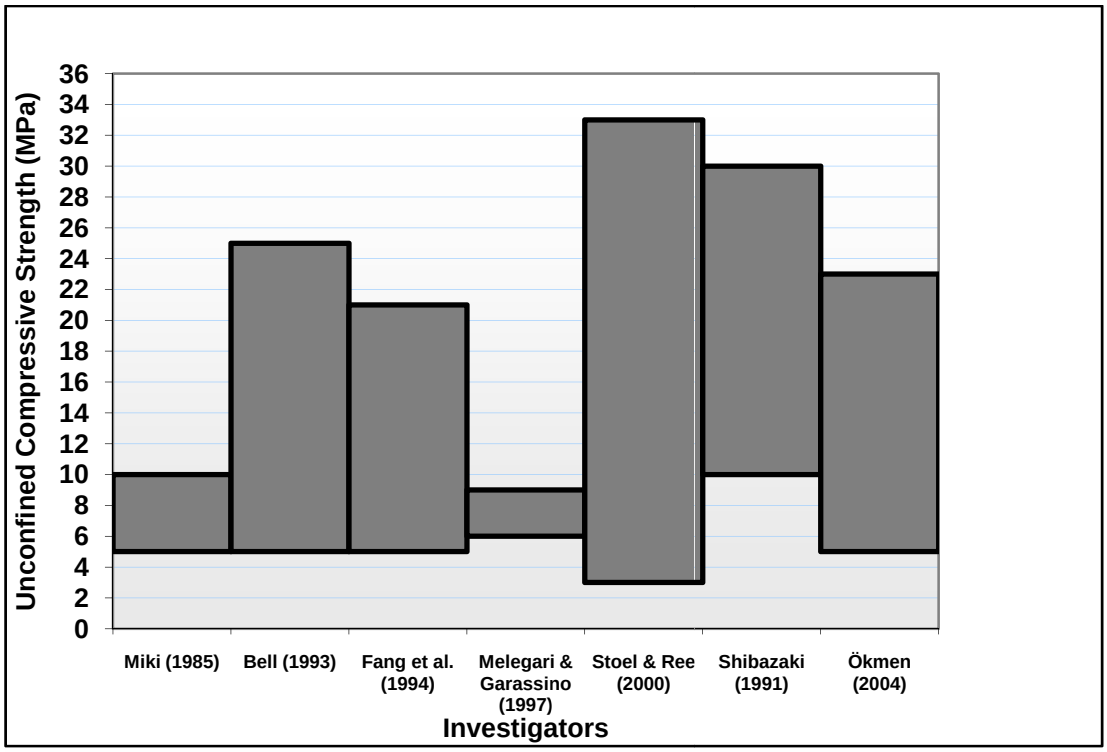

Figure 2. 11 Comparison of the unconfined compressive strength values of sandy soilcrete according to literature.

CHAPTER THREE

DEFINITION OF THE PROBLEM AND FINITE ELEMENT PARAMETERS OF THE METARIALS

3.1 Scope

This study concerns the construction of a cut and cover tunnel. The geometric model of the problem is inspired by Karşıyaka subway tunnel construction.

The retaining system consists of bored piles and jet grout columns intersecting with bored piles. The jet grout columns were used to prevent the seepage. Jet grouting struts were used below the excavation level to reduce the wall displacements and moments. The jet struts also help to reduce the soil displacements at the excavation level and at the ground surface behind the retaining system. Temporary steel struts were used for the safety of the excavation. Sandy and clayey soils of variable thicknesses and properties have been encountered at the construction site.

In this study, the geometric properties of the cut and cover tunnel such as depth of the excavation, span of the excavation and the length of the retaining wall have been taken from Karşıyaka Subway Tunnel Project. Soil parameters are selected as average values for medium dense sand and medium plastic clay. Retaining system was considered as a diaphragm wall to make easy modeling in the finite element analyses. Two level steel struts have been used in the analyses in spite of one level strut used in Karşıyaka Tunnel application.

Various jet strut configurations were formed and analyzed. These include variations in pattern type, soilcrete location, treated soil area ratio and soilcrete stiffness. Jet strut type used in Karşıyaka Tunnel has also been included in the analyses.

In this chapter, geometric properties of the problem, soilcrete patterns types, construction stages and material properties (diaphragm wall, steel strut, jet struts and soils) used in finite element analyses have been explained. Plaxis 2D and 3D will be used in the finite element analyses (Brinkgreve, 2002), (Brinkgreve & Swolfs, 2007)

3.2 The Geometry the Problem

The excavation is 10 m wide and the final depth is 10 m. It extends in longitudinal direction for a large distance. The sides of the excavation are supported by 20 m long diaphragm walls, which are braced by two leveled horizontal struts. Along the excavation surface no surcharge has been considered.

The jet struts are located below the excavation level in between the diaphragm walls. Finite element analyses have been performed for sand and clay profiles separately. The soil parameters are selected as averages values (medium dense sand and medium plastic clay). Water table is assumed at 2 m below the ground surface. The schematic cross section of the system is presented in Fig. 3. 1.

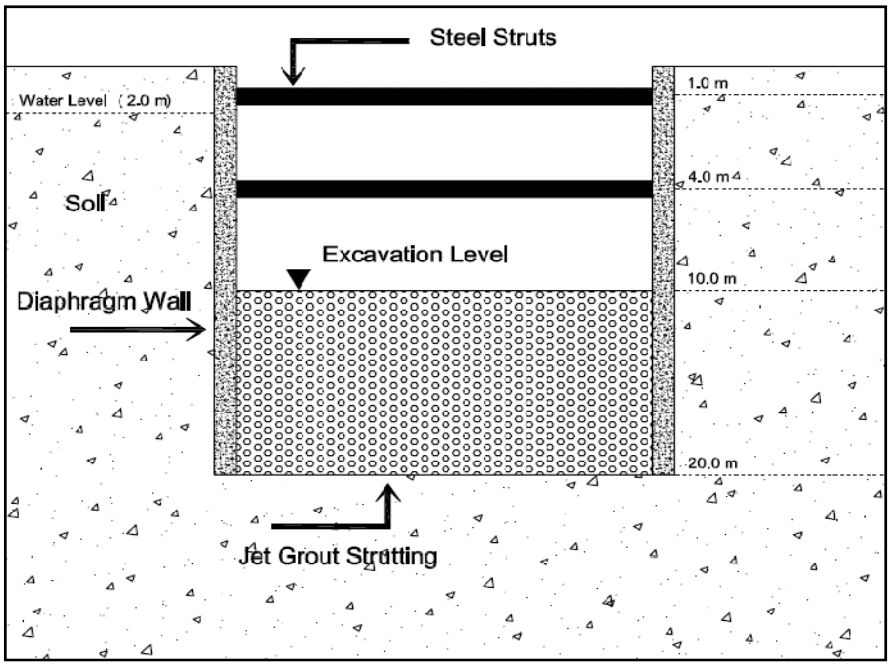

Figure 3. 1 Schematic cross section view of the excavation for cut and cover tunnel

3.3 Description of the Construction

Construction begins by installation of the diaphragm walls. Jet strutting process follows the installation of the diaphragm walls. Jet struts are made in different forms for sand and clay.

Sands have high permeability that causes excessive seepage flow into excavation channel. This worsens the construction conditions and discharging the water out is

usually difficult. It may cause the soil collapse at the excavation level. Therefore, jet grouting is performed as overlapping columns on the excavation base to prevent the excess water movement and damage of soil body. So the problem in this case can be handled as 2 dimensional and finite element analyses can be performed with Plaxis 2D. The schematic plan view of the overlapping jet grout columns is shown in Fig. 3. 2 below.

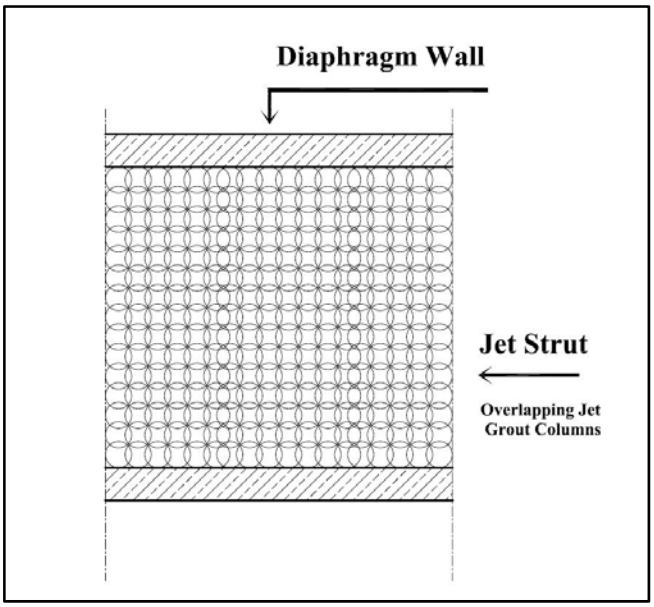

Figure 3. 2 Schematic plan view of the overlapping columns

Clays have low permeability so full overlapping of jet grout columns to prevent seepage is not needed. Various treated soil geometries can be applied. Four different patterns of jet strutting were used in the analyses. Due to the 3D geometry of the problem the analyses is performed by using Plaxis 3D. The jet strut patterns used are presented in Table 3. 1 below. The schematic plan views of these four patterns are shown in Fig. 3. 3.

Table 3. 1 Properties of soils used in finite element analyses

Pattern	Explanations
I	Jet strut extending transversely between diaphragm walls
II	Pattern I with longitudinal jet strut adjacent to diaphragm wall
III	Longitudinal jet strut adjacent to diaphragm wall
IV	Hexagonal jet strut pattern (honeycomb)

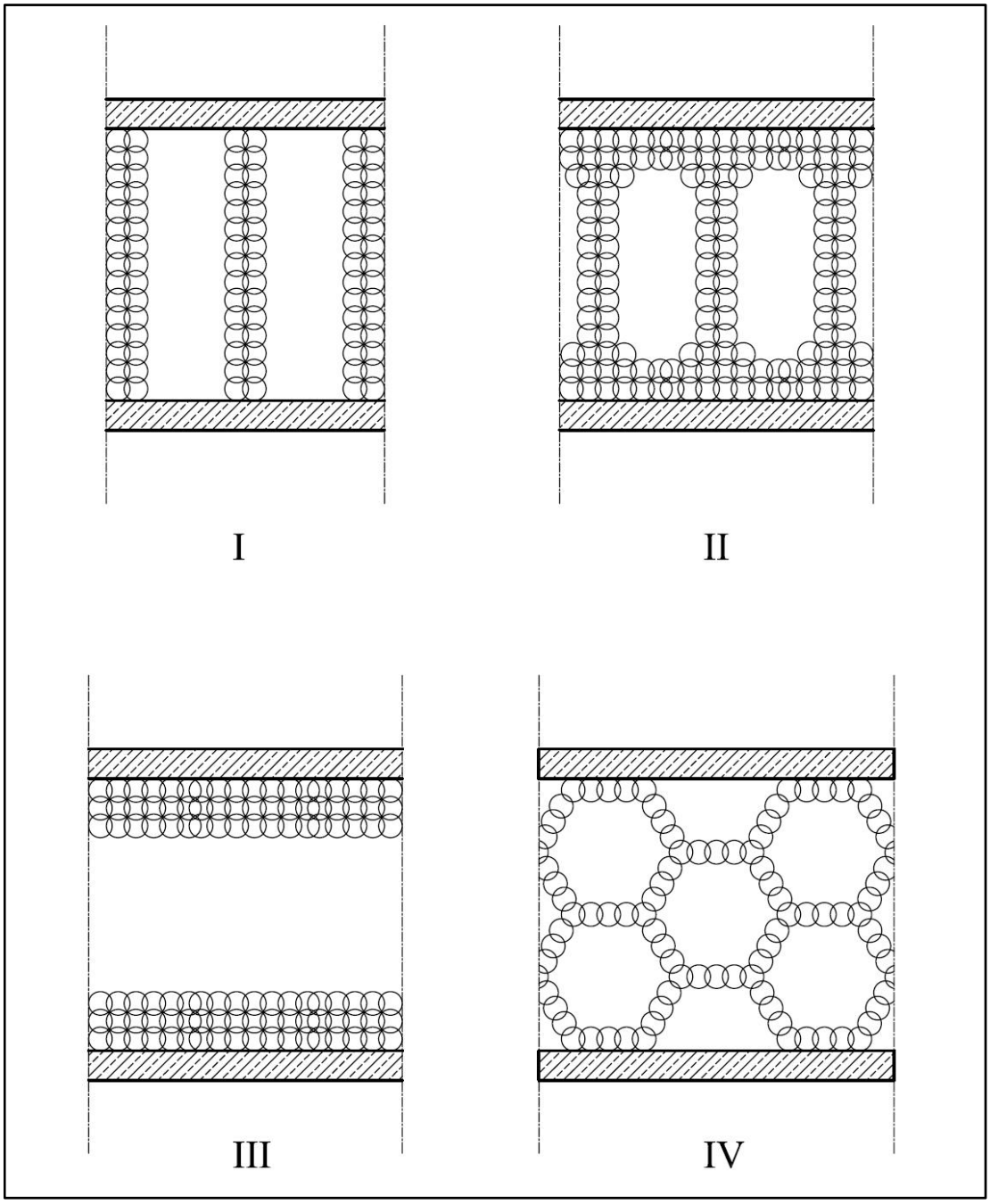

Figure 3. 3 Schematic plan view of the jet grout patterns for clayey soil.

Following the construction of jet strut columns, soil is excavated just below the first row of steel struts. This stage is called as the first excavation phase. After the first excavation phase, steel struts are installed. Second excavation phase follows installation of the first row of the steel struts. After the second excavation phase, second row of steel struts are installed. Final excavation phase is performed after the installation of the second row of the steel struts.

Analyses are performed taking into account the effective thickness of the jet grout columns that have straight edges. Consideration of the effective thickness of the overlapping jet grout columns is shown in Fig. 3. 4.

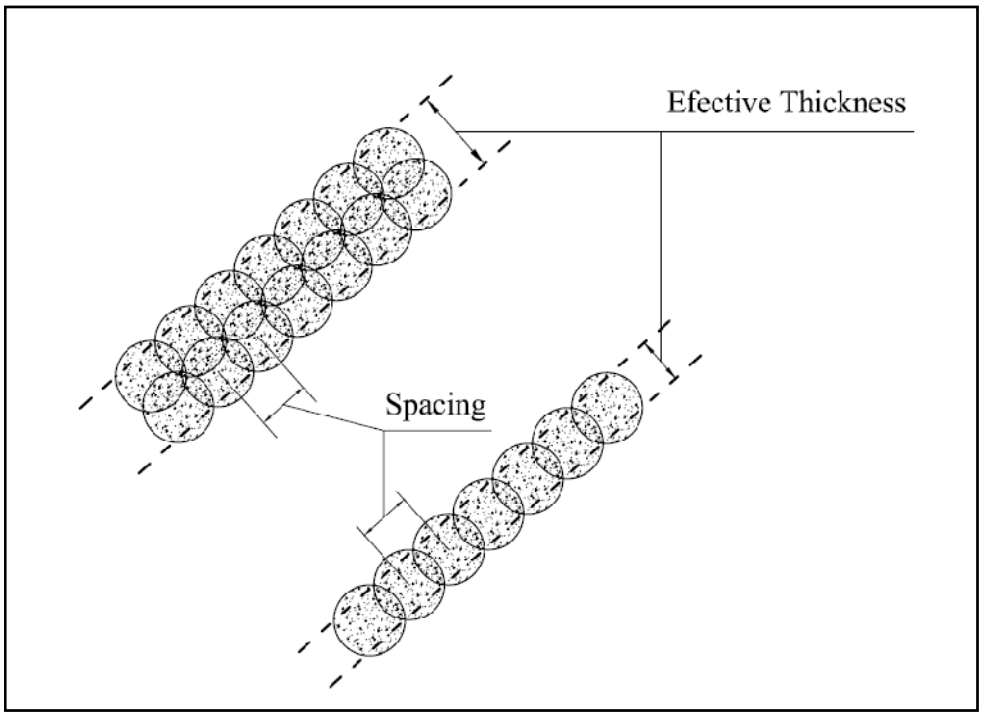

Figure 3. 4 Consideration of the effective thickness of the overlapping jet grout columns.

3D Finite element analyses have been performed for various treated soil area ratios. Treated soil ratio is the ratio of the amount of the improved soil area to total soil area. Treated soil area ratio (I_r) can be calculated simply as follows:

$$I_r = \frac{A_j}{A_t} \tag{6}$$

Where; A_j: the area of jet grout columns in the unit area, A_t: unit area.

Construction Phases of the problem are presented in the Table 3. 2 below. Schematic explanation of the phases is shown in Fig. 3. 5 and Fig. 3. 6.

Table 3. 2 Construction phases used in finite element analyses

Phases	Explanations
Phase I	Initial Phase; There is only native soil.
Phase II	Construction of the diaphragm walls.
Phase III	Construction of jet grout struts below the excavation level.
Phase IV	Excavation from ground surface to a depth of 2 meters.
Phase V	Installation of the first row of steel struts at 1 meter depth.
Phase VI	Excavation to 6 meters depth.
Phase VII	Installation of the second row of steel strut at 5 meters depth.
Phase VIII	Excavation to 10 meters depth (final depth).

3.4 Material Properties Used in Finite Element Analyses

In this section, properties of soils, diaphragm walls, steel struts and jet struts are explained for use in finite element analyses by Plaxis 2D and 3D programs.

3.4.1 Properties of Soils

Untreated soil parameters are assigned regardless of any specific data. Average soil values are taken into consideration for finite element analyses (Bowles, 1997). The untreated soil parameters for both clay and sand are explained in Table 3. 3 below. The untreated soil parameters are unit weight (γ) and saturated unit weight (γ_{sat}), cohesion intercept (c), friction angle (ϕ), Poisson ratio (ν), modulus of elasticity (E) and coefficient of permeability (k). Finite element analyses will be performed as long term analyses. Interface strength (R_{inter}) was considered as 2/3.

Table 3. 3 Properties of soils used in finite element analyses

Material	**γ**	**γ_{sat}**	**c'**	**ϕ '**	**ν**	**E**	**k**
	kN/m^3	**kN/m^3**	**kN/m^2**	**degrees**	**-**	**kN/m^2**	**m/s**
Sand	17	20	1	33	0.30	25000	10^{-3}
Clay	18	21	1	27	0.35	12500	10^{-6}

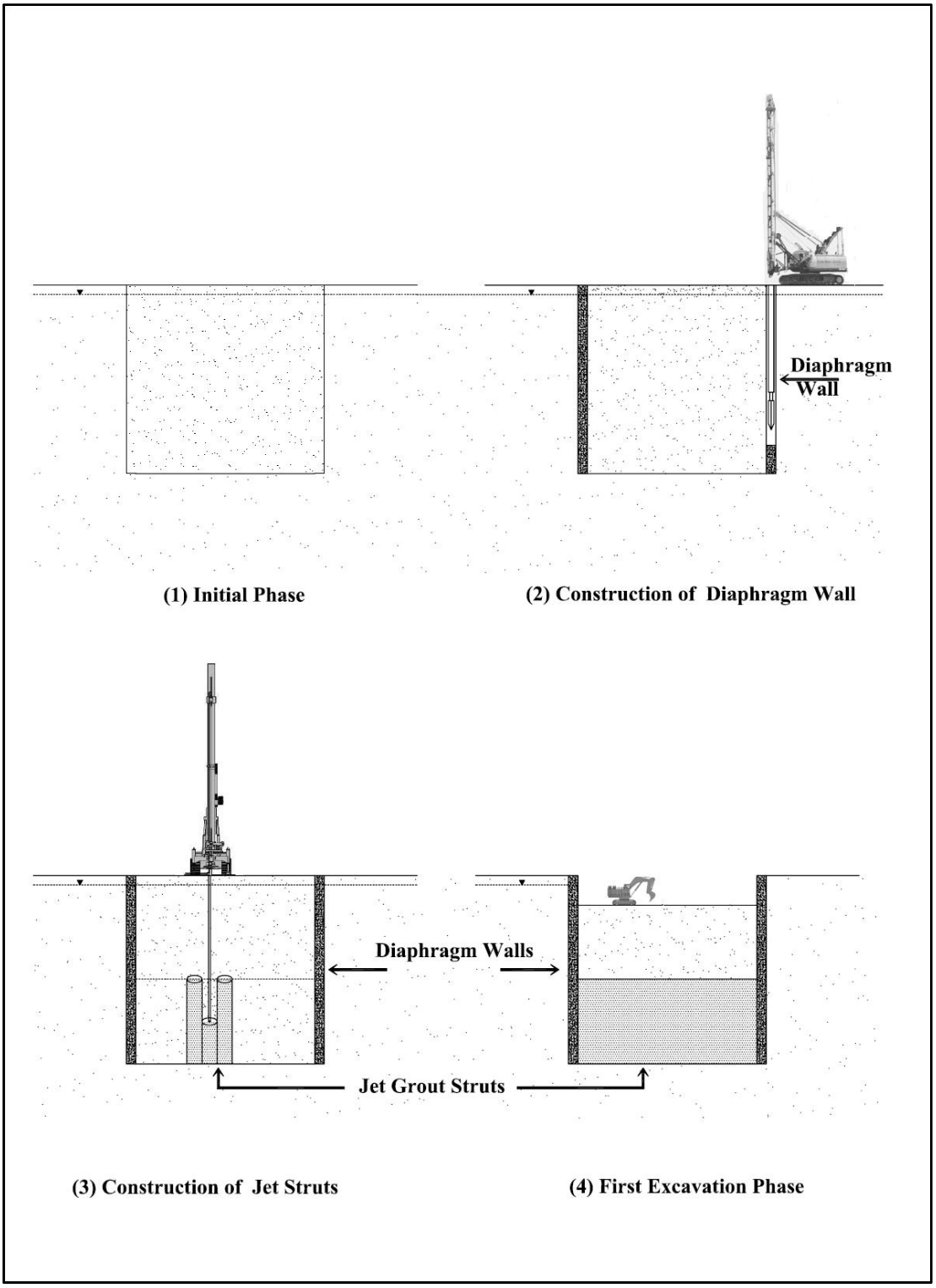

Figure 3. 5 Construction stages of I, II, III and IV.

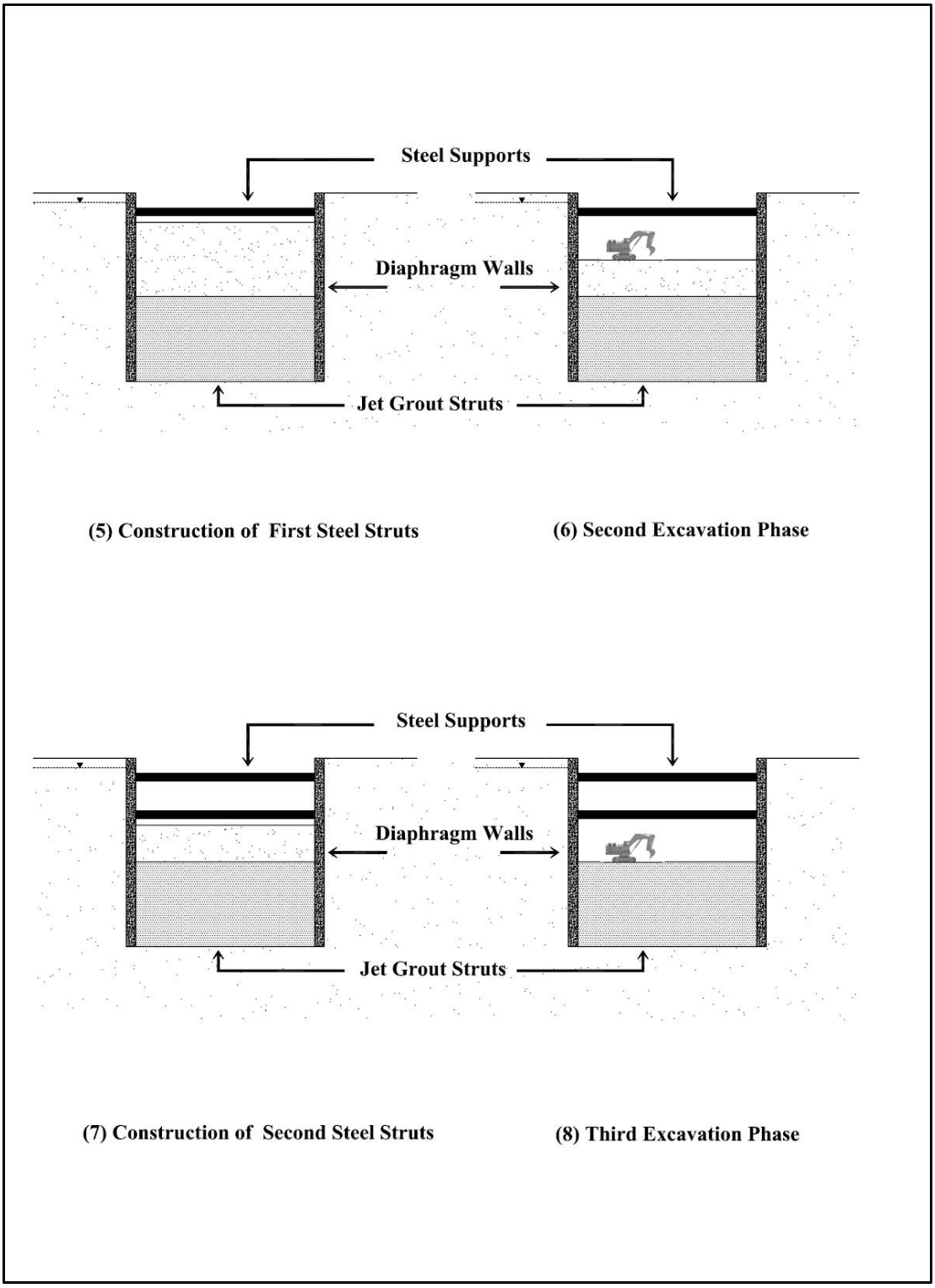

Figure 3. 6 Construction stages of V, VI, VII and VIII.

3.4.2 Properties of Diaphragm Walls

The thickness *(d)* of the diaphragm wall is assumed as 1 meter. Values of *E, A and I* are follows;

Diaphragm walls are assumed to be constructed with C20 quality concrete and modulus of elasticity is taken as

$$E_c = 30.000 \text{ MPa}$$

Area of diaphragm wall per one meter is

$$A = 1x1 = 1m^2$$

Inertia of diaphragm wall is

$$I_d = b.h^3/12 = 1.1^3/12 = 0.08m^4$$

Unit weight of the concrete ($\gamma_{concrete}$) is

$$\gamma_{concrete} = 24kN/m^3$$

Modulus of elasticity (E), thickness (d), moment of inertia (I_d), Poisson ratio and unit weight (γ) of the diaphragm wall is presented in Table 3. 4 below.

Table 3. 4 Properties of diaphragm wall used in finite element analyses

Material	**Modulus of Elasticity (E)**	**Thickness (d)**	**Moment of Inertia (I_d)**	**Poisson Ratio (v)**	**Unit Weight (γ)**
Reinforced Concrete	kN/m^2	m	m^4	-	kN/m^3
	30.000.000	1.0	0.08	0.20	24

3.4.3 Properties of Steel Struts

Two level steel supports are used above the excavation level. Lateral spacing of the struts is 5 meters. The inner diameter (D'') and the external diameter (D') of the steel pipe strut is 800 mm and 812 mm respectively. The modulus of elasticity of the steel is

$$E_{steel} = 200,000,000 \text{ kN/m}^2$$

The cross sectional area of the steel pipe is

$$A_{steel} = \pi.\frac{D^2}{4} = \frac{\pi}{4}(D'^2 - D''^2) \quad (7)$$

$$A_{\ steel} = \frac{\pi}{4}(0.812^2 - 0.80^2)$$

$$A_{steel} \cong 0.0152\ m^2$$

Moment of inertia (I) of the steel strut is

$$I_{steel} = \pi.\frac{D^4}{64} = \frac{\pi}{64}(D'^4 - D''^4) \quad (8)$$

$$I_{steel} = \frac{\pi}{64}(0.812^4 - 0.8^4)$$

$$I_{steel} \cong 0.00123m^4$$

Modulus of elasticity (E), Poisson ratio (ν), unit weight (γ) and lateral spacing of the steel strut for the analyses are presented in the Table 3. 5 below.

Table 3. 5 Properties of Steel Strut used in Finite Element Analyses

Material	**Modulus of Elasticity (E)**	**Poisson Ratio (ν)**	**Unit Weight (γ)**	**Lateral Spacing**
Steel	kN/m^2	-	kN/m^3	m
	200,000,000	0.3	78	5

3.4.4 Properties of Jet Struts

The behavior of the soil and soilcrete are modeled with Mohr-Coulomb model. Friction angle (ϕ) and cohesion (c) of soil and soilcrete are required for finite element analysis. To obtain these parameters for soilcretes following equations were employed (Nishimatsu, 1972).

$$c = \frac{q_u q_t}{2[q_t(q_u - 3q_t)]^{0.5}} \quad (9)$$

And

$$tg\phi = \frac{{q_u}^2 - 4{q_u}^2}{4q_u c} \quad (10)$$

Where, c: Cohesion intercept, ϕ : Angle of internal friction, q_u: Unconfined compressive strength, q_t: Brazilian indirect tensile strength

Tensile strength (q_t) was reported between 8 to 14% of unconfined compressive strength for improved soils by deep mixing method (Bruce and Bruce, 2003). For finite element analysis tensile strength is considered as 14% of unconfined compressive strength; because, low values of tensile strength produce very high friction angle which is not reasonable.

Friction angle (ϕ) and cohesion intercept (c) calculated for soilcrete in the clay and in the sand are presented in Table 3.6 and Table 3.7, respectively. The unconfined compressive strength (q_u) values given in Table 3.6 and Table 3.7 are the selected values for parametric analyses. These values are consistent with the ones suggested in the literature.

Modulus of elasticity of soilcrete in clay and in sand is calculated as $100q_u$ and $150q_u$ respectively that are averages values of the given in the literature. The values of modulus of elasticity are also calculated in Table 3. 6 and Table 3. 7.

Table 3. 6 Properties of soilcrete in the clay used in finite element analyses

q_u	**q_t**	**c**	**ϕ**	**E**
kN/m^2	kN/m^2	kN/m^2	degrees	kN/m^2
3000	420	737	38	300000
6000	840	1474	38	600000
9000	1260	2211	38	900000

Table 3. 7 Properties of soilcrete in the sand used in finite element analyses

q_u	**q_t**	**c**	**ϕ**	**E**
kN/m^2	kN/m^2	kN/m^2	degrees	kN/m^2
5000	700	1229	38	750000
10000	1400	2457	38	1500000
15000	2100	3685	38	2250000

Bell (1993) reported expected values of permeability (k) in treated soils as between 10^{-7} and 10^{-10} m/s for sandy, silty and clayey soils. For gravelly soils, permeability of treated soil is between 10^{-7} and 10^{-9} m/s. Permeability of treated soils both the clay and the sand is considered as 10^{-9} m/s in finite element analysis and shown Table 3. 8.

Poisson ratio (ν) of jet grouted soilcrete produced in the clay and in the sand has been selected as 0.25 according to Fang et al. (1994).

Unsaturated and saturated unit weights, Poisson ratio (ν), and coefficient of permeability (k) of the soilcretes are presented in Table 3. 8.

Table 3. 8 Additional properties of soilcrete used in finite element analyses

Material	γ_{unsat}	γ_{sat}	**ν**	**k**
	kN/m^3	kN/m^3	-	m/s
Soilcrete	18	21	0.25	10^{-9}

3.4.5 Hardening-Soil Model Parameters of the Soil and Soilcrete

The Hardening-Soil model is an advanced model for simulating the behavior of different types of soil, both soft soils and stiff soils (Schanz, 1999). Soil displacements may not occur as realistic, both at the ground surface and at the excavation level when Mohr-Coulomb model is used. In some of the analyses magnitude and direction of the soil displacements have been found very different from the expected. For this reason Hardening-Soil model is also used in the analyses to obtain realistic results.

This study is related with an excavation problem. Unloading is the main action. In Hardening-Soil model, E values are taken different in the cases of loading and unloading. The value of E for unloading is $^1/_3$ of the E for loading. Hence, wall deformations and moments, ground surface displacements can be more realisticly obtained.

The values of the basic parameters of the Hardening-Soil model for the soil stiffness are presented in Table 3. 9 below. Failure parameters (c, ϕ) are assumed as

in Mohr-Coulomb model. Advanced parameters of the Hardening-Soil model have been used as the default values.

Table 3. 9 Hardening-Soil model properties of soils used in finite element analyses

Modulus of Elasticity	**Sand**	**Clay**	**Soilcrete**					
			in the clay (UCS, MPa)			**in the sand (UCS, MPa)**		
			3	**6**	**9**	**5**	**10**	**15**
E_{50}^{ref} (kN/m^2)	25000	12500	300000	600000	900000	750000	1500000	2250000
E_{od}^{ref} (kN/m^2)	25000	12500	300000	600000	900000	750000	1500000	2250000
E_{ur}^{ref} (kN/m^2)	75000	37500	900000	1800000	2700000	2250000	4500000	6750000

Where; E_{50}^{ref} : Secant stiffness in Standard drained triaxial test, E_{ur}^{ref} : Tangent stiffness for primary oedometer loading ($E_{ur}^{ref} = 3\,E_{50}^{ref}$), E_{od}^{ref} : Unloading / reloading stiffness.

CHAPTER FOUR

FINITE ELEMENT ANALYSES

4.1 General

Purpose of the finite element analyses is to investigate the contribution of jet grout strutting on the stability of deep retaining systems. The required parameters of the materials used in the finite element analyses and excavation stages of the problem have been explained in the previous chapter. The finite element analyses have been performed using Plaxis 2D and Plaxis 3D for the jet grout strutting in the sand and in the clay, respectively.

The detailed cross-sections of the problem both for the case of sand and the clay soils will be explained in this chapter. Analyses combinations have been formed according to the stiffness, location and thickness of the soilcretes. Soilcrete plan patterns and treated soil area ratios are additional parameters for analyses combinations in the clay.

Analyses have been performed basically using Mohr-Coulomb model both for the sand and the clay profiles. Finite element analyses with Hardening-Soil model have also been performed for representative cases and obtained results have been compared with the solutions of Mohr-Coulomb model.

Moments and lateral displacements curves of the diaphragm wall have been presented comparatively with respect to due to analyses combinations. Vertical soil displacement curves at the excavation level and at the ground surface have been plotted according to the analyses combinations and presented condensly in this chapter. The detailed displacements and moments curves were presented in the sections of Appendices for the sand and the clay profiles.

4.2 Alternative Cross Sections

Jet struts have been located at four different depth intervals. The first interval is between 10.0 m – 20.0 m below the ground surface. Hence, the thickness of the jet

struts is 10 meters. This configuration of jet strutting is named as Location I (Figure 4.1). The other configurations are called as Location II, Location III and Location IV. Thicknesses of jet struts in all these alternatives are equal to 3 meters. Depth intervals of jet grouting struts in Location II, Location III and Location IV are 10.0 m – 13.0 m, 13.5 – 16.5 m and 17.0 m – 20.0 m, respectively. Cross sections of last three alternatives are given in Figures 4.2, 4.3 and 4.4, respectively. Soil profile is completely composed of either sand or clay. Water level is at 2 m below the ground surface. The length of the diaphragm wall is 20 m. Excavation level is at 10 m depth and the span of the excavation is 10 m. Steel struts are at 1 m and 5 m depths below the ground surface and lateral spacings of the supports are 5 m.

4.3 Two Dimensional Finite Elements Analyses for the Sand Profile

4.3.1 Analyses Combinations for the Sand Profile

Jet grouting process has been assumed to be composed of overlapped soilcrete columns in the sand profile. The values of the finite element parameters have been explained in the previous chapter. Analyses combinations are presented in Table 4.1.

Table 4.1 Analyses combinations for the sand profile.

Analyses No	Jet Grouting Strut Layer				Soil Model
	Location Type	UCS (MPa)	Thickness (m)	Depth Intervals (m)	
1	No Jet Gouting Strut	-	-	0 - 20	MC
2		-			HS
3	I	5	10	10.0 – 20.0	MC
4		5			HS
5		10			MC
6		15			MC
7	II	5	3	10.0 – 13.0	MC
8		5			HS
9		10			MC
10		15			MC
11	III	5	3	13.5 – 16.5	MC
12		5			HS
13		10			MC
14		15			MC
15	IV	5	3	17.0 – 20.0	MC
16		5			HS
17		10			MC
18		15			MC

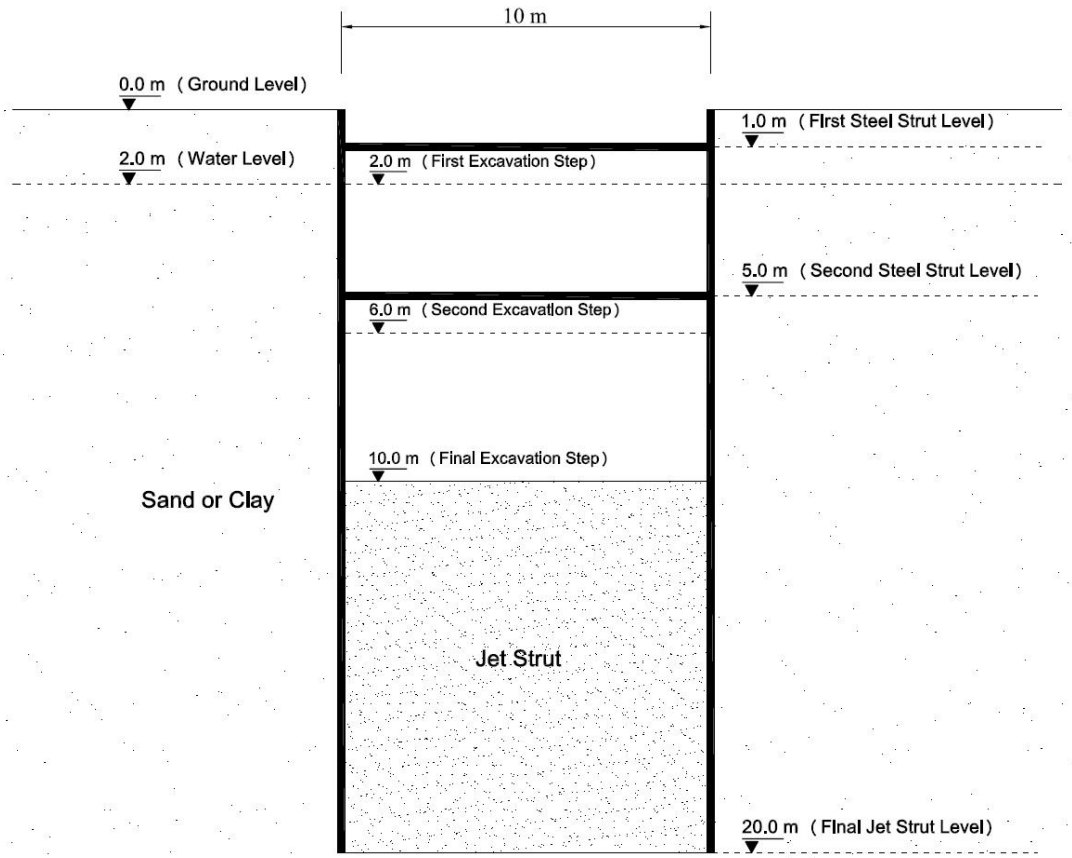

Figure 4.1 Jet Grouting Strut Location I: Jet struts between 10 m and 20 m

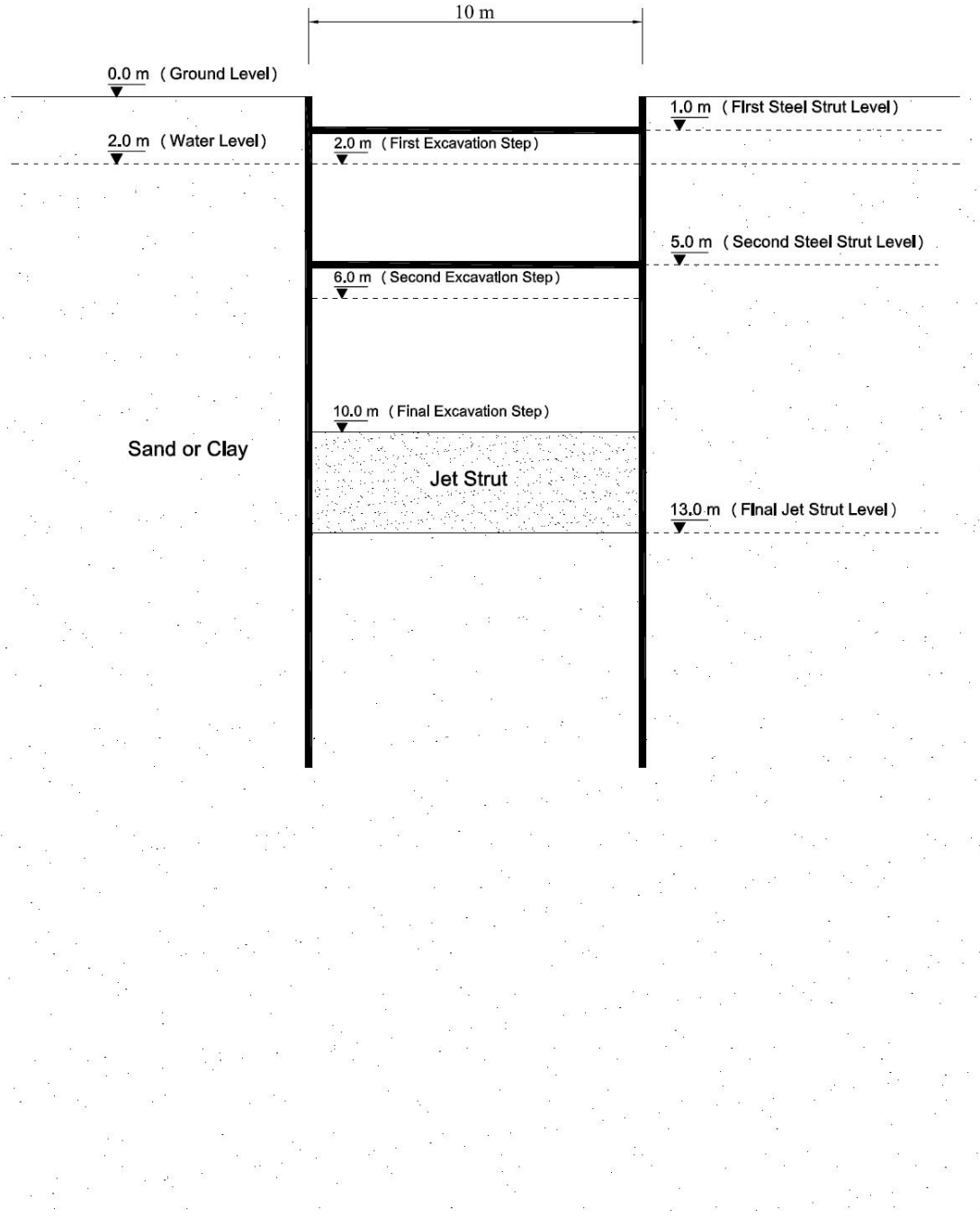

Figure 4.2 Jet Grouting Strut Location II: Jet struts between 10.0 m and 13.0 m

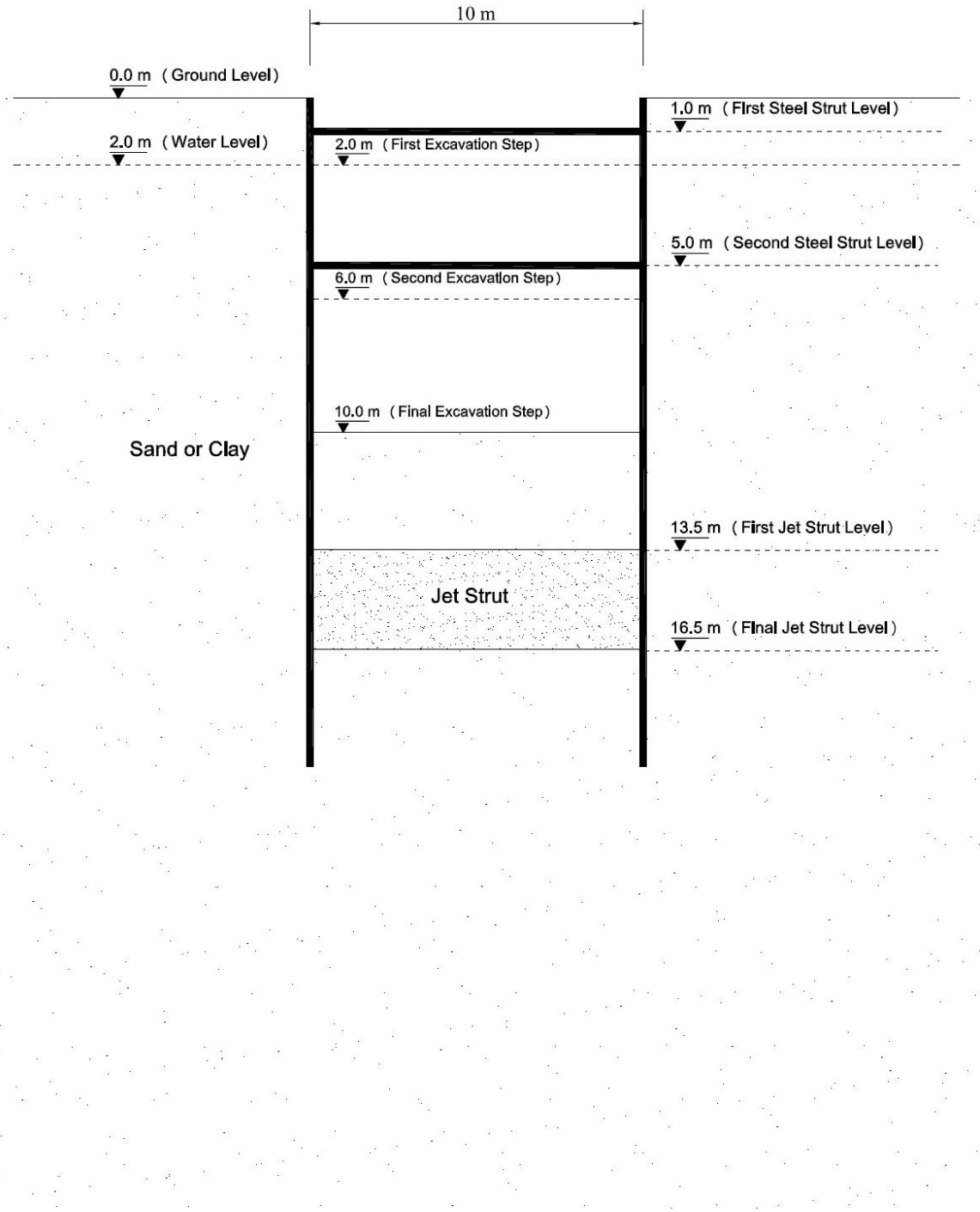

Figure 4.3 Jet Grouting Strut Location III: Jet struts between 13.5 m and 16.5 m

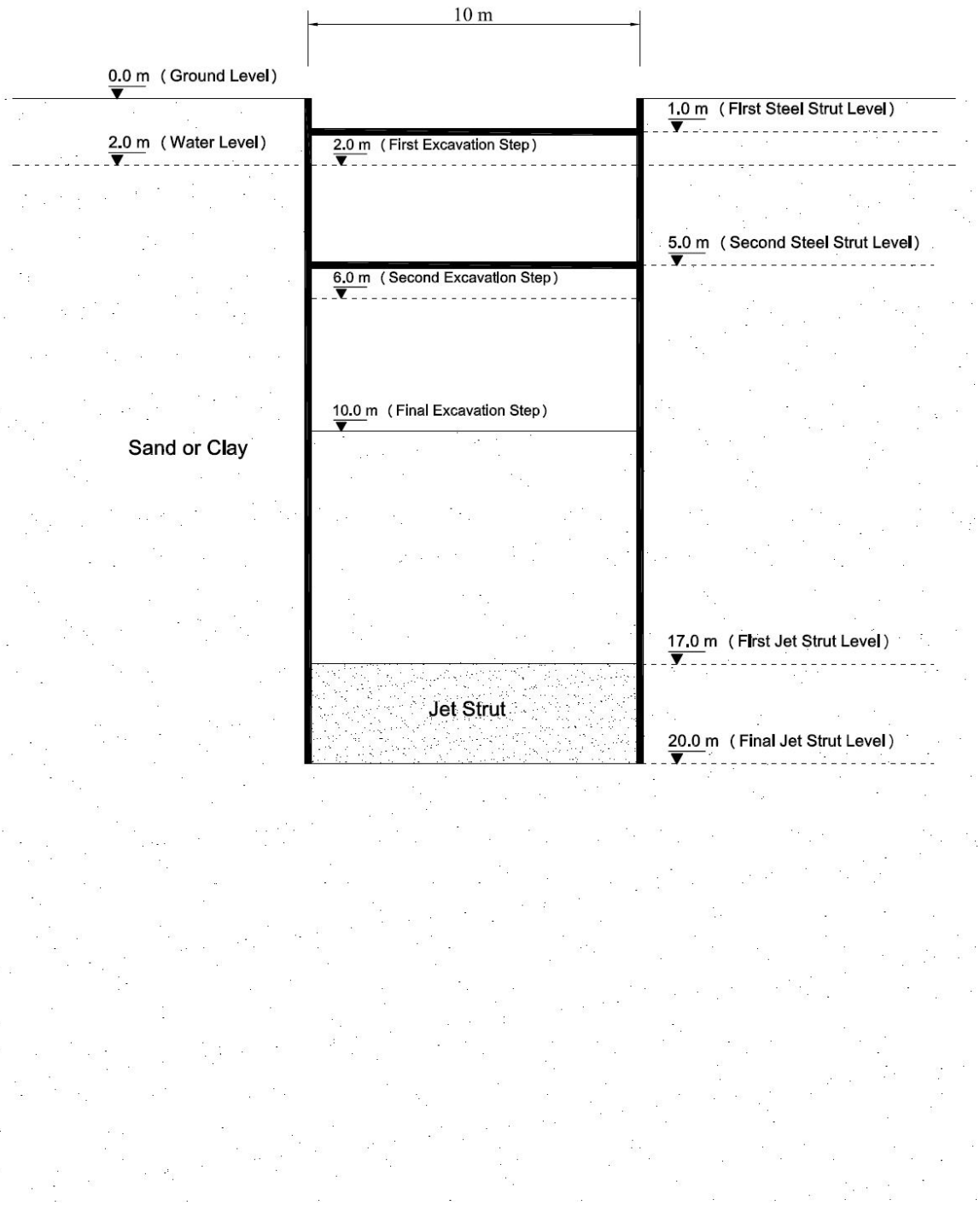

Figure 4.4 Jet Grouting Strut Location IV: Jet struts between 17 m and 20 m

Finite element analyses have been performed according to the combinations of location and soilcrete stiffness for the sand. Since the problem is symmetric, only one half (the left side) of cross section is considered in the analyses. Deformed mesh of the sandy profile with no jet grouting strut is shown in Fig. 4.5 in order to present the modeling of the problem in the Plaxis 2D.

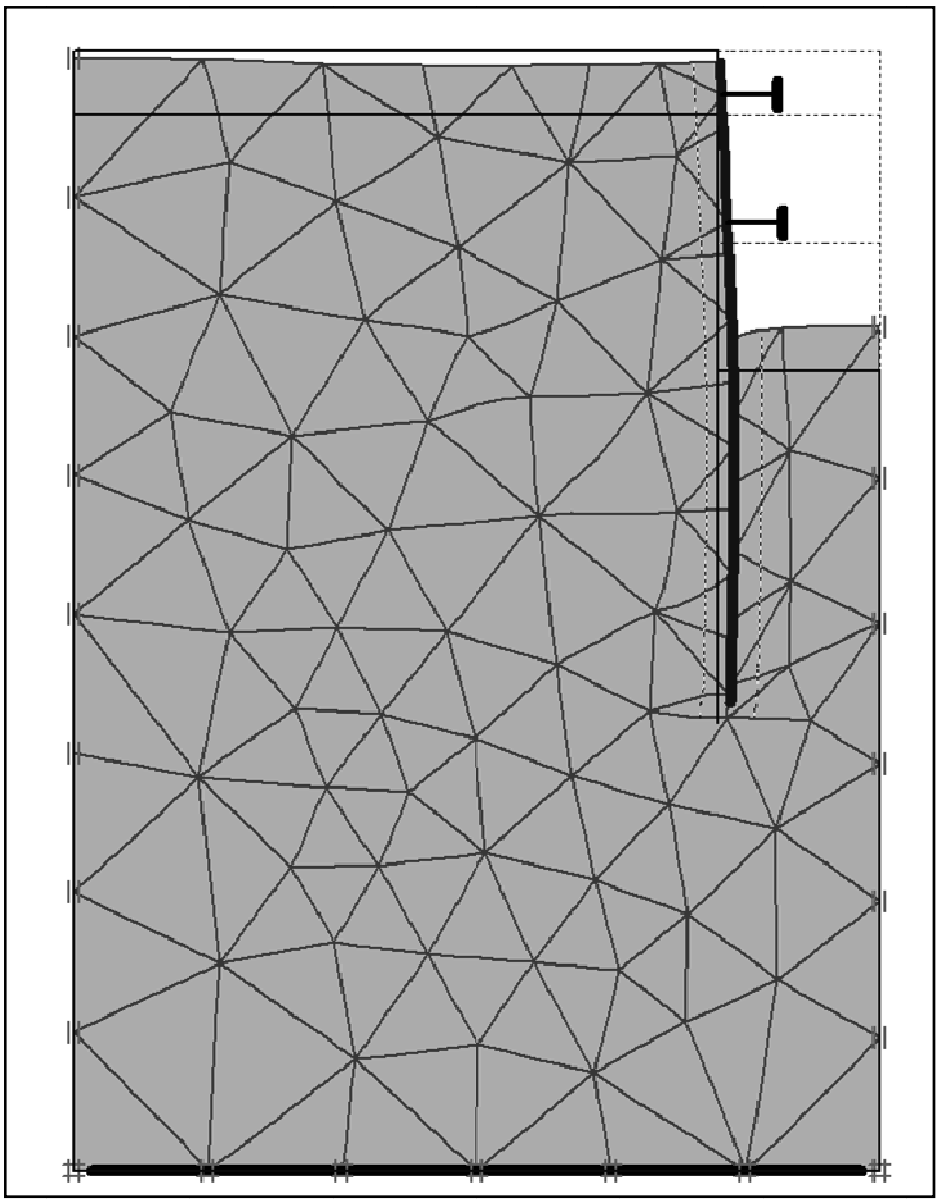

Figure 4.5 Deformed mesh of the problem for the sand profile.

4.3.2 Results and Discussions of Finite Element Analyses for the Sand Profile

Totally 18 different 2D finite element analyses have been performed for the sand profile. Finite element analyses without jet strutting have been performed initially using Mohr-Coulomb and Hardening-Soil models as base analysis.

Then finite element analyses for 4 different locations of jet grout strut layer have been performed. For each location 3 different analyses have been done for different soilcrete stiffnesses (5, 10, 15 MPa). In these analyses, Mohr-Coulomb (MC) model has been adopted. The results of these analyses showed no significant difference according to soilcrete stiffness increment. Therefore, hardening-Soil (HS) model analyses have been performed for only UCS=5 MPa.

Results of finite element analyses have been presented in Table 4.2. Diaphragm wall lateral displacements and moments, vertical ground displacements on the excavation level and behind the diaphragm wall have been given in this table.

Comparative diagrams of depth versus displacement, depth versus moment, and distance versus vertical ground displacements on the excavation level and behind the diaphragm wall have been generated. The detailed curves have been given according to Mohr-Coulomb model in the Appendix A.

Diaphragm wall lateral displacements for three different soilcrete stiffnesses for jet strut Location I have been presented comparatively in Fig 4.6.

The maximum displacement occurs at the middle part of the wall without jet grout strutting. The displacements decrease towards both top and tip of the wall.

All jet strutting cases reduce the wall displacements practically. Jet strutting between 10 m – 20 m depths reduces the wall displacements practically to zero within this depth interval. On the other hand, diaphragm wall top displacements are slightly more than the displacements obtained in the case of without jet strutting. It is clear that increase of soilcrete stiffness has no significant affect on the wall displacements (Fig. 4.6)

Table 4.2 Finite Element Analyses Results for Sand Profile

Analysis No	Jet Grout Strut Layer				Soil Model	Diaphragm Wall Displacements&Moments							Ground Displacements (δ)						
						Displacements (δ)					Max. Moments		On the Excavation Level			Behind the Diaphragm Wall			
						Depths (m)			Max. Disp.				Distance (m)			Distance (m)		Max. Disp.	
	Location Type	UCS (MPa)	Thickness (m)	Depth Interval		0	10	20	(δ_{max}) (mm)	Depth (m)	M_{max} (kNm/m)	Depth (m)	0	2.5	5.0	0	20	(δ_{max}) (mm)	Depth (m)
1	No Jet Strut	-	10	-	MC	3.2	17.9	15.7	18.5	12.5	800.9	9.5	-0.6	49.4	48.3	-0.9	-9.1	-9.1	20
2		-			HS	3.2	15.7	4.9	15.7	10.0	1051.4	10.0	0.1	16.5	18.4	-18.1	-16.1	-24.5	7.0
3	I	5	10	10m-20m	MC	6.1	2.2	-0.4	6.1	0.0	428.4	11.0	-0.6	1.9	2.3	-1.3	-2.0	-2.0	20
4		5			HS	5.3	2.7	-0.6	5.8	3.5	469.2	5.2	-8.9	-8.7	-8.7	-12.4	-7.1	-12.4	20
5		10			MC	6.1	1.5	-0.9	6.1	0.0	501.6	10.5	-0.5	1.4	1.7	-1.4	-1.9	-1.9	20
6		15			MC	6.1	1.2	-1.1	6.1	0.0	556.7	10.5	-0.5	1.3	1.6	-0.2	-1.8	-1.8	20
7	II	5	3	10m-13m	MC	5.5	1.9	10.4	10.4	20.0	982.5	10.8	3.6	9.3	10.9	0.0	-3.2	-3.2	20
8		5			HS	3.7	2.4	4.3	4.3	20.0	546.6	10.8	-3.1	-0.7	0.2	-11.1	-8.5	-11.3	2.0
9		10			MC	5.6	0.9	9.9	9.9	20.0	1038.7	10.8	3.8	8.0	9.1	0.0	-2.8	-2.8	20
10		15			MC	5.6	0.5	9.6	9.6	20.0	1038.4	10.8	3.8	7.5	8.5	0.0	-2.7	-2.7	20
11	III	5	3	13.5m-16.5m	MC	5.3	6.4	3.6	8.3	6.5	745.1	8.0	1.5	19.8	20.3	0.0	-2.8	-2.8	20
12		5			HS	4.5	7.1	1.3	8.6	7.0	827.2	8.0	1.0	4.5	4.0	-11.4	-8.3	-13.5	4.5
13		10			MC	5.5	5.5	2.6	7.8	6.0	741.0	8.0	1.6	18.5	18.9	0.0	-2.4	-2.4	20
14		15			MC	5.5	5.1	2.3	7.6	6.0	739.0	7.5	1.7	18.1	18.4	0.0	-2.2	-2.2	20
15	IV	5	3	17m-20m	MC	4.4	14.0	-1.7	14.2	9.5	1133.7	9.5	-0.2	32.1	31.5	0.0	-4.5	-4.5	20
16		5			HS	3.7	13.1	-1.4	13.4	9.0	1153.0	9.5	1.0	12.3	14.1	-12.9	-10.4	-17.8	5.5
17		10			MC	4.5	13.3	-2.7	13.7	8.5	1141.6	9.5	-0.1	31.1	30.5	0.0	-4.1	-4.1	20
18		15			MC	4.6	13.0	-3.2	13.4	8.5	1141.9	9.5	-0.1	30.7	30.1	0.0	-3.9	-3.9	20

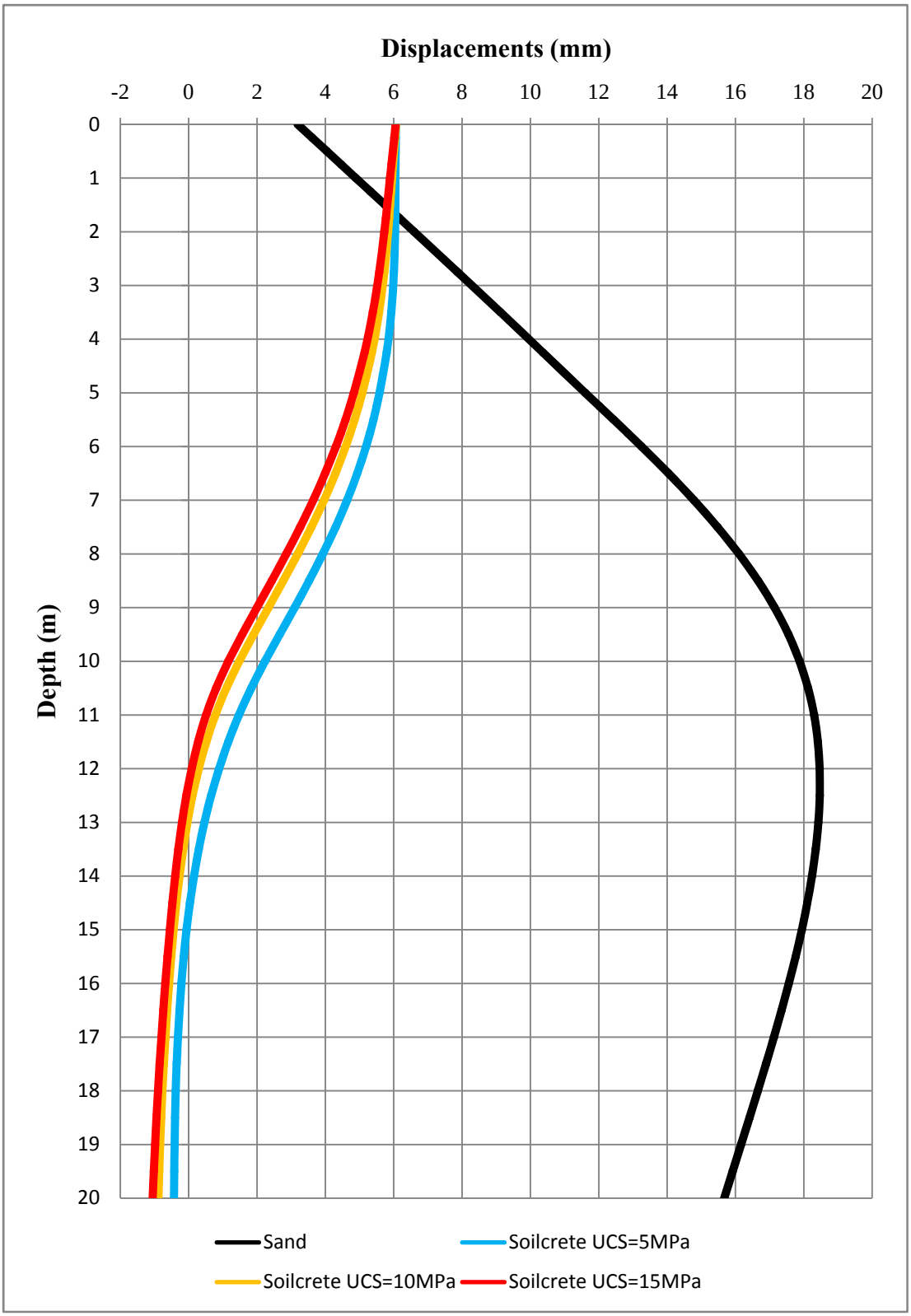

Figure 4.6 Diaphragm wall displacements according to UCS for location I, sand profile

The displacements have been compared according to jet strut location types for both Mohr-Coulomb and Hardening-Soil models in Fig. 4.7. For all locations of jet grout struts, the minimum diaphragm wall displacements occurred at the jet strutting application depth intervals. The displacements tend to increase outside of these areas. The top displacement values of the diaphragm wall are in a narrow range. Generally, minimum displacements have been observed in jet grout strut application of location I (JGSLI) and location II (JGSLII). Their displacements are closer above the excavation level. But below the excavation level, JGSLI has lower displacements than JGSLII. Displacements of JGSLII and JGSLIII are closer relatively close to each other below the excavation level. But above the excavation level, JGSLIII has higher displacement value of displacements than JGSLII. Displacements obtained with MC and HS models are generally in agreement with each other. But for the case of non jet grout strutting. MC and HS displacements are significantly different especially at the bottom of the wall.

Diaphragm wall moments with respect to soilcrete stiffnesses have been given in Fig 4.8. In Fig. 4.9, moments have been presented comparatively according to location types of jet struts for both MC and HS models.

Practically, all jet strutting cases reduce the wall moments. Maximum moment is the highest in JSGLIV. Increment of the soilcrete stiffness has no significant affect on the moments. The lowest value of the maximum moment has been observed in JGSLI. JGSLII and Non JGS application have higher maximum moment value than JGSLI but, the moments get closer with HS model. The worst moments have been observed in JGSLIV and non jet grout strut application cases.

The vertical displacements on the excavation level according to soilcrete stiffnesses have been presented in Fig. 4.10. Comparative distance versus vertical displacements curves have been given in Fig. 4.11 for both MC and HS models.

Rise of ground surface (heave) have been observed at the excavation level in all cases. The vertical displacement values have been reduced in jet strutting cases. Increase of soilcrete stiffnesses did not cause any significant difference in vertical displacements at the excavation level.

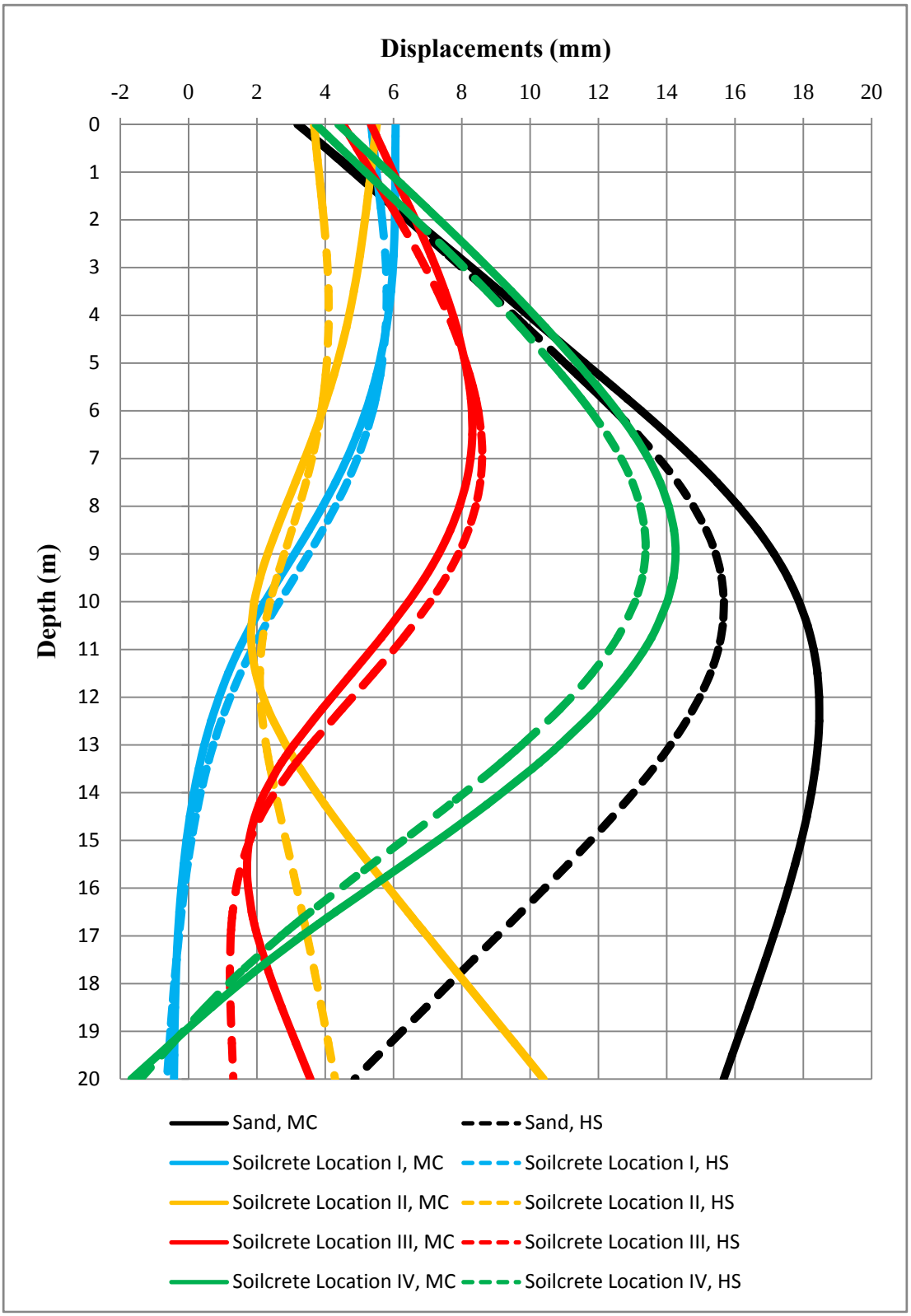

Figure 4.7 Diaphragm wall displacements according to location types for UCS=5 MPa with MC and HS models, sand profile

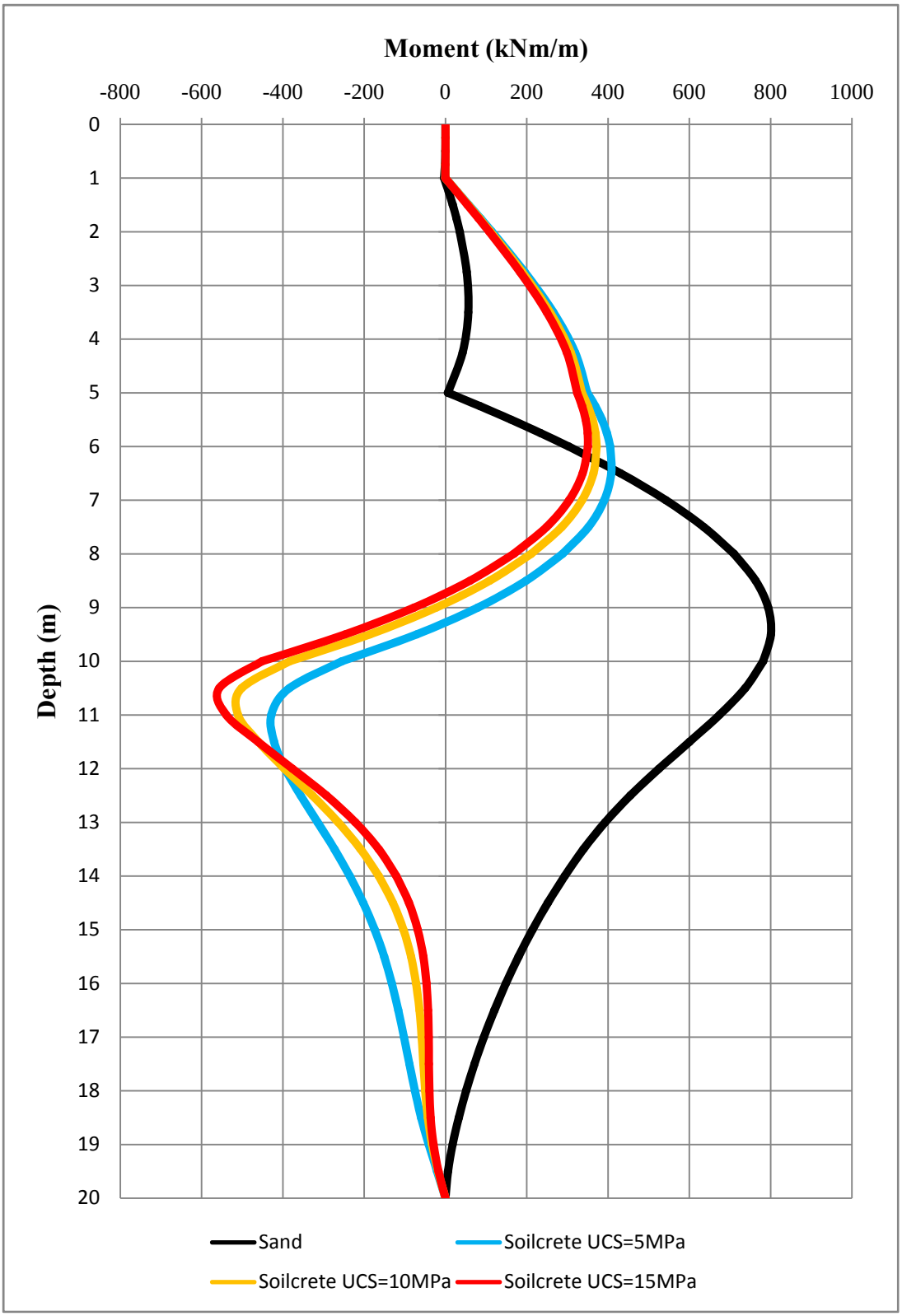

Figure 4.8 Diaphragm wall moments according to UCS for location I, sand profile

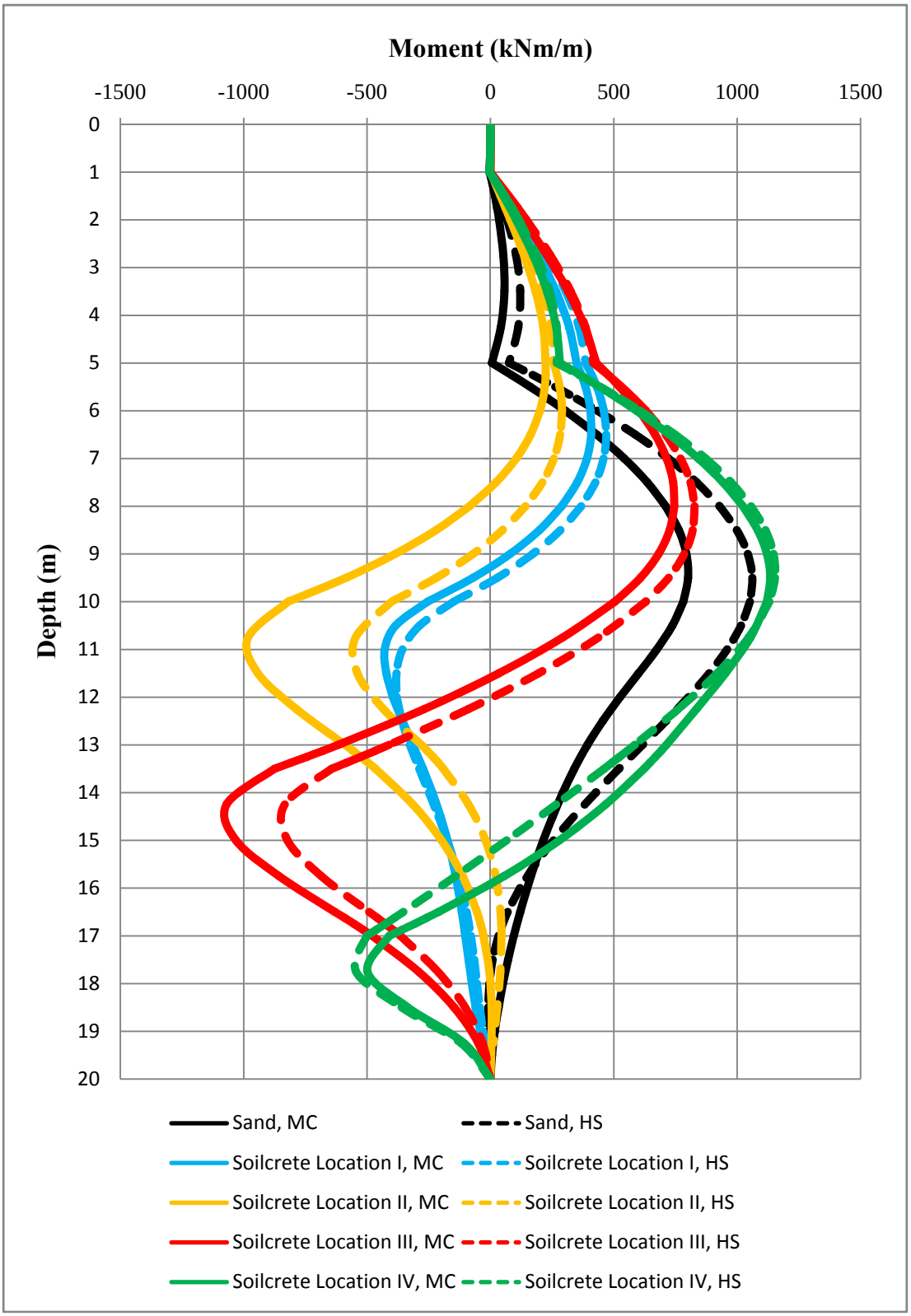

Figure 4.9 Diaphragm wall moments according to location types for UCS=5 MPa with MC and HS models, sand profile

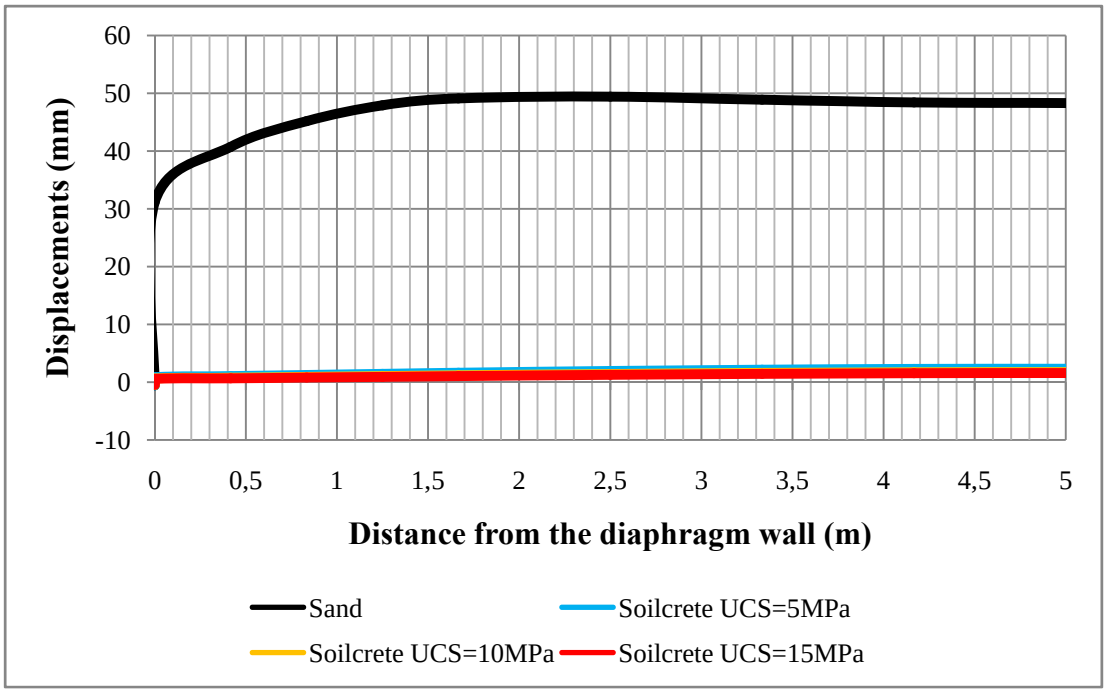

Figure 4.10 Vertical Displacements on the excavation level according to UCS for location I, sand profile

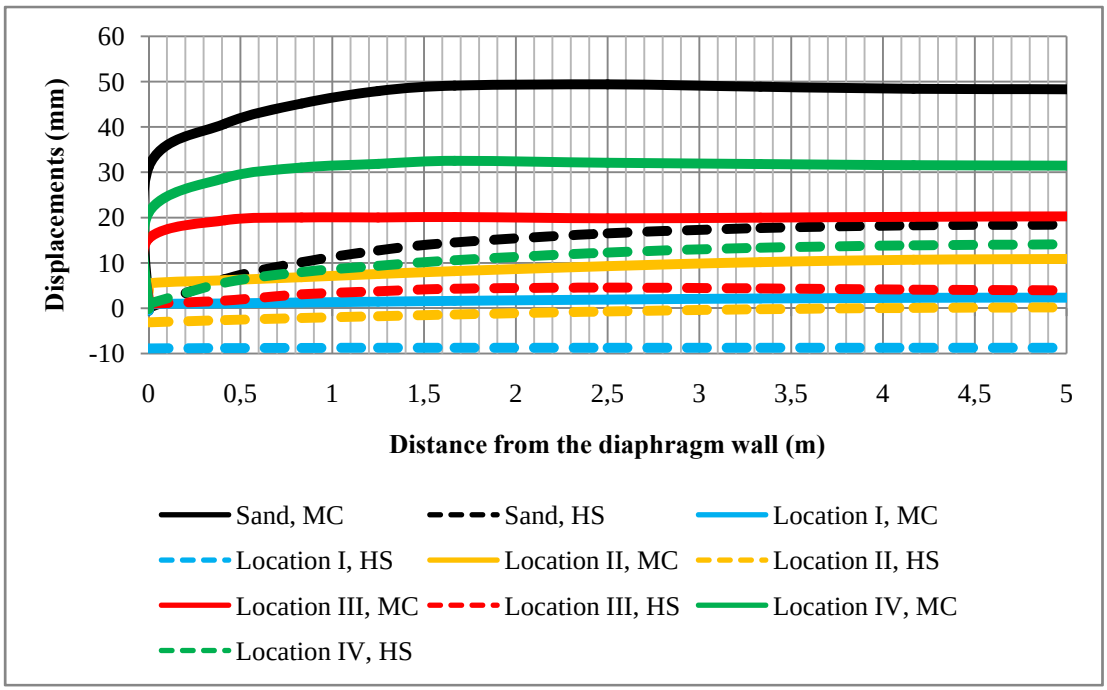

Figure 4.11 Vertical displacements on the excavation level according to locations types for UCS=5 MPa with MC and HS models, sand profile

Value of heave from highest to lowest is obtained in succession of non jet grout strut application, JGSLIV, JGSLIII, JGSLII and JGSLI, respectively. This sorting is the same according to Hardening-Soil model. But the displacement results are lower than Mohr-Coulomb model.

Comparative distance versus vertical displacement curves have been given in Fig. 4.12 for both Mohr-Coulomb and Hardening-Soil models

Increment of soilcrete stiffness did not cause any significant difference on the vertical displacements. The vertical displacement values are almost same for JGSLI, JGSLII and JGSLIII which have minimum displacements. JGSLIV has higher displacements than JGSLI, JGSLII and JGSLIII. Non jet grout strut application is the worst. Hardening-Soil model has the same trend but the displacement values are higher than Mohr-Coulomb model.

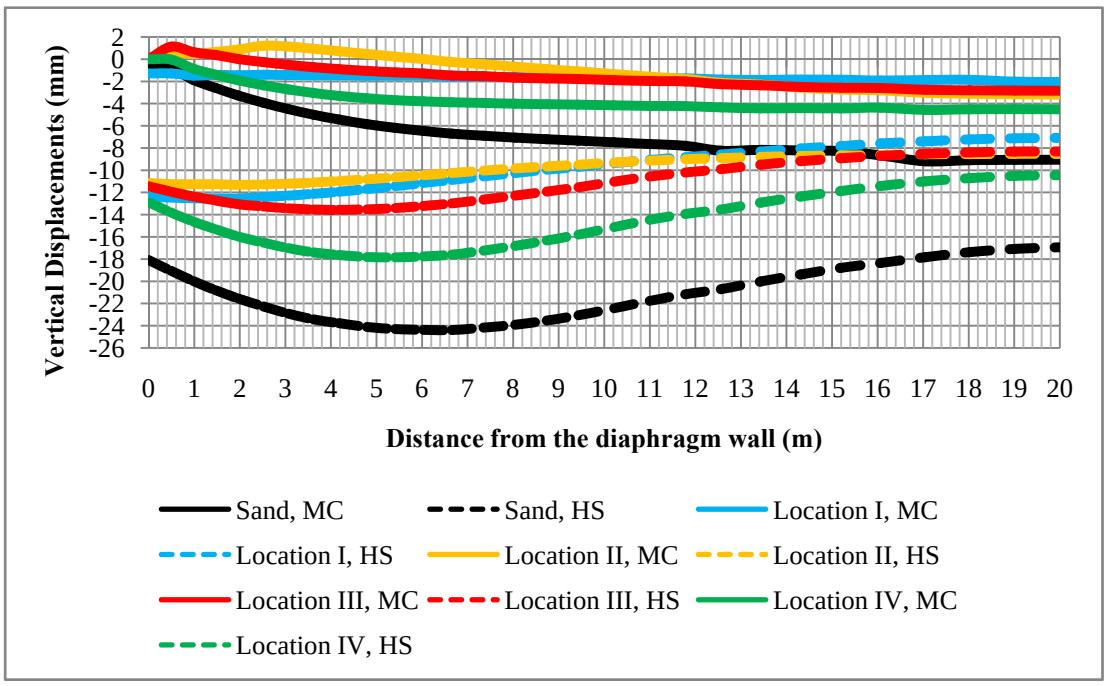

Figure 4.12 Vertical displacements behind the diaphragm wall according to locations types for UCS=5 MPa with MC and HS models, sand profile

4.4 Three Dimensional Finite Element Analyses on the Clay Profile

4.4.1 Analyses Combinations for Clay Profile

The finite element analyses have also been performed for the clay profile using Plaxis-3D. Four types of patterns have been used in these analyses. Pattern types are given in the previous chapter.

It is assumed that the clay is impervious and full treatment with jet grouting is not required. The treated soil area ratios (I_r) are used as %0, %20, %40, %60, %80 and 100% for the all patterns types. There different soilcrete stiffness values (3 MPa, 6 MPa and 9 MPa) are considered.

The location types have been considered for completely overlapping jet grouting in the finite element analyses. So, analyses of completely overlapping jet grouting for the clay soil profile have been performed using Plaxis 2D.

The analyses combinations used in the finite element analyses have been presented in Table 4.3. Location types, pattern types, treated soil area ratios, soilcrete stiffnesses, thicknesses of the layers, depths of the layers and soil models are given in the table.

The schematic plan view of the problem has been presented in the Fig. 4.13. The displacements and moments will be given on the Axis 1. The problem is symmetric, only one half (the left side) is considered in the analyses. Deformed mesh of the clay soil profile is shown in Fig. 4.14.

Table 4.3. Analyses combinations for the clay profile.

No	Location Type	Pattern Type	(Ir) (%)	UCS (MPa)	H_{Layer} (m)	Depth (m)	Soil Model
1	No Jet Strut	-	0	-	-	0-20	MC
2							HS
3	I	-	100	3	10	10-20	MC
4							HS
5				6			MC
6				9			MC
7		I	20	3			MC
8			40				MC
9							HS
10			60				MC
11			80				MC
12		II	20				MC
13			40				MC
14							HS
15			60				MC
16			80				MC
17		III	20				MC
18			40				MC
19							HS
20			60				MC
21			80				MC
22		IV	20				MC
23			40				MC
24							HS
25			60				MC
26			80				MC
27	II	-	100		3	10-13	MC
28							HS
29	III					13.5-16.5	MC
30							HS
31	IV					17-20	MC
32							HS

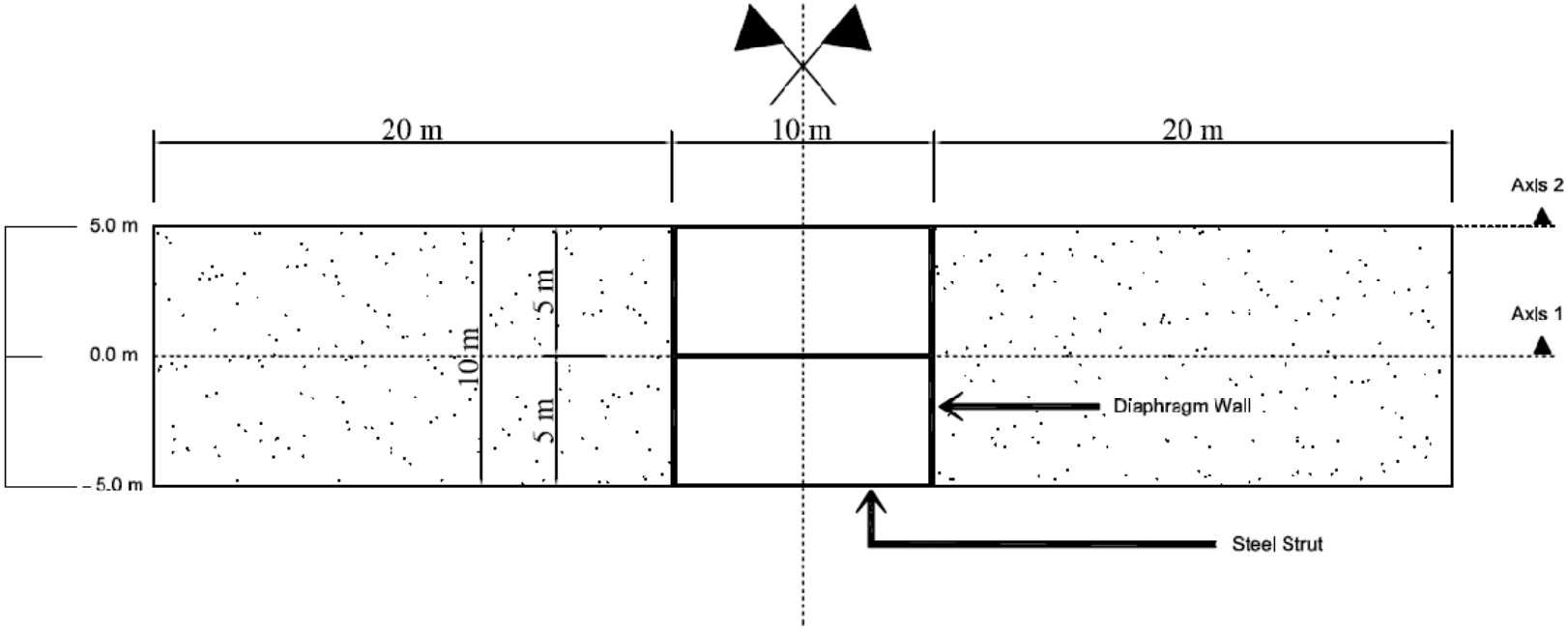

Figure 4.13 Plan view of the problem.

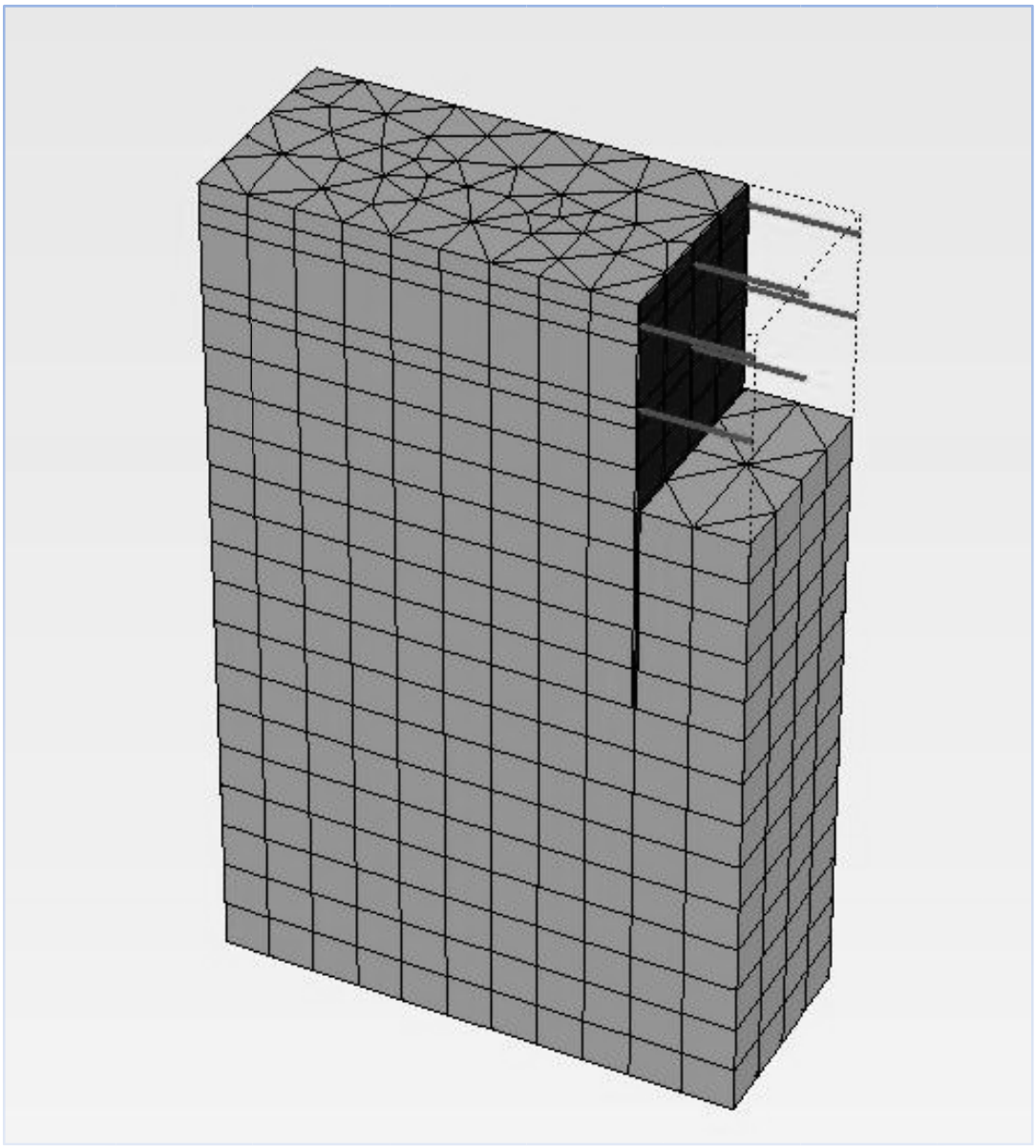

Figure 4.14 Three dimensional view of the problem.

4.4.2 Finite Element Analyses Results for the Clay Profile

Finite element analyses results for clay profile have been presented in Table 4.4 and Table 4.5. Diaphragm wall lateral displacements and moments are given in the Table 4.4. Vertical ground displacements on the excavation level and behind the diaphragm wall on the ground surface have been given in the Table 4.5.

Comparative depth versus displacement, depth versus moment and distance versus vertical displacement on the excavation level and behind the diaphragm wall curves has been generated. Detailed diagrams according to Mohr-Coulomb model have been given in the Appendix B. 2D Plaxis analyses diagrams have been given in the Appendix C.

Diaphragm wall lateral displacements for three different soilcrete stiffnesses for JGSLI have been presented comparatively in Fig 4.15. The displacements have been compared according to treated soil area ratios (I_r) for pattern I and UCS=3 MPa in Fig. 4.16. The displacements have also been compared according to pattern types and location types with Mohr-Coulomb and Hardening-Soil models in the Fig. 4.17 and Fig. 4.18, respectively.

Increment of soilcrete stiffnesses did not cause any significant differences on the displacements. On the other hand, increase of treated soil area ratio decrease the lateral displacements of the diaphragm wall.

The displacements have been recorded from worst to best as non JGS application, JGS Pattern III (JGSPIII), JGSPIV, JGSPII and JGSPI, respectively. For soilcrete location types, the displacements have been recorded from worst to best as non JGS application, JGSLIV, JGSLIII, JGSLII and JGSLI, respectively. For the Hardening-Soil model above mentioned displacement behavior are the same but the displacement values are lower than the Mohr-Coulomb model.

Table 4.4 Diaphragm Wall Displacements and Moments for Clay Profile

Anaylses No	Jet Grouting Layer					Soil Model	Diaphragm Wall						
							Displacements					Moments (kNm/m)	
	Location Type	Pattern Type	(Ir) (%)	UCS (MPa)	Thickness (m)		0 m	10 m	20m	(δ_{max}) (mm)		(M_{max})	Depth (m)
										δ_{max}	Depth (m)		
1	-	-	0	-	-	MC	5.9	36.6	32.5	40.1	13.8	1564	12.5
2						HS	4.1	32.7	-0.6	34.9	12.5	1761	12.5
3	I	-	100	3	10	MC	10.0	4.2	-1.6	10.0	0.0	430	6.0
4						HS	8.0	4.9	-1.6	8.5	3.5	535	8.0
5				6		MC	9.7	2.9	-2.0	9.7	0.0	420	12.5
6				9		MC	9.6	2.3	-2.1	9.6	0.0	420	10.0
7		I	20	3		MC	9.3	10.8	3.0	12.1	7.0	692	8.0
8			40			MC	9.6	7.3	0.2	10.1	5.5	565	8.0
9						HS	7.6	8.8	-1.5	10.7	6.0	844	8.0
10			60			MC	9.8	5.7	-0.8	9.8	0.0	487	6.0
11			80			MC	9.8	4.8	-1.5	9.8	0.0	459	6.0
12		II	20			MC	9.0	13.8	5.7	14.3	8.0	722	8.0
13			40			MC	9.5	8.9	1.3	10.9	6.0	587	8.0
14						HS	7.4	10.2	-0.6	11.5	7.0	845	8.0
15			60			MC	9.8	6.2	-0.6	9.9	3.5	483	8.0
16			80			MC	9.8	4.8	-1.4	9.8	0.0	452	6.0
17		III	20			MC	6.9	28.4	22.4	29.7	12.5	1251	10.0
18			40			MC	7.5	23.5	16.0	24.0	11.3	1057	10.0
19						HS	6.0	18.9	3.5	18.9	10.0	1273	10.0
20			60			MC	8.5	17.6	7.8	17.6	10.0	811	10.0
21			80			MC	9.3	11.0	0.9	11.9	9.0	628	8.0
22		IV	20			MC	9.0	15.3	6.6	15.5	9.0	747	8.0
23			40			MC	9.6	9.8	1.4	11.5	6.0	631	8.0
24						HS	7.4	12.1	-0.7	13.0	8.0	939	8.0
25			60			MC	9.9	6.6	-0.6	10.2	3.5	544	8.0
26*	II	-	100		3	MC	9.8	5.3	18.6	18.6	20.0	1222	10.8
27*						HS	9.0	6.6	6.4	9.2	3.5	555.7	11.5
28*	III					MC	10.5	11.4	6.2	13.6	6.0	1128	14.3
29*						HS	9.0	11.8	2.1	13.6	7.0	991	8.5
30*	IV					MC	9.1	23.3	-1.4	23.5	9.0	1606	10.0
31*						HS	7.8	20.5	-2.2	20.6	9.0	1552	10.0

*Plaxis 2D Anayses

Table 4.5. Ground Displacements for clay profile.

Analyses No	Jet Grouting Strut Layer					Soil Model	Ground Displacements (δ) (mm)						
							On the Excavation Level			Behind the Diaphragm Wall			
												δ_{max}	
	Location Type	Pattern Type	(Ir) (%)	UCS (MPa)	Thickness (m)		0.0 (m)	2.5 (m)	5.0 (m)	0.0 (m)	20.0 (m)	(δ_{max})	Depth (m)
1	-					MC	178.0	215.3	213.5	9.5	-12.3	-12.3	20
2						HS	80.1	125.1	127.1	-27.8	-31.5	-40	7.0
3	I	-	100	3	10	MC	40.7	43.2	43.9	18.2	9.6	21.7	3.5
4						HS	-4.8	-4.2	-4.7	-12.4	-11.1	-12.4	0.0
5				6		MC	40.1	41.6	42.1	18.4	10.0	22.2	3.5
6				9		MC	40.0	41.1	41.6	18.4	10.1	22.3	3.5
7		I	20	3		MC	40.2	53.9	59.0	19.1	5.9	19.1	0.0
8			40			MC	40.3	45.2	47.2	19.2	8.0	20.2	2.4
9						HS	-5.0	-0.1	1.0	-12.7	-11.1	-13.6	2.4
10			60			MC	41.1	44.5	45.7	19.5	9.0	21.5	3.0
11			80			MC	40.9	43.8	44.7	19.4	9.4	22.1	3.5
12		II	20			MC	40.0	63.4	72.4	19.2	4.9	19.2	0.0
13			40			MC	40.5	47.8	54.6	18.4	7.5	20.3	3.5
14						HS	-5.0	2.3	9.2	-12.2	-11.4	-14.4	7.0
15			60			MC	41.0	44.2	45.9	18.6	8.8	21.2	3.5
16			80			MC	41.2	43.8	44.8	18.4	9.3	21.6	3.5
17		III	20			MC	35.9	159.1	163.0	19.9	-2.9	19.9	0.0
18			40			MC	40.0	101.2	155.6	21.3	0.7	21.3	0.0
19						HS	-6.3	35.6	71.5	-11.7	-13.5	-19.2	7.0
20			60			MC	40.8	58.0	127.7	21.1	4.2	21.1	0.0
21			80			MC	41.1	51.0	87.3	20.0	7.3	20.7	3.5
22		IV	20			MC	41.0	109.0	97.6	20.0	4.7	20.0	0.0
23			40			MC	42.2	80.9	71.1	20.1	7.2	20.1	0.0
24						HS	-5.7	34.1	21.1	-12.6	-11.6	-13.6	10.0
25			60			MC	41.1	57.9	59.5	20.5	8.6	20.5	0.0
26*	II	-	100		3	MC	-13.1	0.6	4.3	-27.8	-38.4	-38.4	20.0
27*						HS	-38.2	-33.7	-32.3	-45.9	-46.2	-46.6	4.2
28*	III					MC	11.8	18.8	19.9	-28.1	-37.8	-37.8	20.0
29*						HS	-26.5	-15.4	-17.1	-46.1	-45.3	-49.6	5.4
30*	IV					MC	27.8	41.4	40.6	-26.4	-41.1	-41.1	20.0
31*						HS	-21.4	-2.6	-0.4	-46.8	-47.3	-54.8	6.0

*Plaxis 2D Anayses

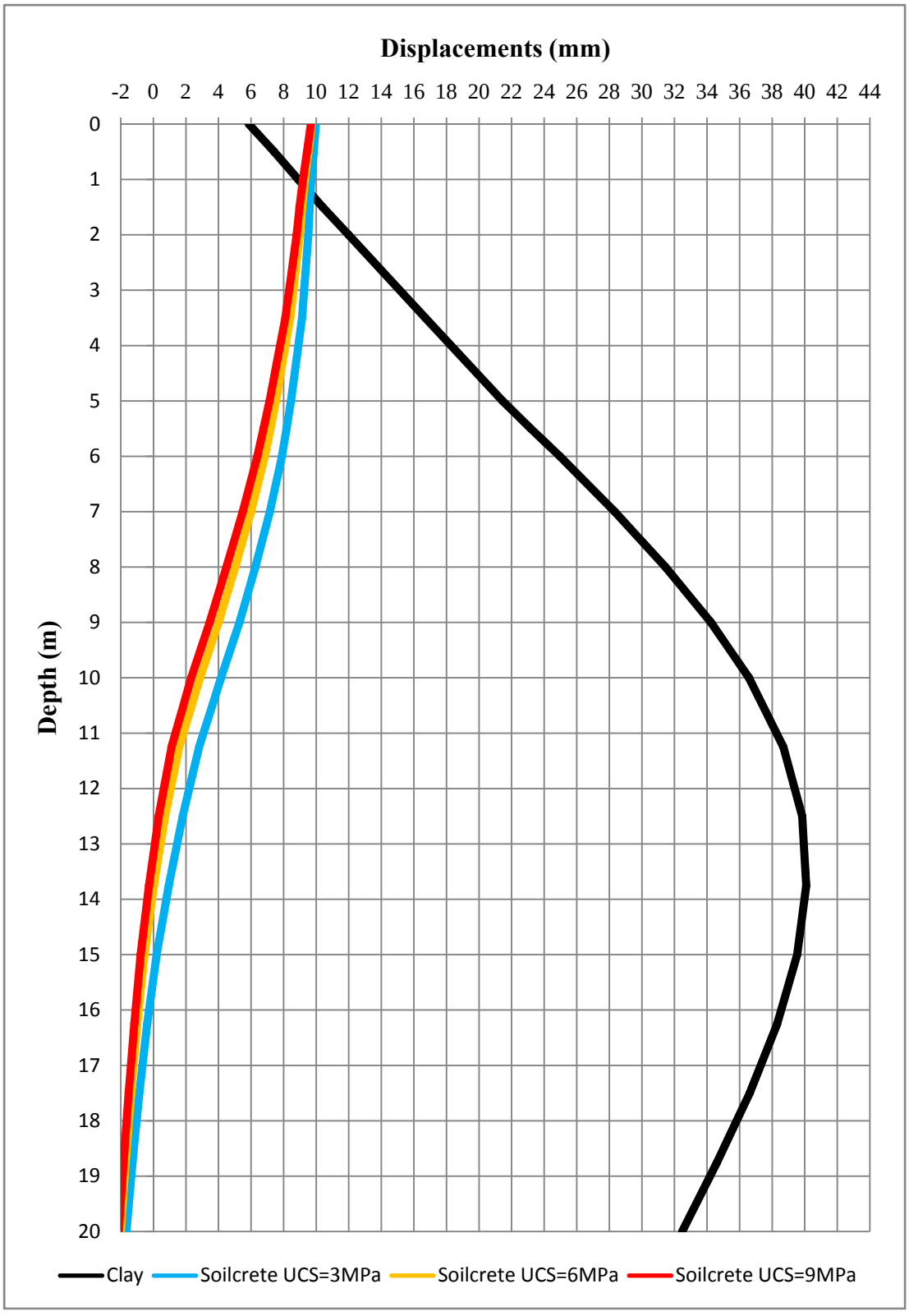

Figure 4.15 Diaphragm wall displacements according to UCS, clay profile, Location I, I_r=100%

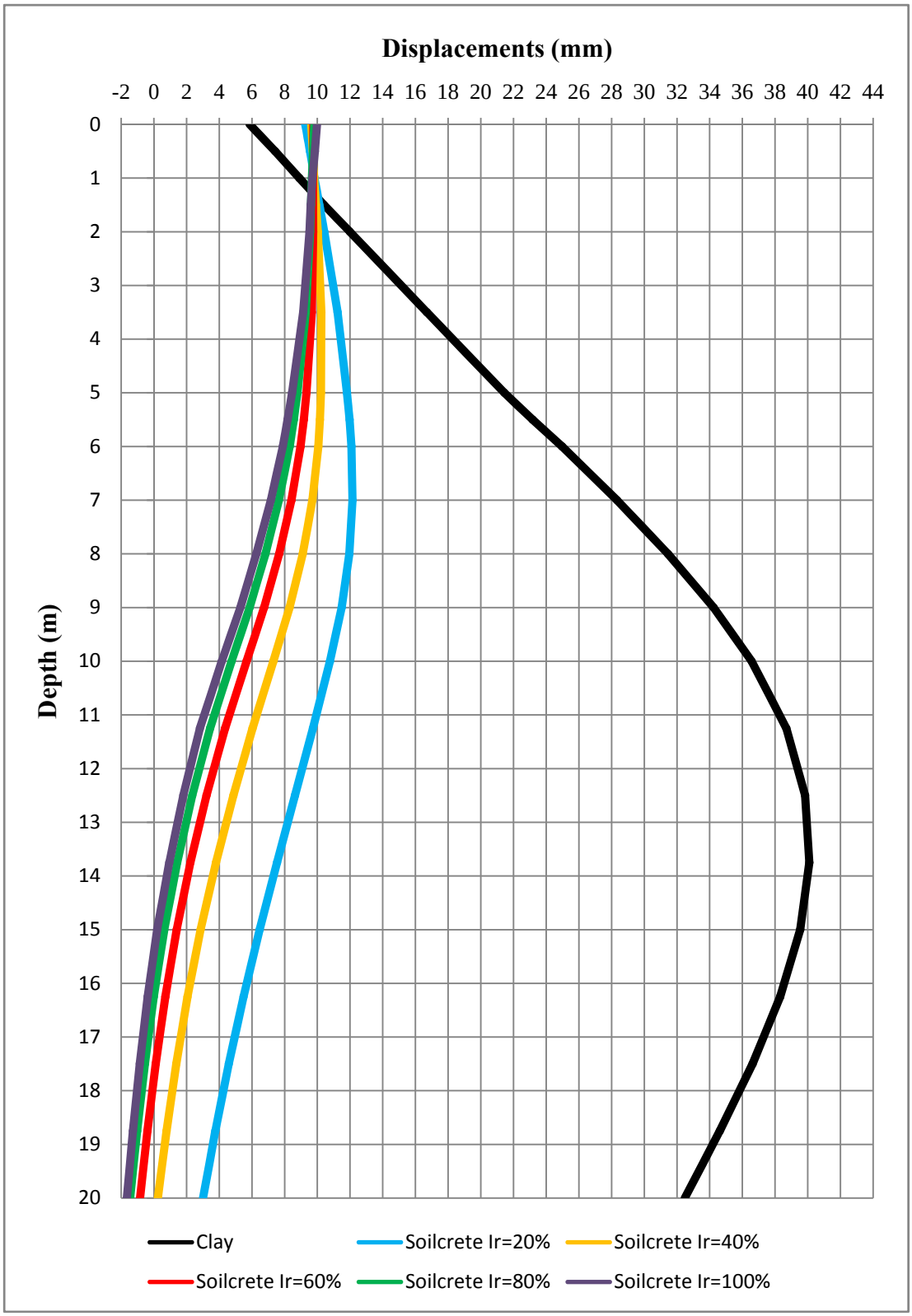

Figure 4.16 Diaphragm wall displacements according to treated soil area ratio (I_r) for pattern I and USC= 3MPa, clay profile, Location I.

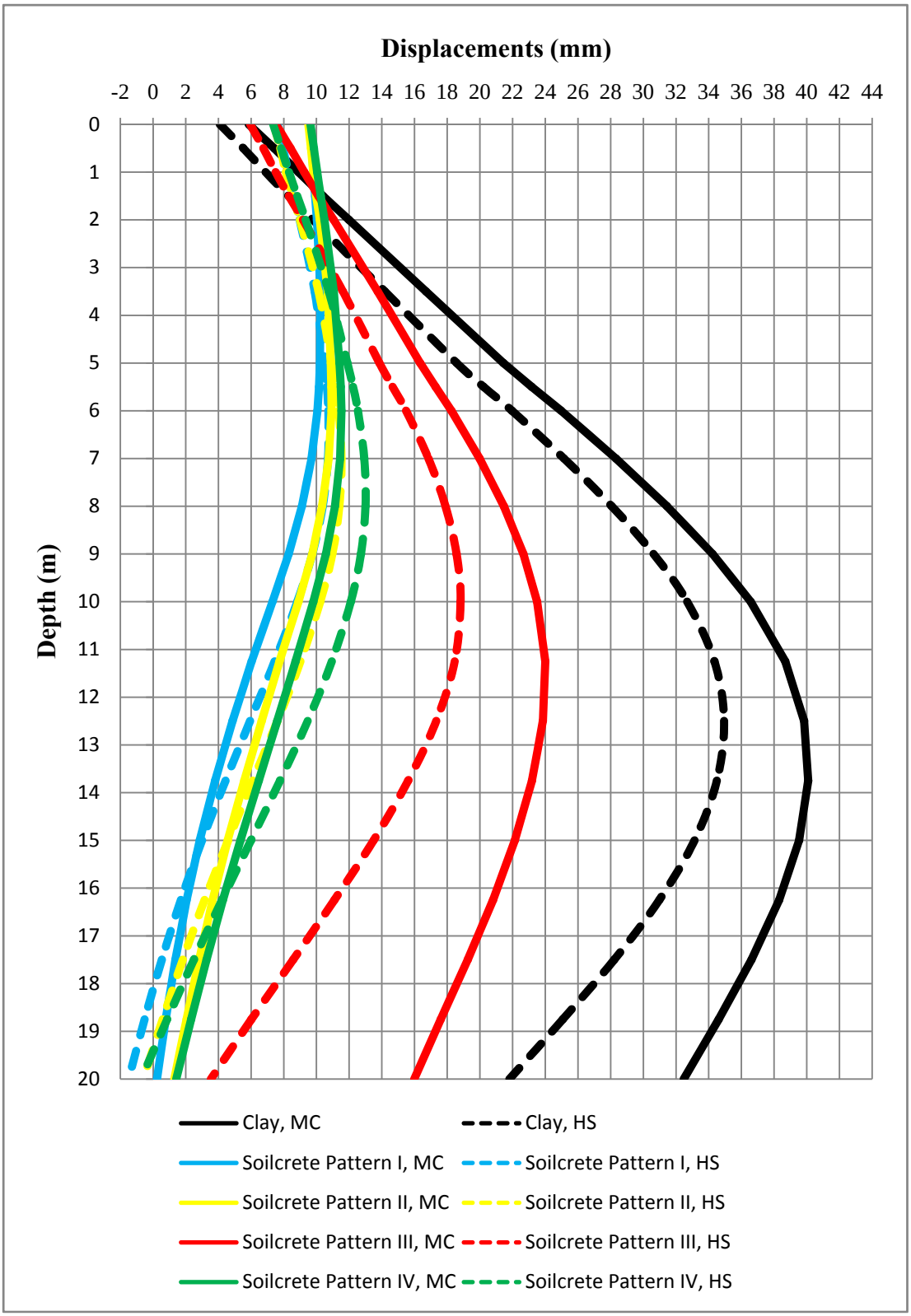

Figure 4.17 Diaphragm wall lateral displacements according to pattern types for UCS= 3MPa with MC and HS models, clay profile, Location I, I_r=40%

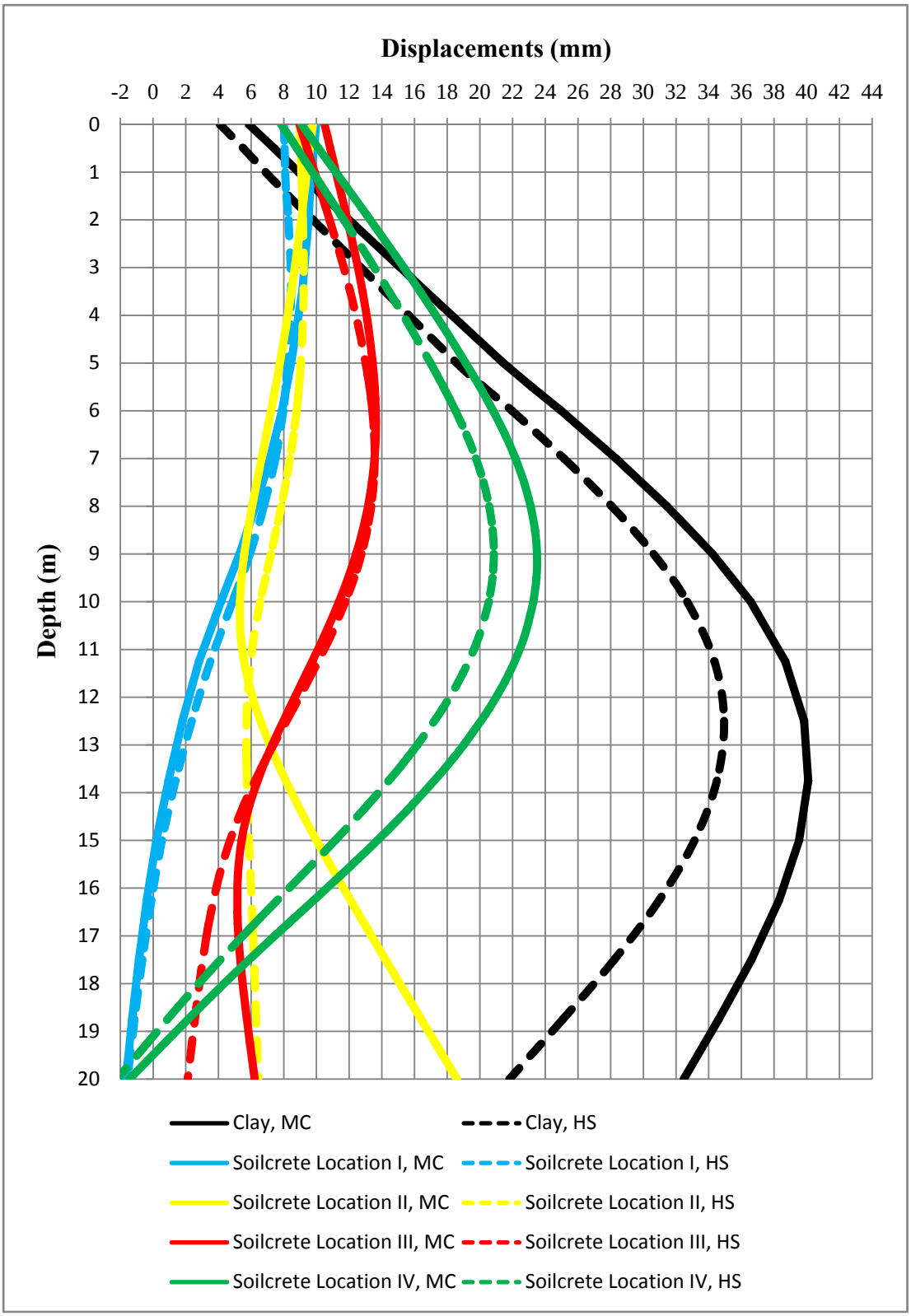

Figure 4.18 Diaphragm wall lateral displacements according to location types for UCS=3MPa with MC and HS models, clay profile, I_r=100%.

Diaphragm wall moments have been compared for three different soilcrete stiffnesses for JGSLI in Fig 4.19. The moments have been given according to treated soil area ratios (I_r) for pattern I and UCS=3 MPa in Fig. 4.20. The moments have also been compared according to pattern types and location types with Mohr-Coulomb and Hardening-Soil models in the Fig. 4.21 and Fig. 4.22, respectively.

Significant moment difference has not been observed with increment of soilcrete stiffness. Maximum moment has been observed in the non JGS application. Moments are descreased with increment of treated soil area ratios. According to pattern types for constant UCS and treated soil area ratio, the worst moment has been observed for JGSPIII after non JGS application.

The moments are obtained from higher to lower in succession of JGSPIII, JGSPIV, JGSPII and JGSPI. According to Hardening-Soil model, they are same but the moments are lower than MC model.

For soilcrete location types, the moments have been recorded from worst to best as non JGS application, JGSLIV, JGSLIII, JGSLII and JGSLI, respectively. Soil model above mentioned displacement behavior are same but the displacement values are lower than Mohr-Coulomb model.

Vertical ground displacements on the excavation level have been given according to soilcrete stiffnesses for JGSLI in Fig 4.23. The vertical displacements have been given according to treated soil area ratios (I_r) for pattern I and UCS=3 MPa in Fig. 4.24. The displacements have also been presented according to pattern types and location types with Mohr-Coulomb and Hardening-Soil models in the Fig. 4.25 and Fig. 4.26, respectively.

Significant displacement difference has not been observed with increment of soilcrete stiffness. Maximum lateral displacement is obtained in the non jet grout strut case. Displacements are decreased with increment of treated soil area ratios. According to pattern types for constant UCS=3MPa and treated soil area ratio (Ir=40%), the worst displacements have been observed for JGSPIII after non JGS application.

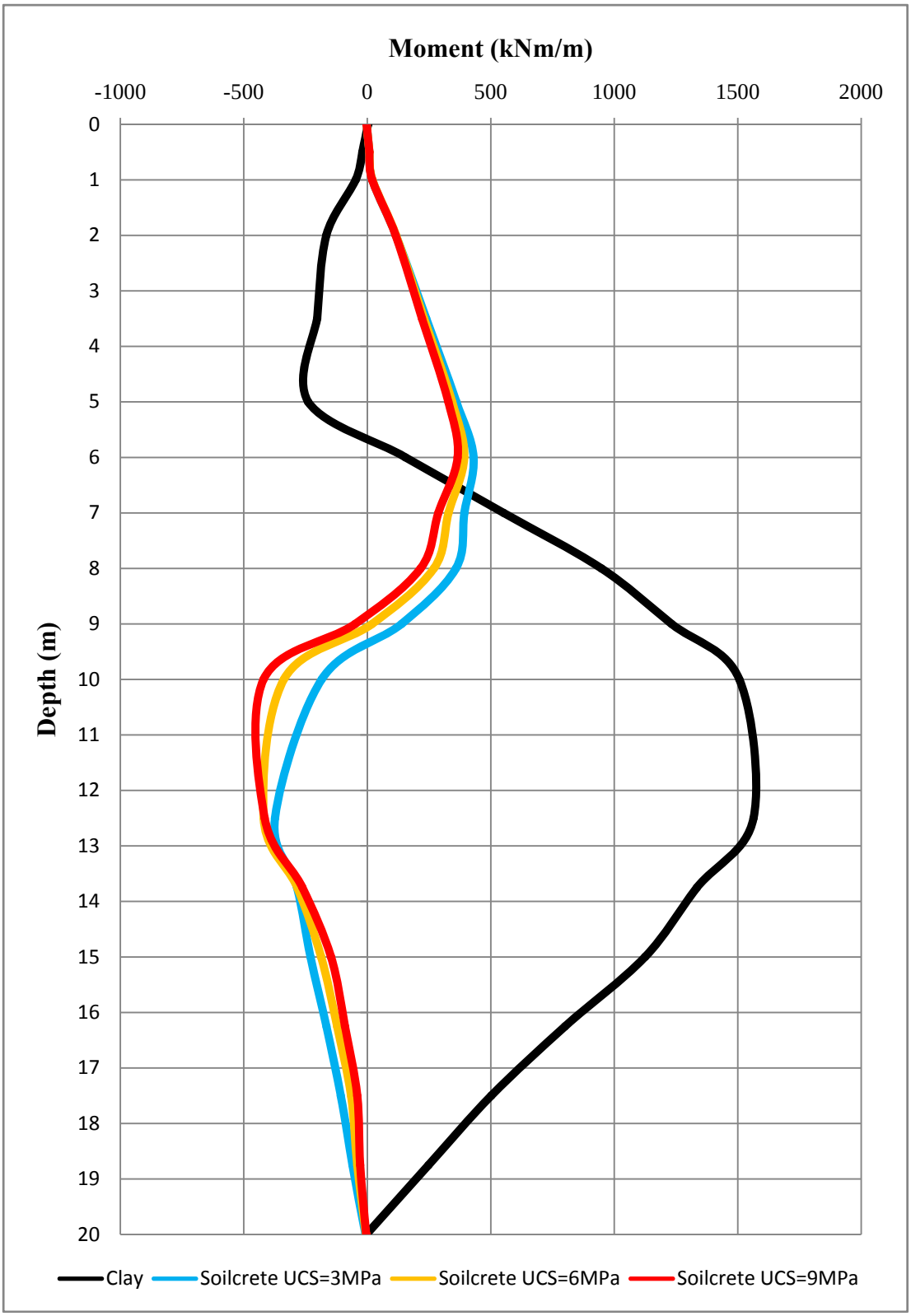

Figure 4.19 Diaphragm wall moments displacements according to UCS, clay profile, Location I, I_r=100%

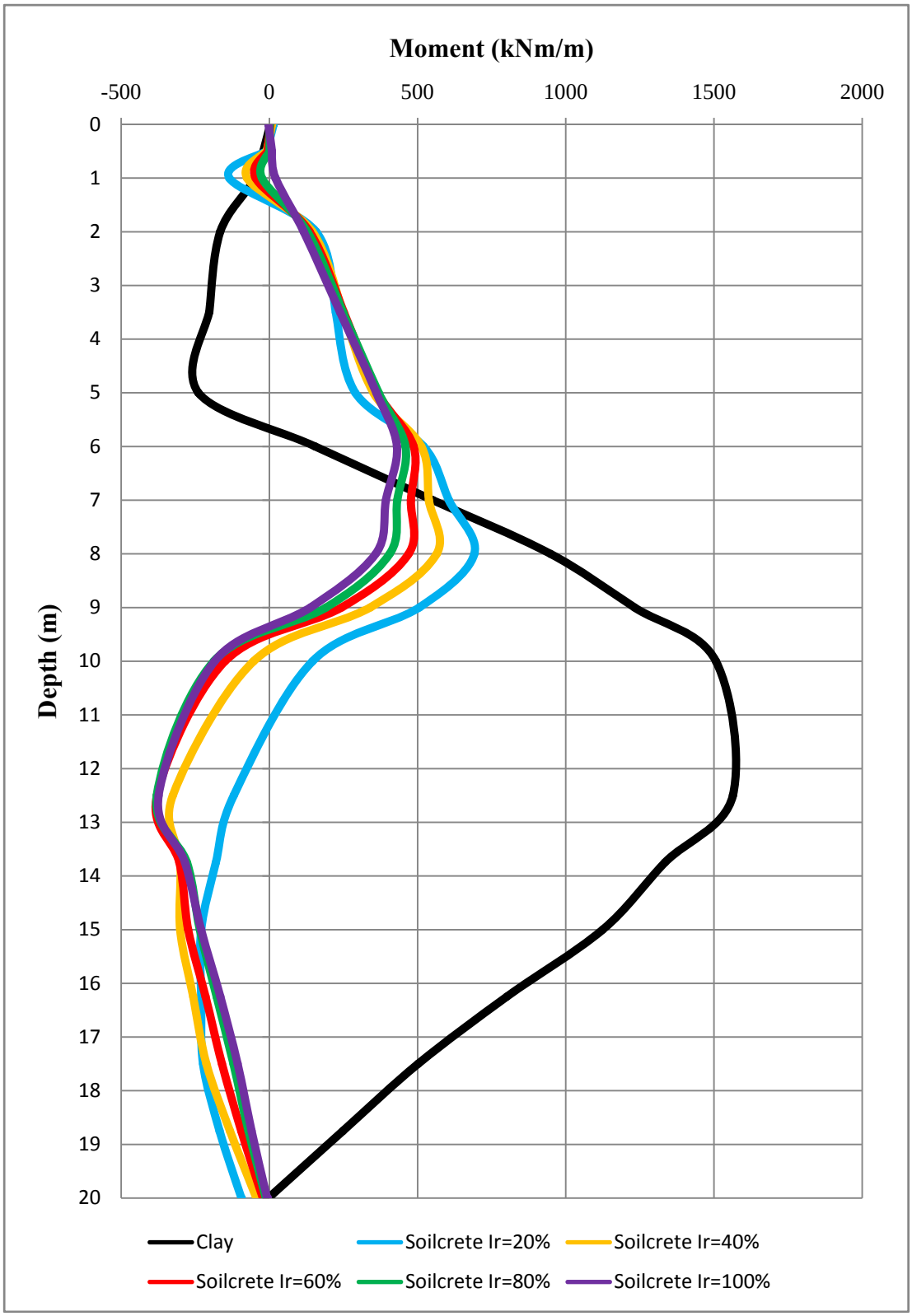

Figure 4.20 Diaphragm wall moments according to treated soil area ratio (I_r) for pattern I and UCS= 3 MPa, clay profile, Location I

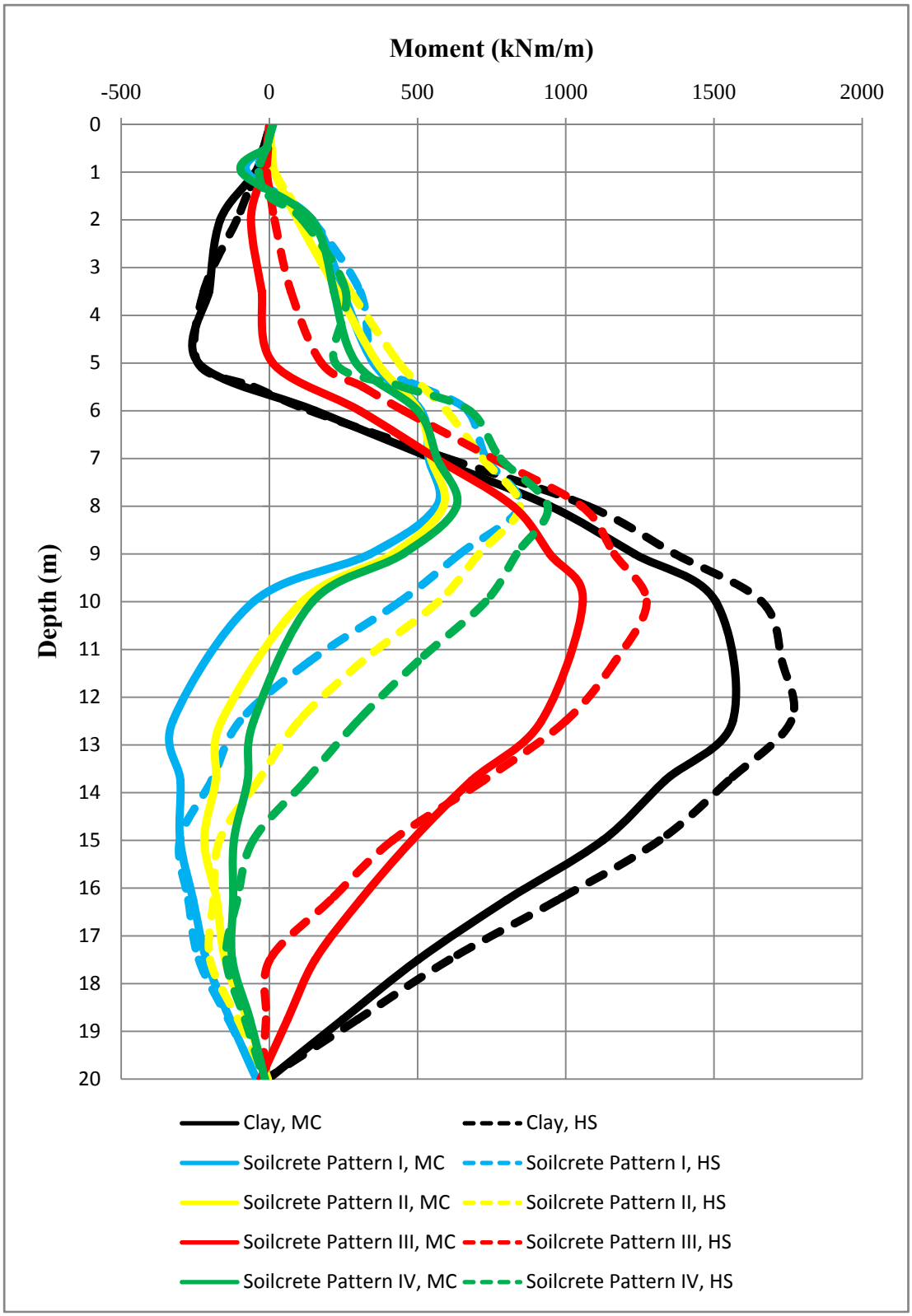

Figure 4.21 Diaphragm wall moments according to pattern types for UCS= 3MPa MC and HS models, clay profile, Location I, I_r=40%

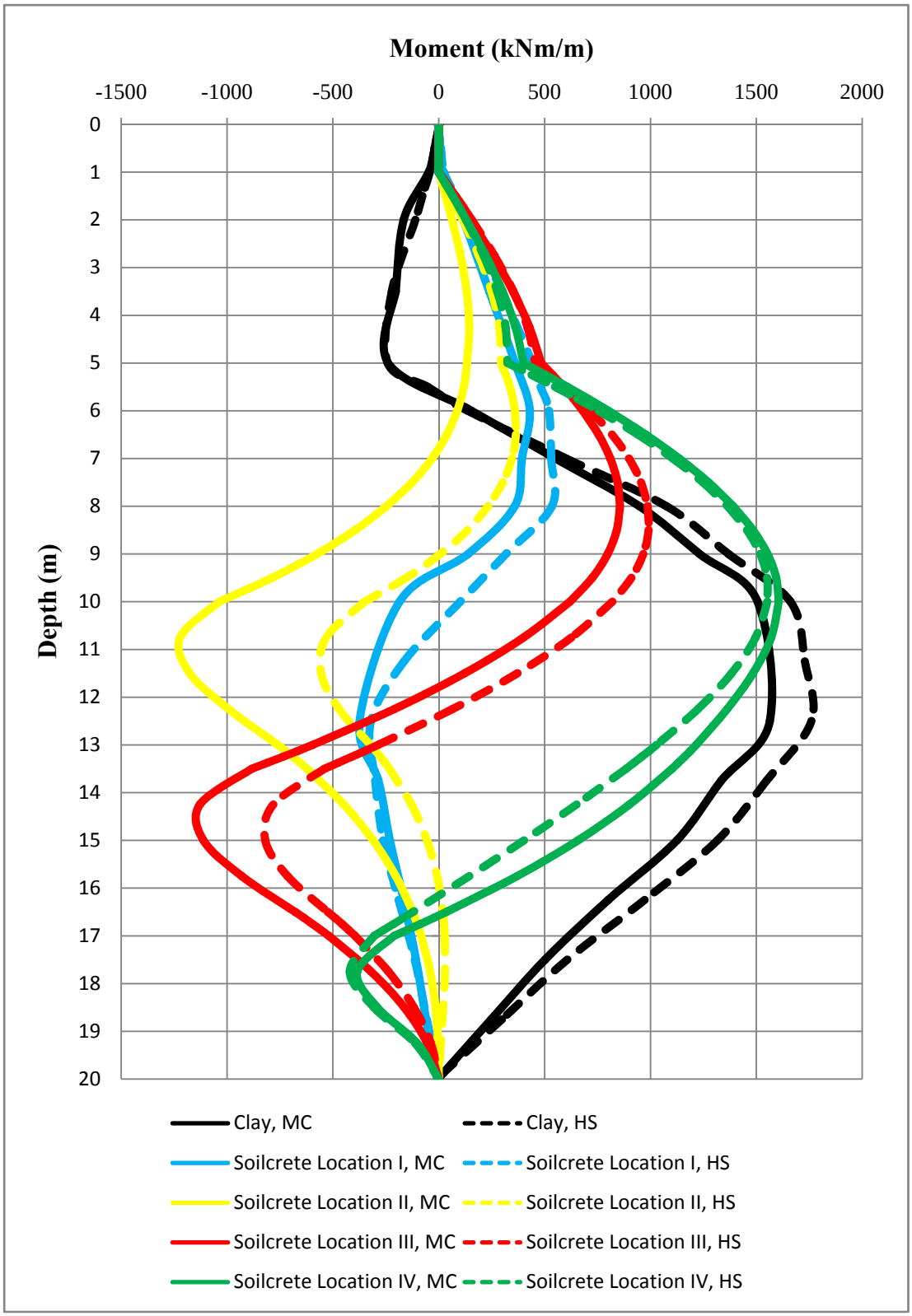

Figure 4.22 Diaphragm wall moments according to location types for UCS= 3 MPa with MC and HS models, clay profile, I_r=100%.

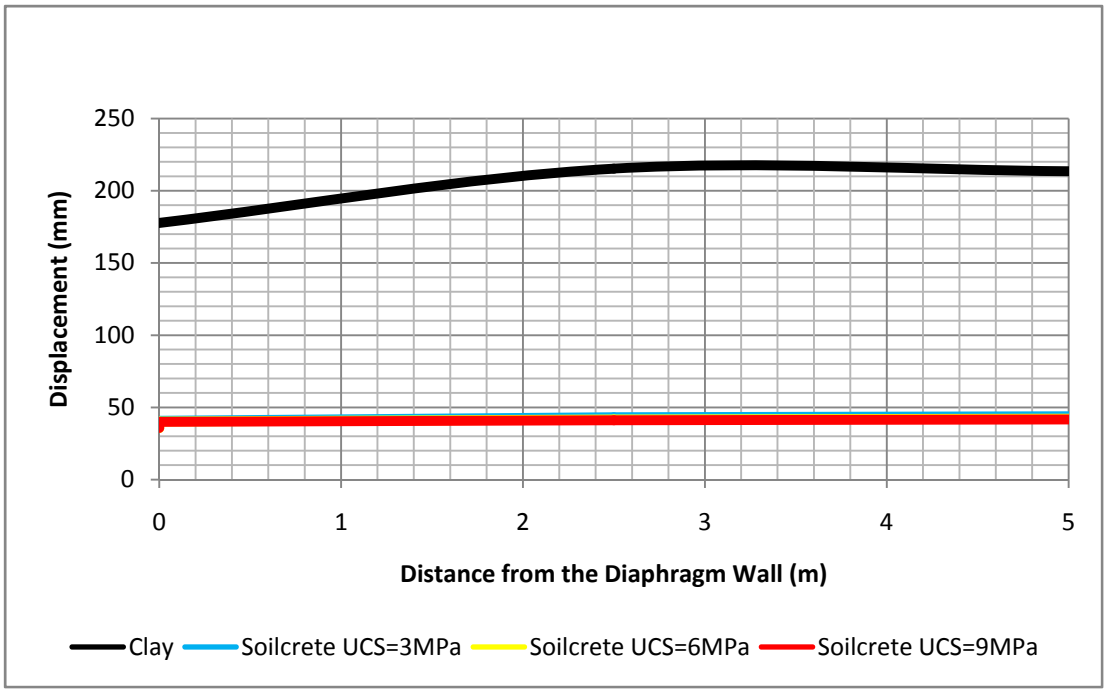

Figure 4.23 Vertical displacements on the excavation level according to USC, clay profile, Location I

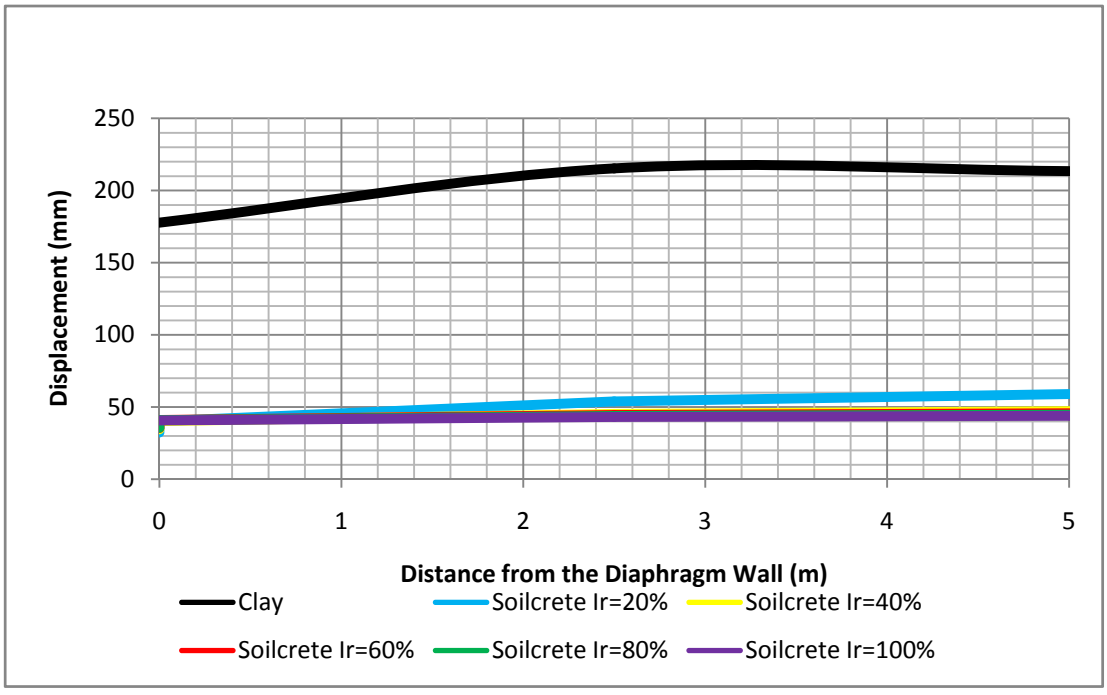

Figure 4.24 Vertical displacements on the excavation level according to treated soil area ratio (I_r) for pattern I and UCS=3 MPa, clay profile, Location I

The vertical ground displacements on the excavation level are obtained in succession of JGSPIII, JGSPIV, JGSPII and JGSPI. According to Hardening-Soil model above mentioned displacement behavior are same but the displacement values are lower than MC model.

For soilcrete location types, the displacements are obtained in succession of non JGS application, JGSLIV, JGSLIII, JGSLII and JGSLI. For the Hardening-Soil model above mentioned displacement behavior are same but the displacement values are lower than Mohr-Coulomb model.

Vertical displacements behind the diaphragm wall have been presented according to soilcrete stiffnesses for JGSLI in Fig 4.27. The vertical displacements have been given according to treated soil area ratios (I_r) for pattern I and UCS=3 MPa in Fig. 4.28. The displacements have also been presented according to pattern types and location types with Mohr-Coulomb and Hardening-Soil models in the Fig. 4.29 and Fig. 4.30, respectively.

Significant displacement difference has not been observed with increment of soilcrete stiffness. Maximum displacement has been occurred in the non JGS application. Displacements are decreased with increment of treated soil area ratios. According to pattern types for constant UCS=3MPa and treated soil area ratio (Ir=40%), the worst displacements have been observed for JGSPIII after non JGS application.

The vertical displacements are obtained in succession of JGSPIII, JGSPIV, JGSPII and JGSPI. According to Hardening-Soil model above mentioned displacement behavior are same but the displacement values are lower than MC model.

For soilcrete location types, the displacements are obtained in succession of JGSLIV, JGSLIII, JGSLII, non JGS application and JGSLI. For the Hardening-Soil model above mentioned displacement behavior but the displacement values are lower than Mohr-Coulomb model.

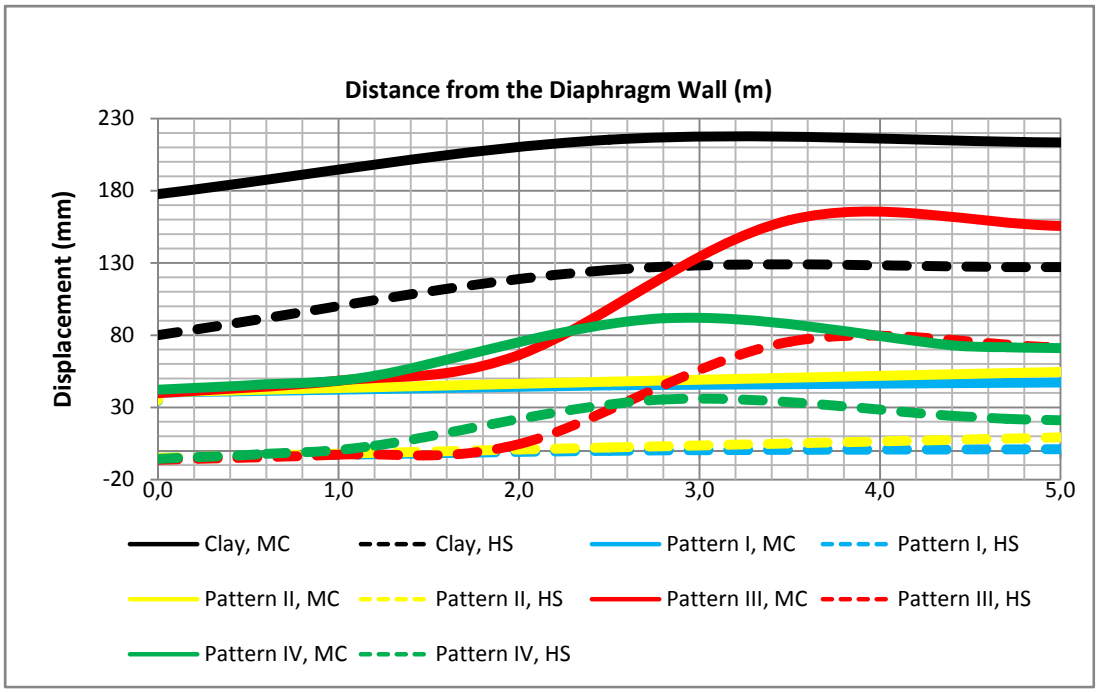

Figure 4.25 Vertical displacements on the excavation level according to pattern types for UCS= 3 MPa with MC and HS models, clay profile, Location I, Ir=40%

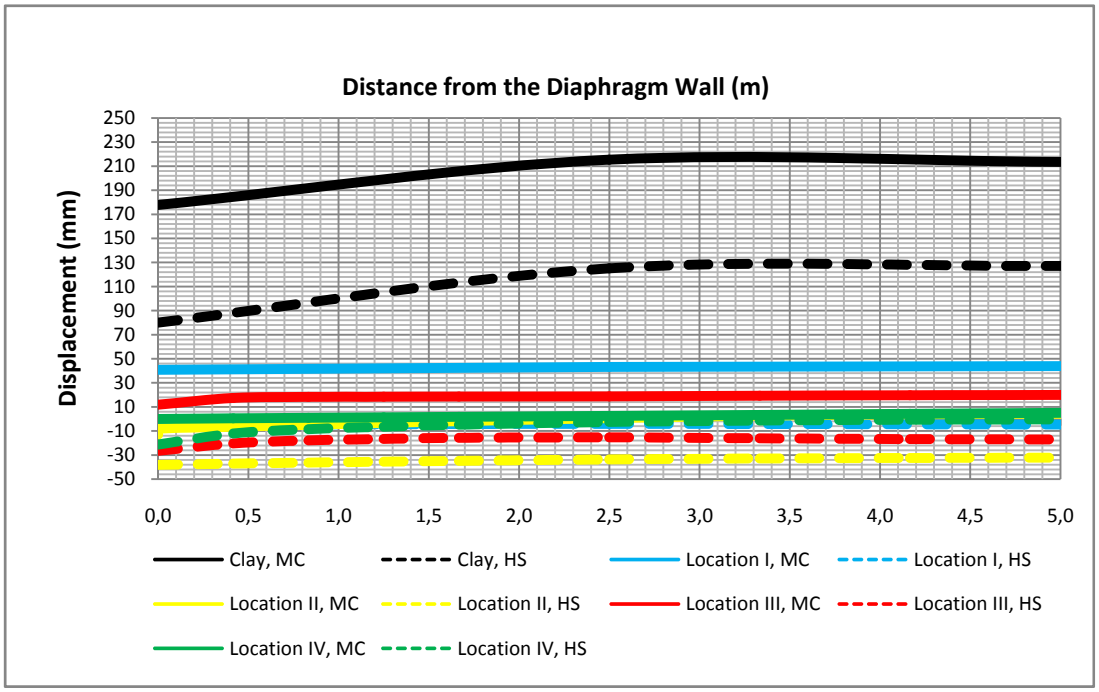

Figure 4. 26 Vertical displacements on the excavation level according to location types for UCS= 3 MPa with MC and HS models, clay profile, Ir=100%

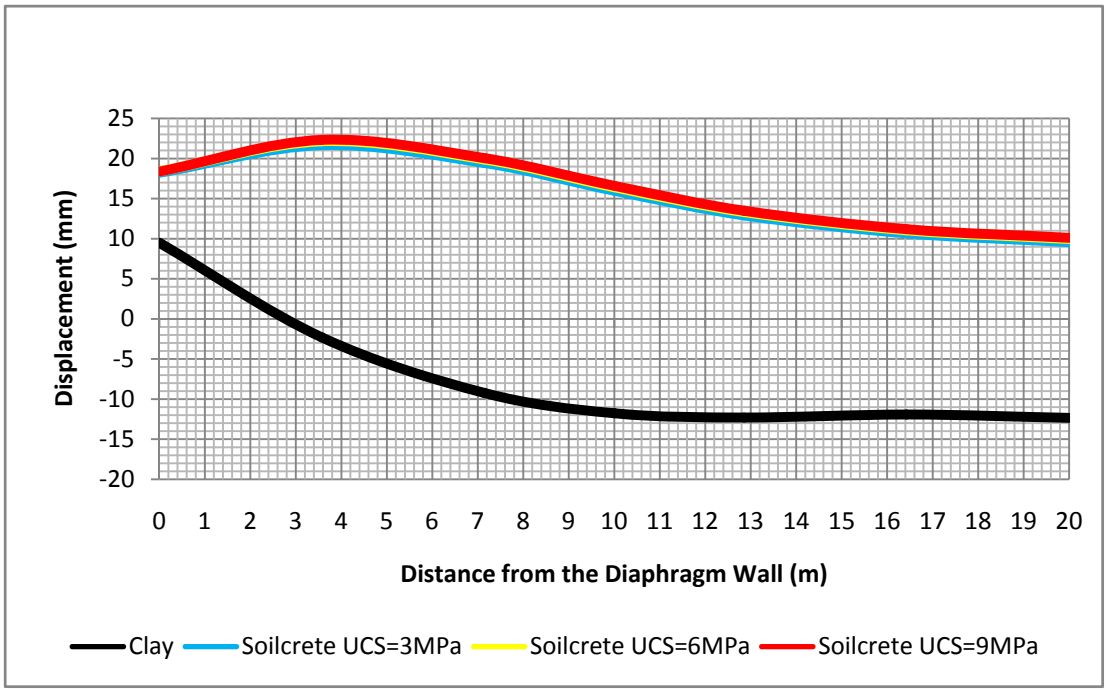

Figure 4.27 Vertical displacements behind the diaphragm wall on the ground surface according to UCS, clay profile, Location I, Ir=100%

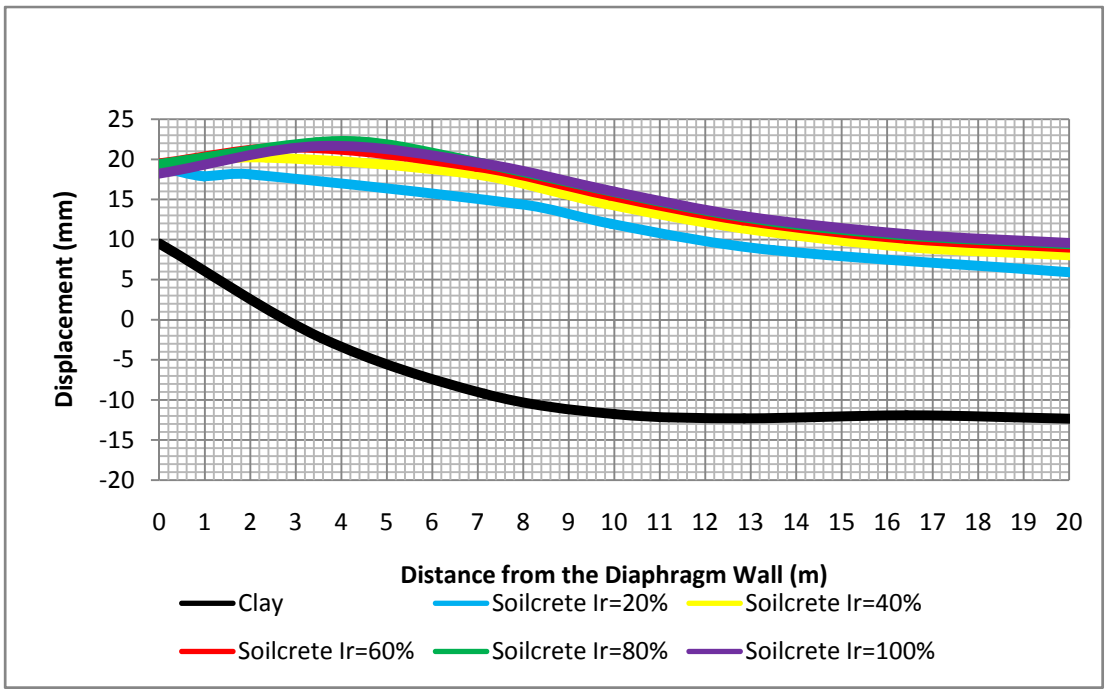

Figure 4.28 Vertical displacements behind the diaphragm wall according to treated soil area ratio (I_r) for pattern I and UCS= 3 MPa, clay profile, Location I

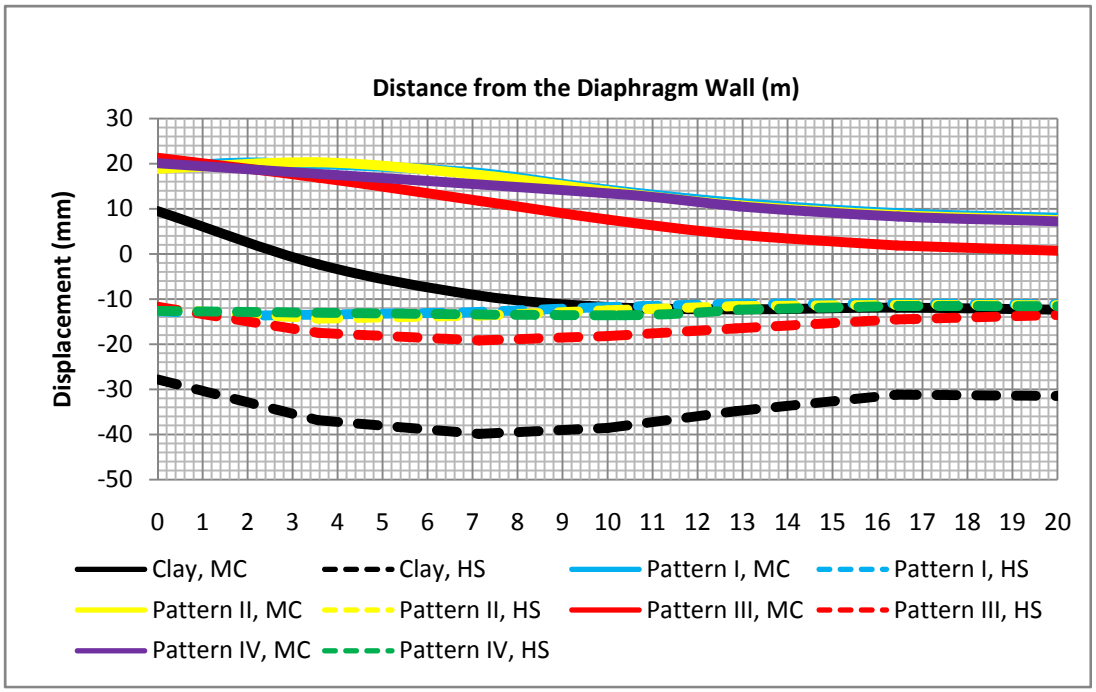

Figure 4.29 Vertical displacements behind the diaphragm wall according to pattern types for UCS = 3 MPa with MC and HS models, clay profile, Location I, Ir=40%

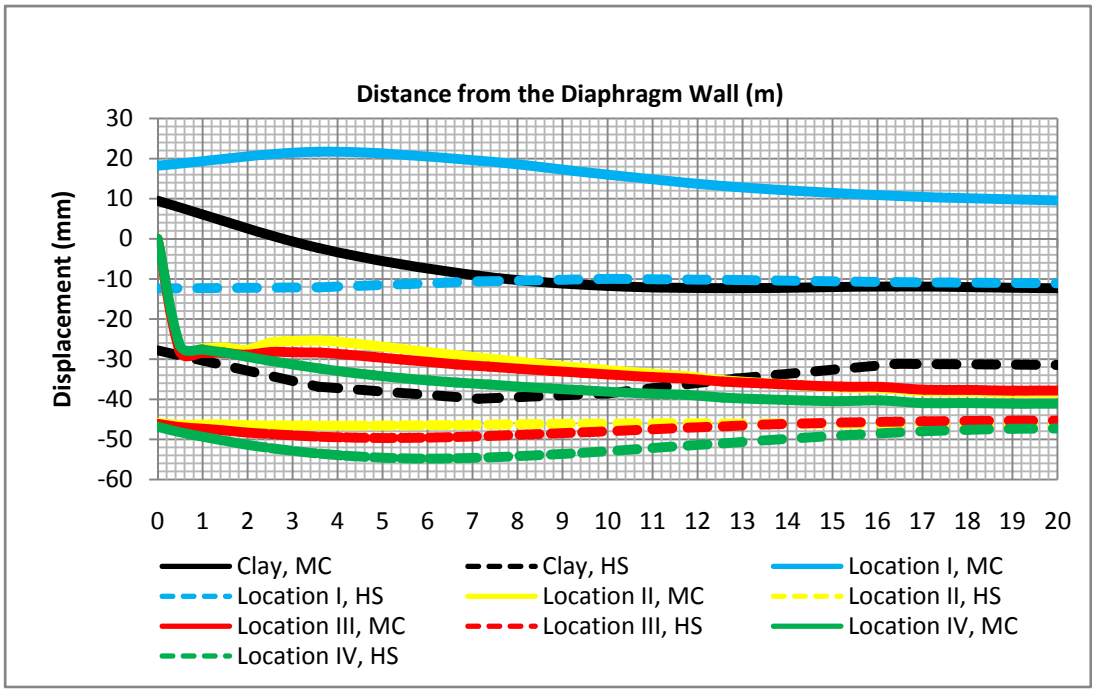

Figure 4.30 Vertical displacements behind the diaphragm wall according to location types for UCS= 3 MPa with MC and HS models, clay profile, Ir=100%

CHAPTER FIVE

RESULTS AND CONCLUSIONS

The contribution of jet grout strutting on the stability of deep retaining systems has been investigated by finite element method. Deep retaining system analyzed related with the construction of a cut and cover tunnel. The geometric model of the tunnel is inspired by Karşıyaka Subway Tunnel construction. The geometric properties of the cut and cover tunnel such as depth of the excavation, span of the excavation and the length of the retaining wall have been taken from the related project. Two different soil profiles have been considered. One is composed of sand and the other one is composed of clay. Soil parameters are selected as average values for medium dense sand and medium plastic clay. Retaining system was considered as a diaphragm wall with two level steel struts.

Engineering properties of jet grouted soilcrete such as modulus of elasticity, cohesion intercept and friction angle are determined due to UCS

Various jet strut configurations were formed and analyzed. These include variations in pattern type, soilcrete location, treated soil area ratio and soilcrete stiffness.

Geometric properties of the problem, soilcrete patterns types, construction stages and material properties (diaphragm wall, steel strut, jet struts and soils) used in finite element analyses (Plaxis 2D and Plaxis 3D) have been explained in detail.

Analyses have been performed basically with Mohr-Coulomb model both for the sand and the clay profiles. Finite element analyses with Hardening-Soil model have also been performed for representative cases and obtained results have been compared with the solutions of Mohr-Coulomb model.

Moment and lateral displacement curves of the diaphragm wall have been presented comparatively with respect to analyses combinations. Vertical soil displacement curves at the excavation level and at the ground surface have been plotted according to the analyses combinations and presented.

The maximum diaphragm wall displacements and moments, vertical displacements on the excavation level and behind the wall has been obtained for the case of no jet grout strutting for both the sand and the clay soil profiles.

The wall displacements and moments are reduced significantly with the application of jet grout strutting. The vertical displacements on the excavation level and behind the wall have also been reduced by jet strutting.

For the sand profile finite element analyses have been done using 4 different locations of jet grout strut layer (I, II, III and IV) and 3 different soilcrete stiffness (5, 10, 15 MPa)

The results of these analyses showed that these exist no significant difference according to soilcrete stiffness increment.

Jet grouting strut location type I (JGSLI) gives the best solution but it is costly because of soilcrete layer thickness (10m) . The results of JGSLII are closer to JGSLI, so it is more economical because of its thickness (3m).

For the clay profile four different locations of jet strut layer (I, II, III and IV) and three different soilcrete stiffness (3, 6, 9 MPa) has been used. The results of these two factors are similar to the results of sand profile.

Treated soil area ratios (0, 20, 40, 60, 80, 100%) and jet strut pattern types (I, II, III and IV) are additional factors for the clay profile.

Increase of the treated soil area ratio reduces the diaphragm wall displacements and moments, ground displacements for all jet strut pattern types. But beyond the 40% of treated soil area ratio, the decrease is not significantly.

Jet grout strut pattern type I (JGSPI) gives the best solution. JGSPII and JGSPIV patterns present acceptable solutions. But JGSPIII is not recommended.

For sandy and clayey soils, jet grout strut location II is recommended. Increment of soilcrete stiffness is not useful, so a low value of stiffness can be selected.

For clayey soils, JGSPI, JGSPII and JGSPIV present good results. But application of JGSPII and JGSPIV is difficult. So, JGSPI is suggested. In the clays, 40% area ratio seems to be adequate.

Above these suggestions for both sandy and clayey soils is believed to present economical and applicable solutions.

REFERENCES

Ayoubian, A., & Nasri, V. (2004). Design of jet grout plugs for base stability and groundwater control. *Geotechnical Engineering for Transportation Projects*, 1905-1914.

Ballarin, L., & Forti, F. (1998). The use of jet-grouting method for the stabilization of the underground. *Geotechnical Hazards*, Belkema, 485-488.

Bell, A. L. (1993). Jet grouting. In Ground Improvement, *Blackie Academic and Professional*, 149-172.

Bertero, M., Marchi, G., Merli, M. and Paviani, A. (1988). Foundation improvement by jet grouting of a historical building in Cerria, Italy - experimental investigation. Proc. *Int. Symp. Engineering Geology of Ancient Works, Monuments and Historical Sites*. Athens, Geece, 381-391.

Bowles, J. E. (1997). *Foundation Analysis and Design (5th. ed.)*, Singapore.

Brinkgreve, R. B. J. (2002) *Plaxis 2D Version 8*, Nertherland.

Brinkgreve, R. B. J., & Swolfs, W. M. (2007) *Plaxis 3D Foundation Version 2*, Nertherland.

British Standard (2001). Execution of special geotechnical works – *Jet grouting. BS EN 12716*, United Kingdom.

Bruce, D. A. and Bruce, M. E. C. (2003). The practitioner's guide to deep mixing. *Proceedings of Rapid Excavation and Tunneling Conference (RETC)*, New Orleans, LO, 474-488.

Chai, J. C, Miura, N., & Koga, H. (2005). Lateral displacement of ground caused by soil-cement column installation. *Journal of Geotechnical and Geoenviromental Engineering*, 131, 623-632.

Coulter, S., & Martin, C. D. (2006). Single fluid jet-grout strength and deformation properties. *Tunneling and Underground Space Technology*, 21, 690-695.

Coulter, S., & Martin, C. D. (2006). Effect of jet-grouting on surface settlements above the Aeschertunnel, Switzerland. *Tunneling and Underground Space Technology*, 21, 542-553.

Fang, Y. S., Liao J. J., & Lin, T. K. (1994). Mechanical Properties of Jet Grouted Soilcrete. *Quarterly Journal of Engineering Geology*, 27, 257-265.

Fang, Y. S., Liao J. J., & Sze, S. C. (1994). An empirical strength criterion for jet grouted soilcrete. *Engineering Geology*, 37, 285-293.

Hsieh, H. S., Wang, C. C., & Ou, C. Y. (2003). Use of jet grouting to limit diaphragm wall displacement of a deep excavation. *Journal of Geotechnical and Geoenvironmental Engineering*, 129, 146-157.

Hsiung, B. C. B., Nash, D. F. T., Cheng, K. H., Huang, C. C., & Hwang, R. N. H. (2000). *Effectiveness of jet-grout slabs and cross-walls in restricting wall movements in deep excavations*. www.maa.com.tw/common/publications.

JSG ASSOCIATION (1986). *JSG method, technical information.* Tokyo, Japan.

Kauschinger, J.L., Perry, E.B., Hankour, R., (1992). Jet-Grouting:State-of-the Practice. Grouting, Soil-Improvement and Geosynthetics, 25-28 Feb. 1992, GSP No:30, pp.169-181, New Orleans

Melegari, C., & Garassino A.L., (1997). *Seminar on Jet Grouting, Singapore*.

Miki, G. (1985). Soil improvement by jet grouting. Third International Geotechnical Seminar, *Soil Improvement Methods*, Singapore, 45-52.

Nishimatsu, Y. (1972). The mechanics of rock cutting. *International Journal of Rock Mechanics and Mining Science*, 9, 261- 270.

Ökmen, Ö. (2003). *A study on strength and deformation behavior of soilcrete in jet grout applications.* M. Sc. Thesis. The Middle East Technical University, Ankara.

Poh, T. Y., & Wong, I. H. (2001). A field trial of jet grouting in marine clay. *Canadian Geotechnical Journal*, 38, 338-348.

Schanz, T., Vermeer P. A. & Bonnier P. G. (1999). The hardening soil model: Formulation and verification. *Beyond 2000 in Computational Geotechnics.*

Shibazaki, M. (2003). State of practice of jet grouting. Grouting and Ground Treatment, *Proceeding of the Third International Conference*, New Orleans, Lousiana, 1, 198-217.

Shirlaw, J. N. (2003). Jet grouting soft clays for tunneling and deep excavations – design and construction issues. Grouting and Ground Treatment, *Proceeding of the Third International Conference*, New Orleans, Lousiana, 1, 257-268.

Stoel, A. E. C., & Ree, H. J. (2000). Strength and stiffness parameters of jet grouting columns: Full scale test Amsterdam. *Geotechnical Aspects of Underground Construction in Soft Ground*, Tokyo, Japan.

Stoel, A. E. C. (2001). *Grouting for pile foundation improvement*. Ph. D. Thesis. Delf University of Technology, Amsterdam, Holland, 233.

Trevi, K. (1994). Columnar Treatment, Illustrative Report, Cesena.

Turkish Standard (2002). Execution of special geotechnical works – *Jet grouting, TS EN 12716*, Ankara

Wang, J. G., Oh, B., Lim, S. W., & Kumar, G. S. (1999). Effect of different jet-grouting installations on neighboring structures. *Field Measurements in Geomechanics*, Rotterdam, 511-516.

Wong, I. H., & Poh, T. Y. (2000). Effects of jet grouting on adjacent ground and structures. *Journal of Geotechnical and Geoenvironmental Engineering*, 126, 247-256.

Wong, L. W., & Hwang, R. N. (1997). Evaluation of jet grouting by in-situ test. *International Conference on Ground Improvement Techniques*, Macau, 641-647.

Wong, L. W., Ju, D. H., & Wu, P. J. (1997). Control of ground movements caused by jet grouting. *International Conference on Ground Improvement Techniques*, Macau, 649-656.

Yohiro, T., Yoshida, H. and Nishi, K., (1975). The development and application of a Japanese grouting system. *Water Power Dam Construction*, 27: 56-69

Yohiro, T., Yoshida, H. and Nishi, K., (1982). Soil improvement method utilizing a high speed water and air jet on the development and application of column solidified construction method (column jet method). 6th Int. Symp. *Jet Cutting Technology*, Univ. Surrey, England, 397-427.

APPENDIX A

DISPLACEMENTS AND MOMENTS CURVES

FOR THE SAND PROFILE

(PLAXIS 2D, MOHR COULOMB SOIL MODEL)

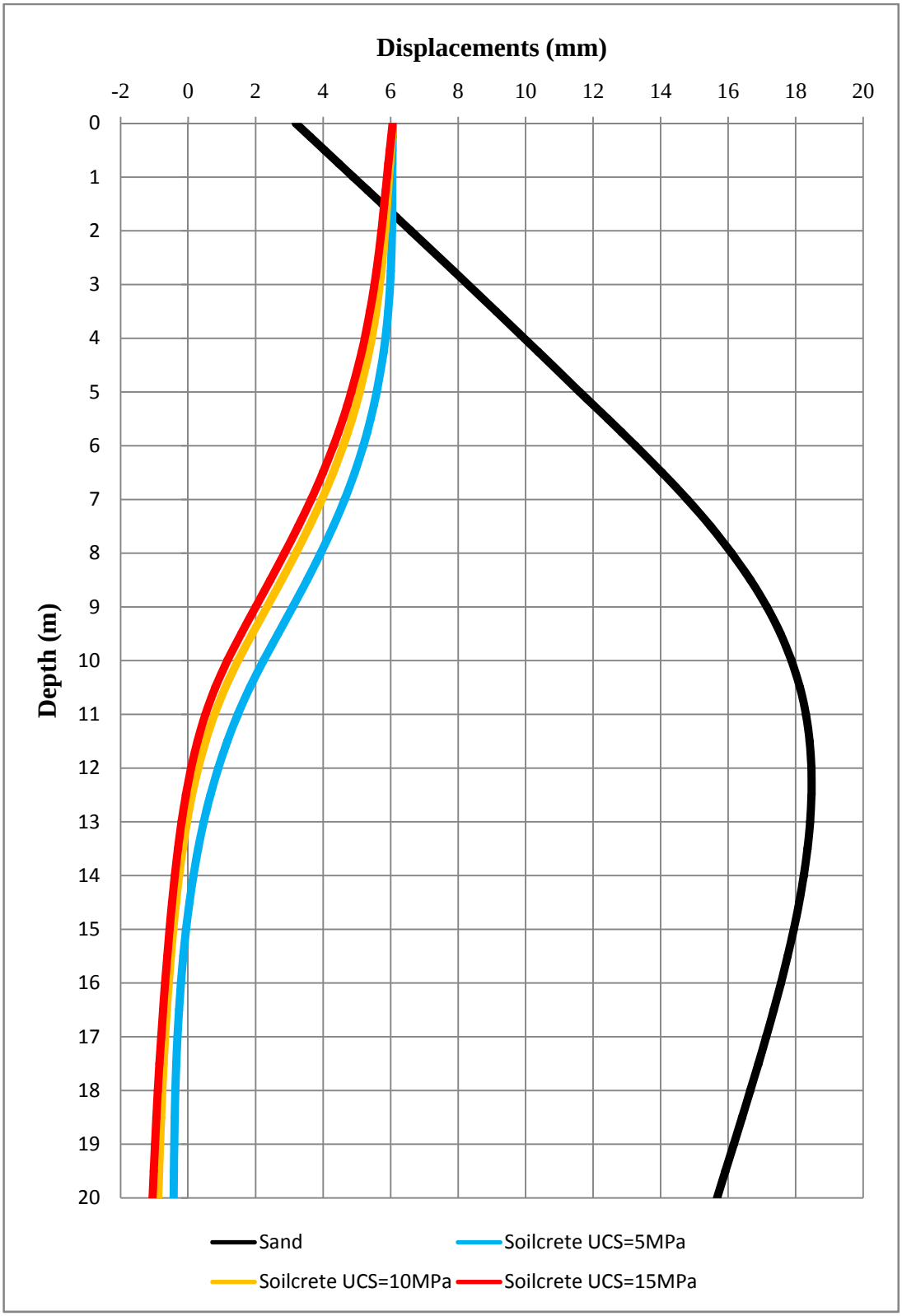

Figure A-1 Diaphragm wall displacements according to USC for location I, sand profile

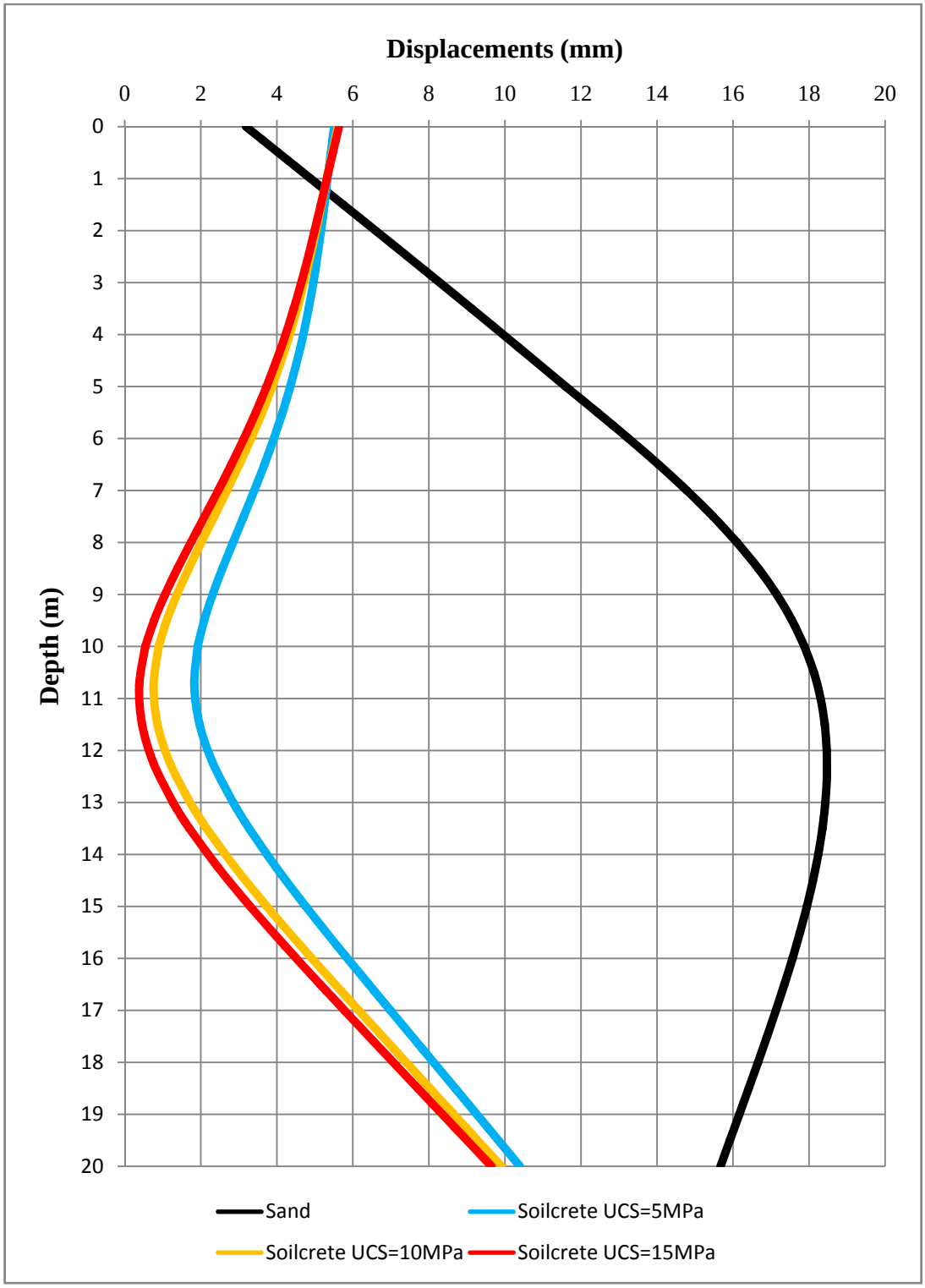

Figure A-2 Diaphragm wall displacements according to USC for location II, sand profile

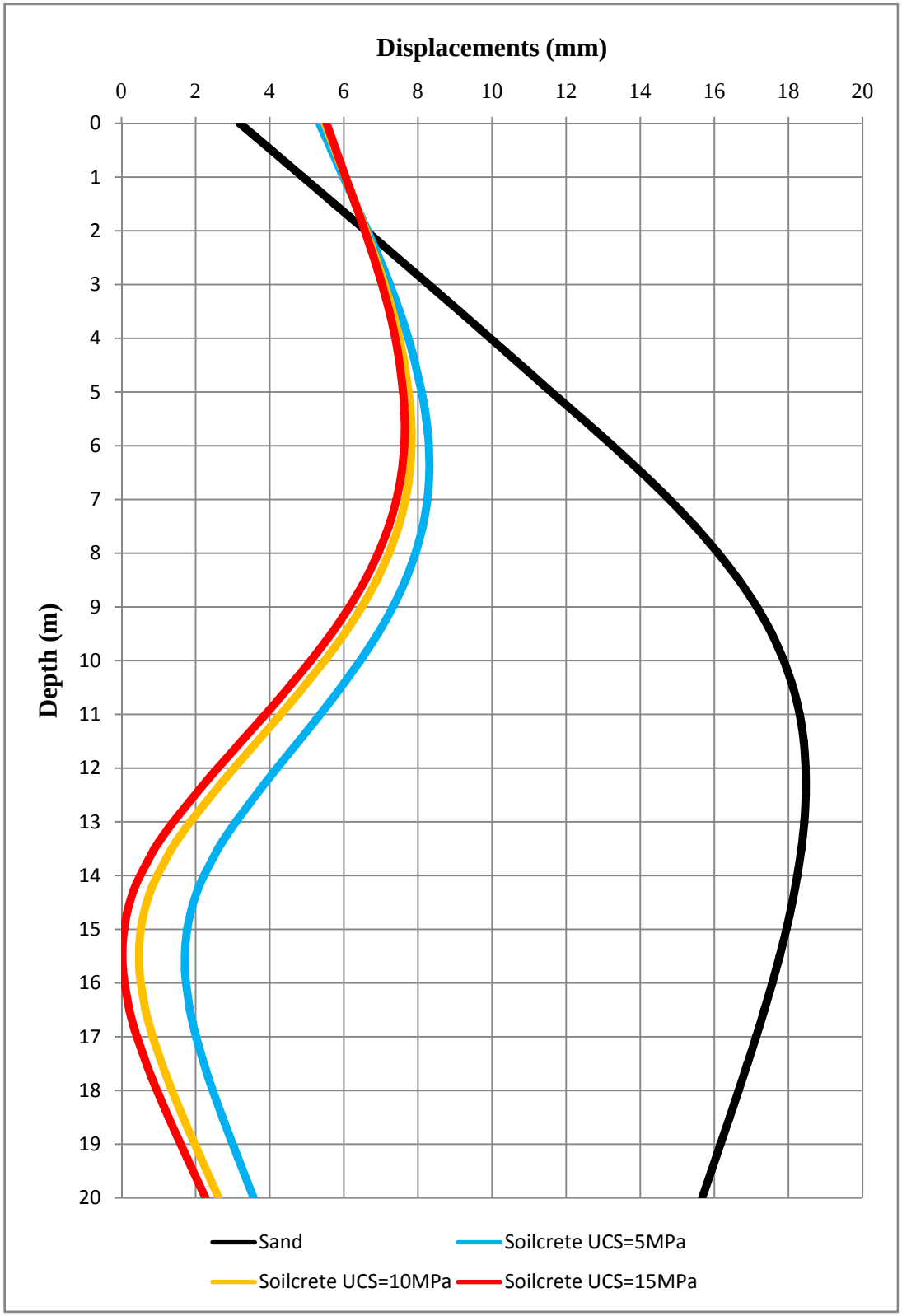

Figure A-3 Diaphragm wall displacements according to USC for location III, sand profile

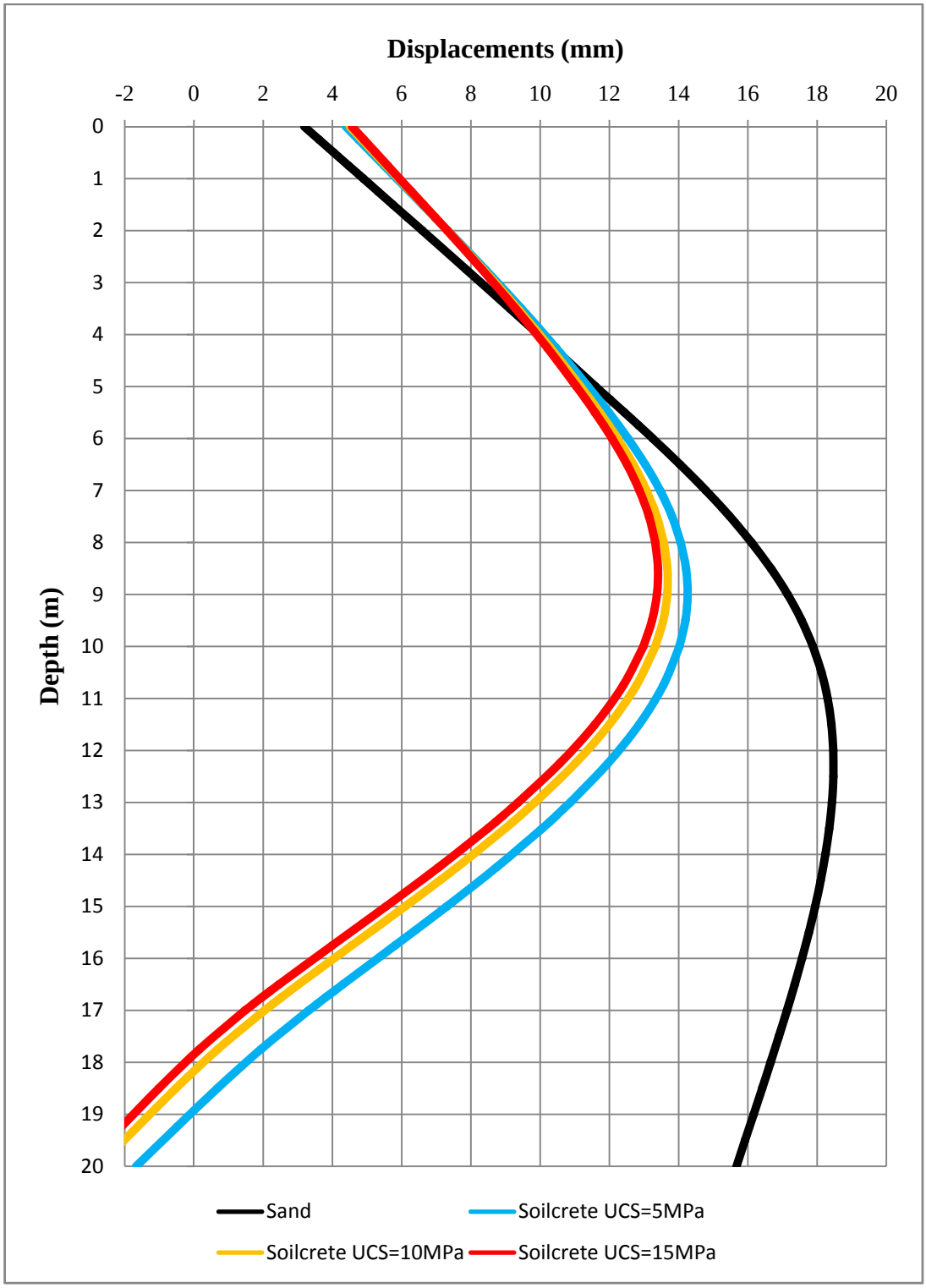

Figure A-4 Diaphragm wall displacements according to USC for location IV, sand profile

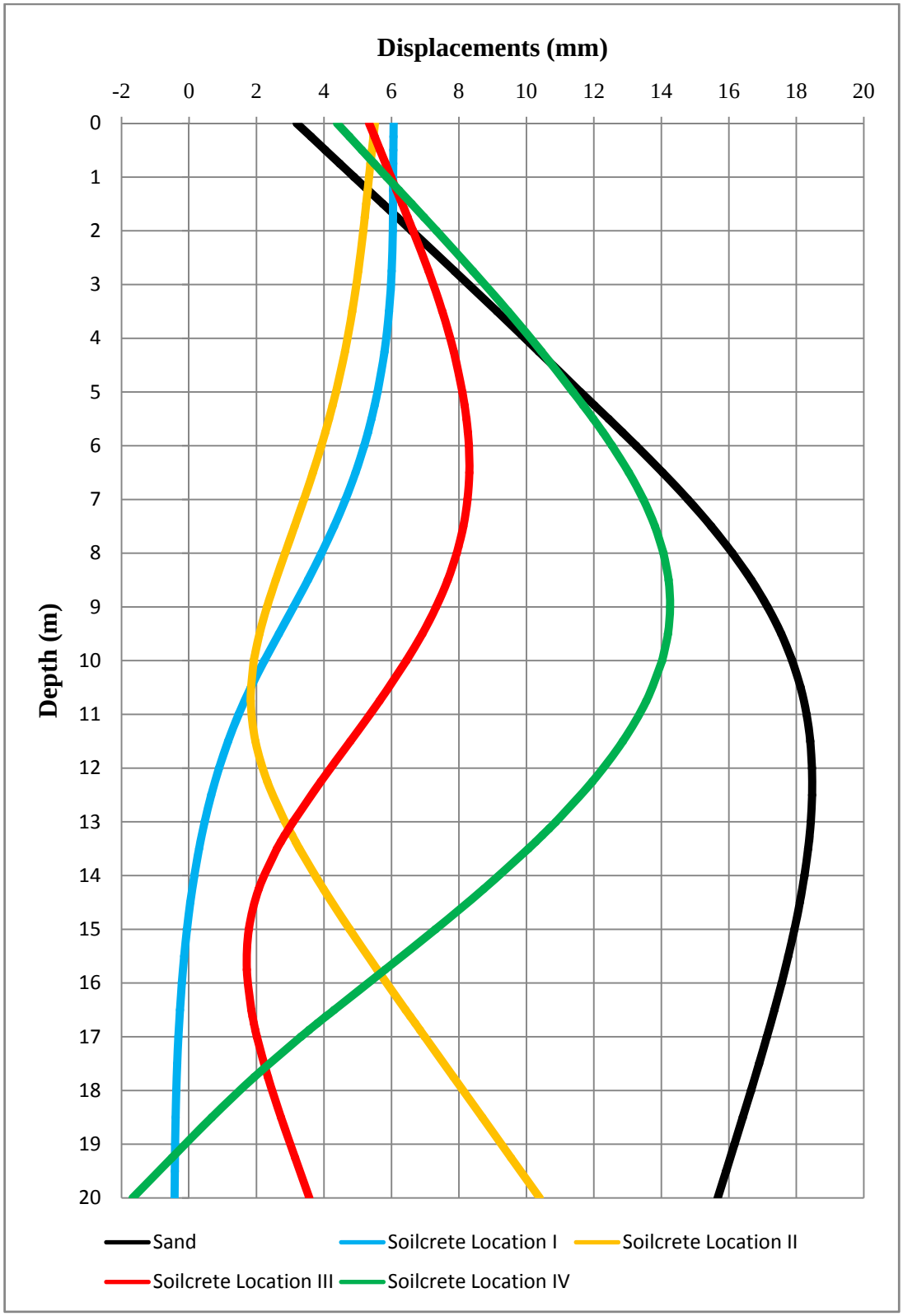

Figure A-5 Diaphragm wall displacements according to location types for UCS=5 MPa, sand profile

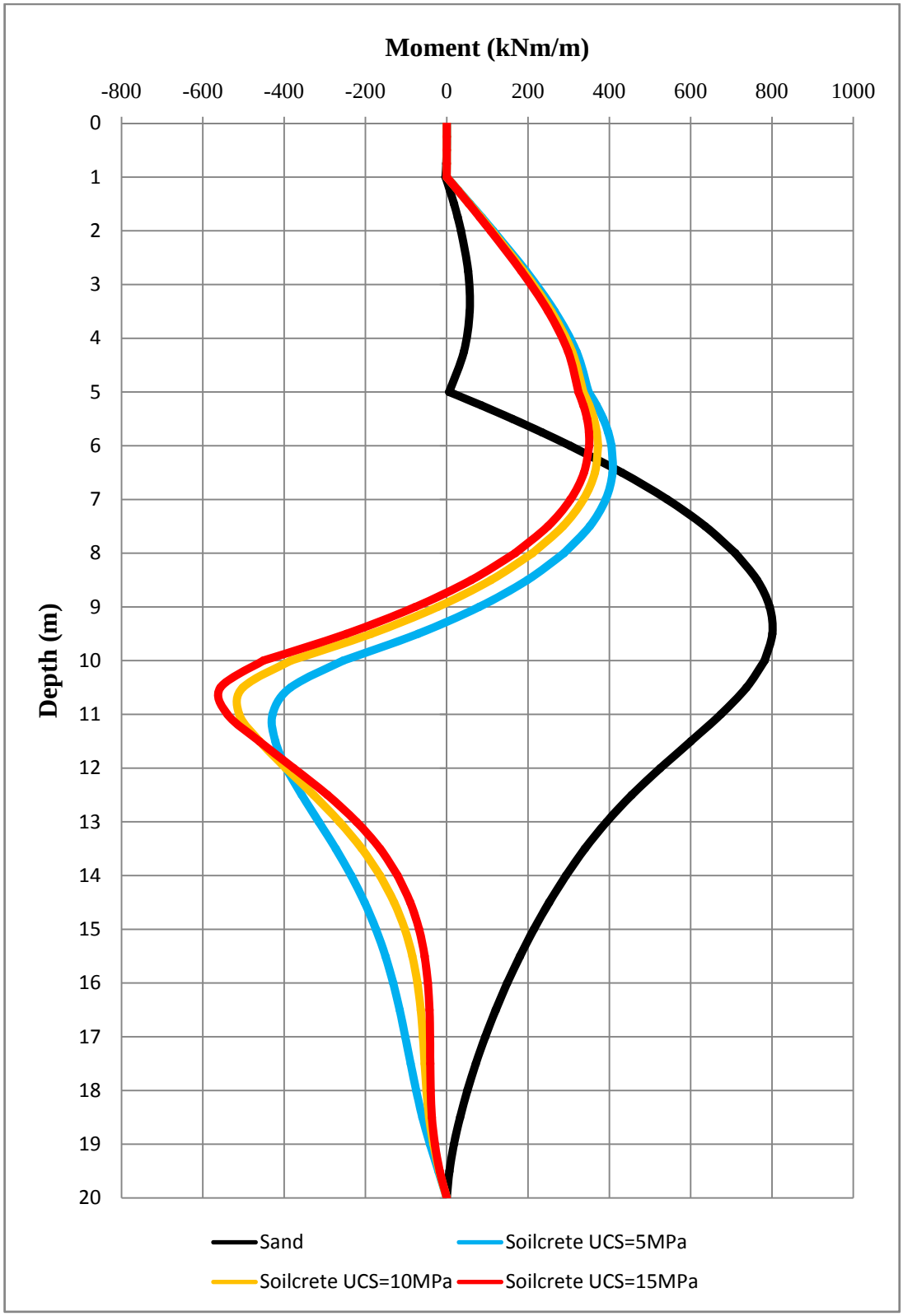

Figure A-6 Diaphragm wall moments according to USC for location I, sand profile

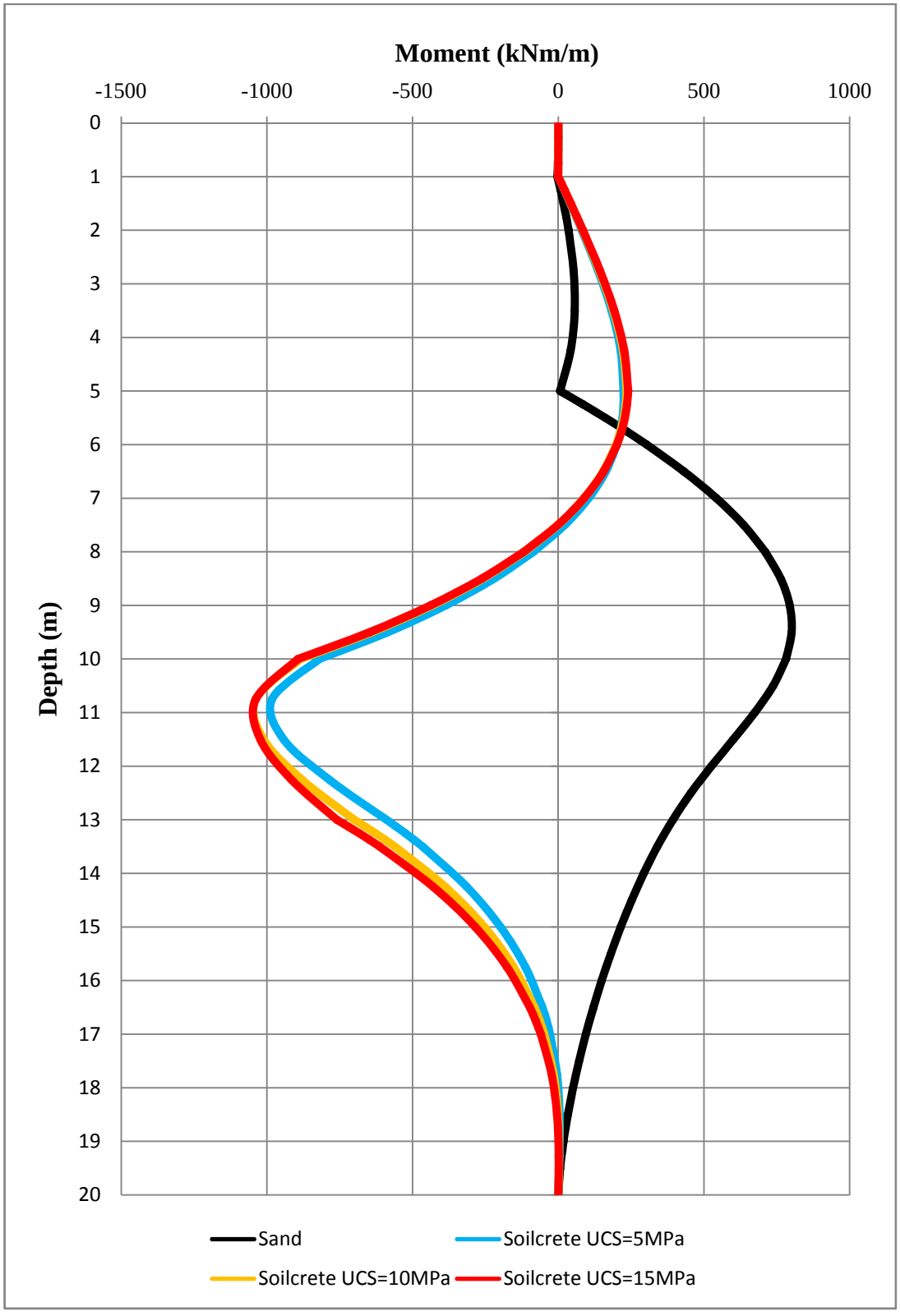

Figure A-7 Diaphragm wall moments according to USC for location II, sand profile

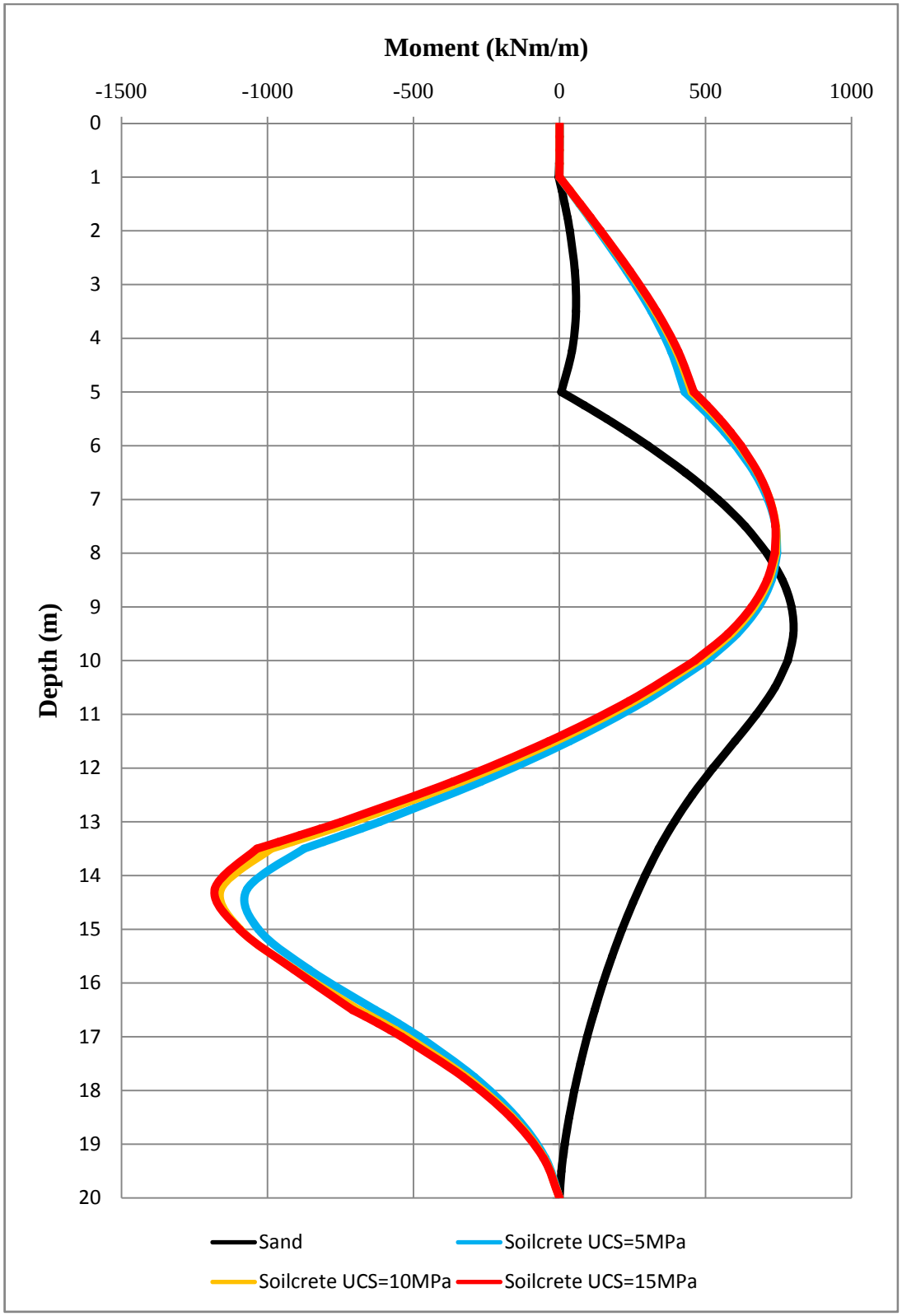

Figure A-8 Diaphragm wall moments according to USC for location III, sand profile

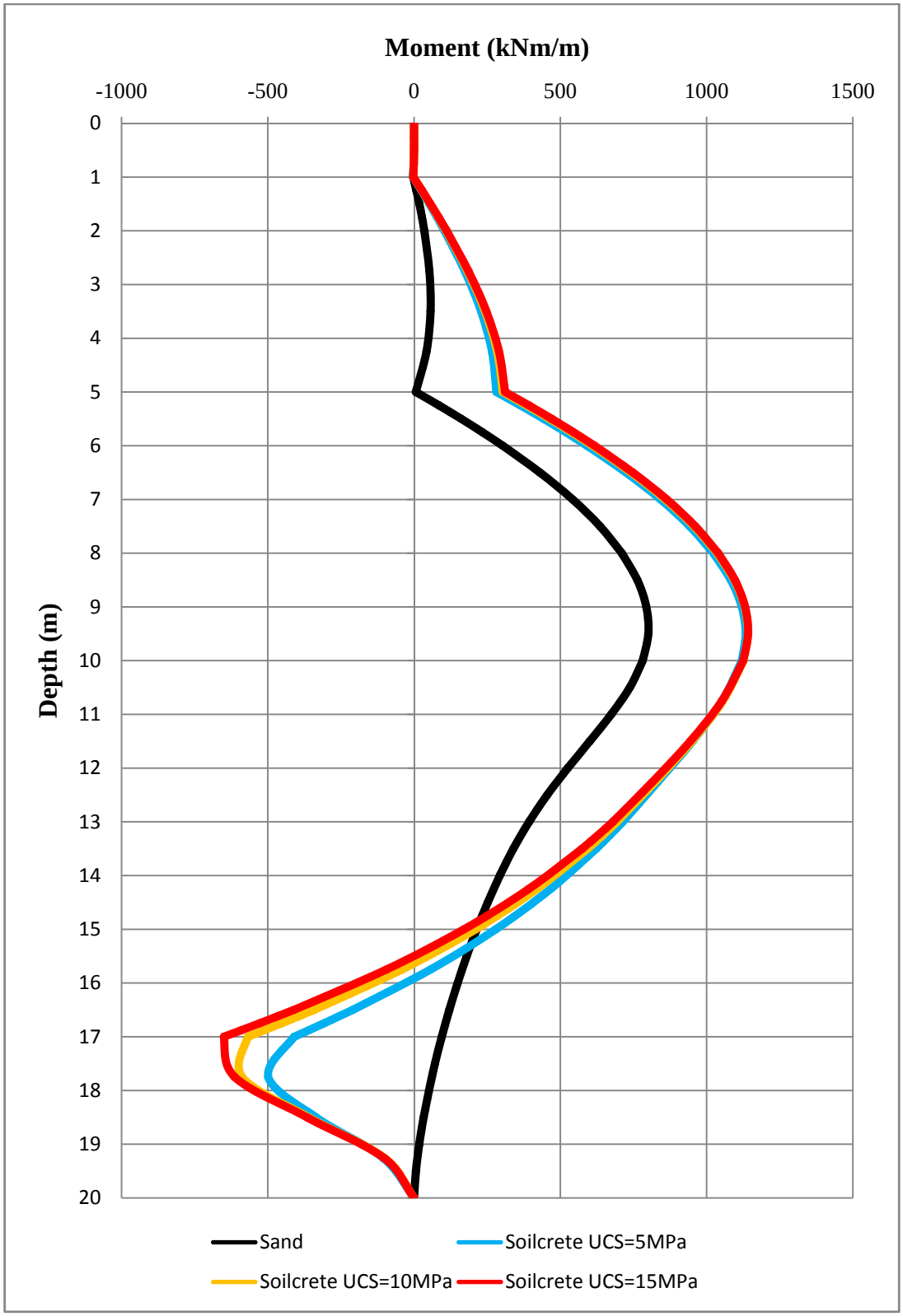

Figure A-9 Diaphragm wall moments according to USC for location IV, sand profile

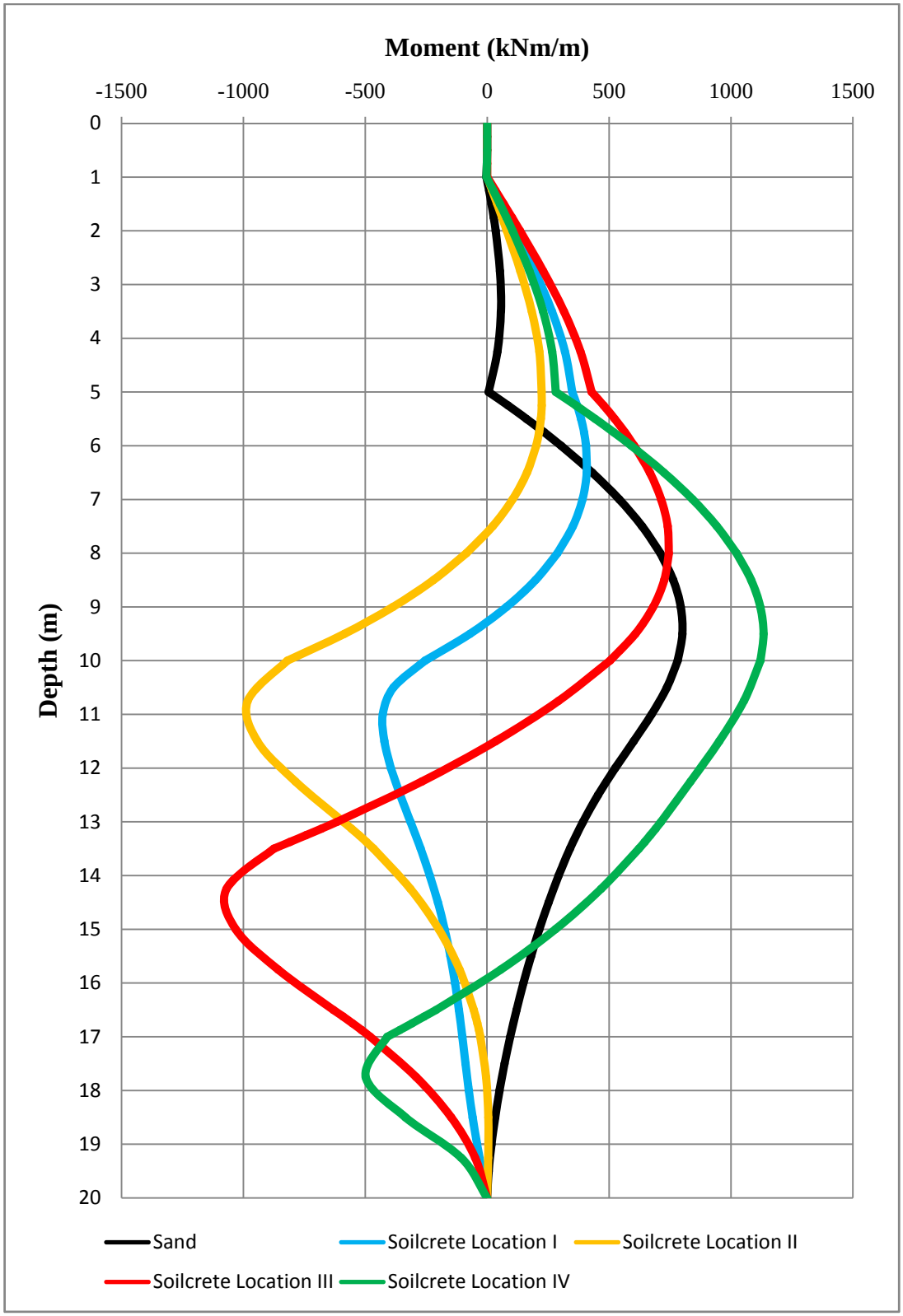

Figure A-10 Diaphragm wall moments according to location types for the UCS=5 MPa, sand profile

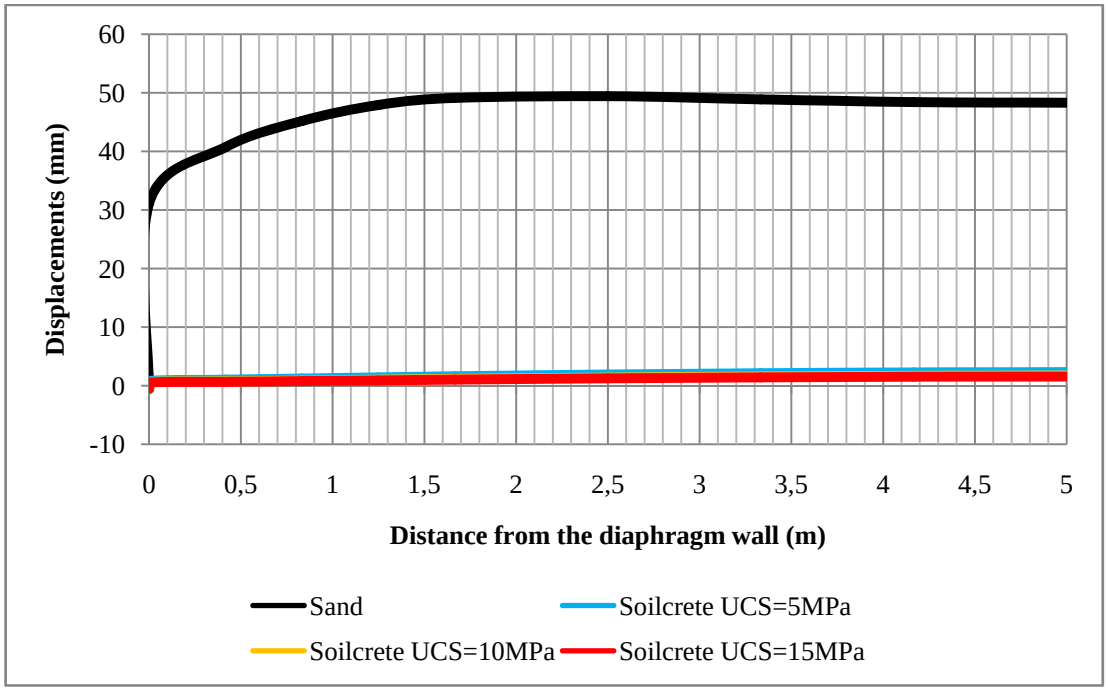

Figure A-11 Vertical displacements on the excavation level according to UCS for location I, sand profile

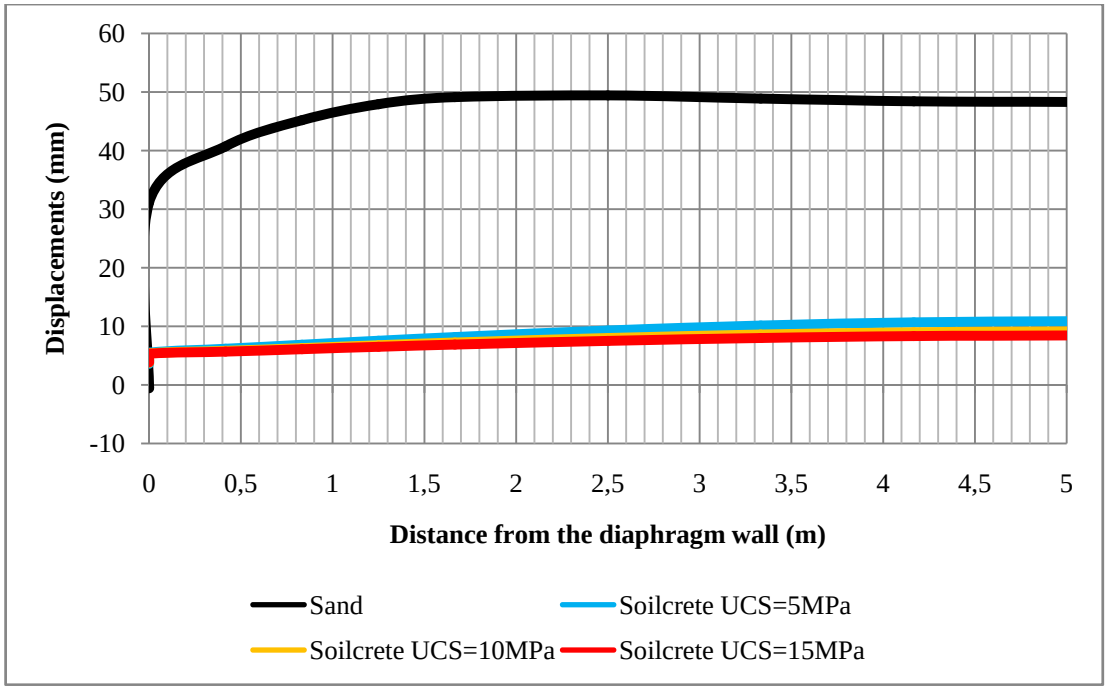

Figure A-12 Vertical displacements on the excavation level according to UCS for location II, sand profile

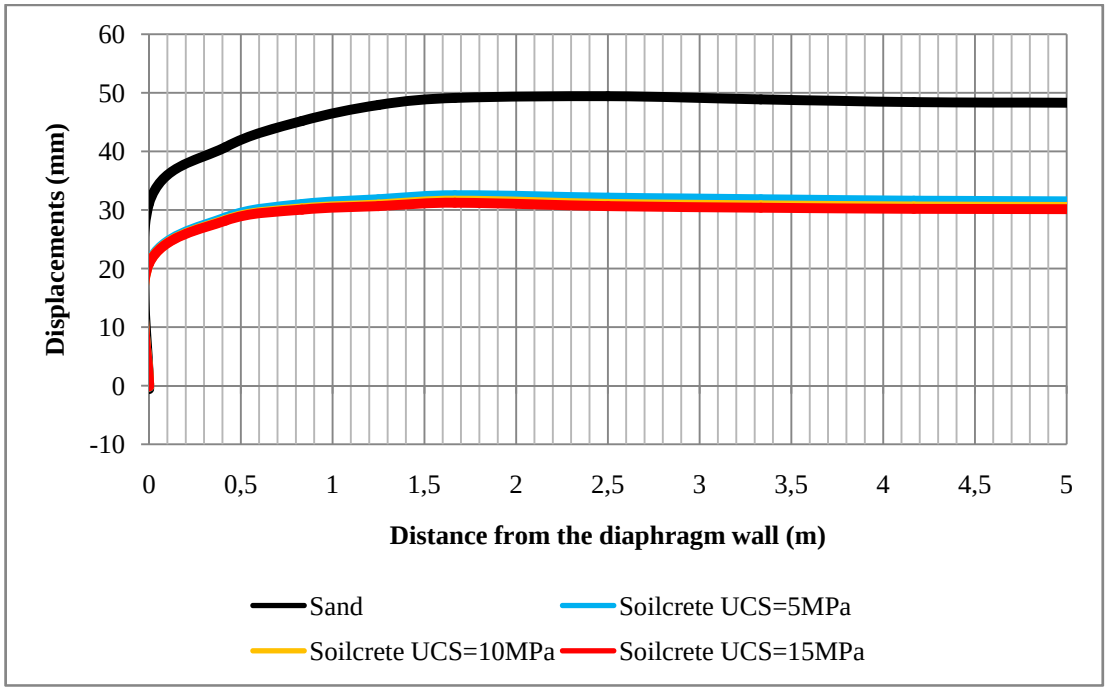

Figure A-13 Vertical displacements on the excavation level according to UCS for location III, sand profile

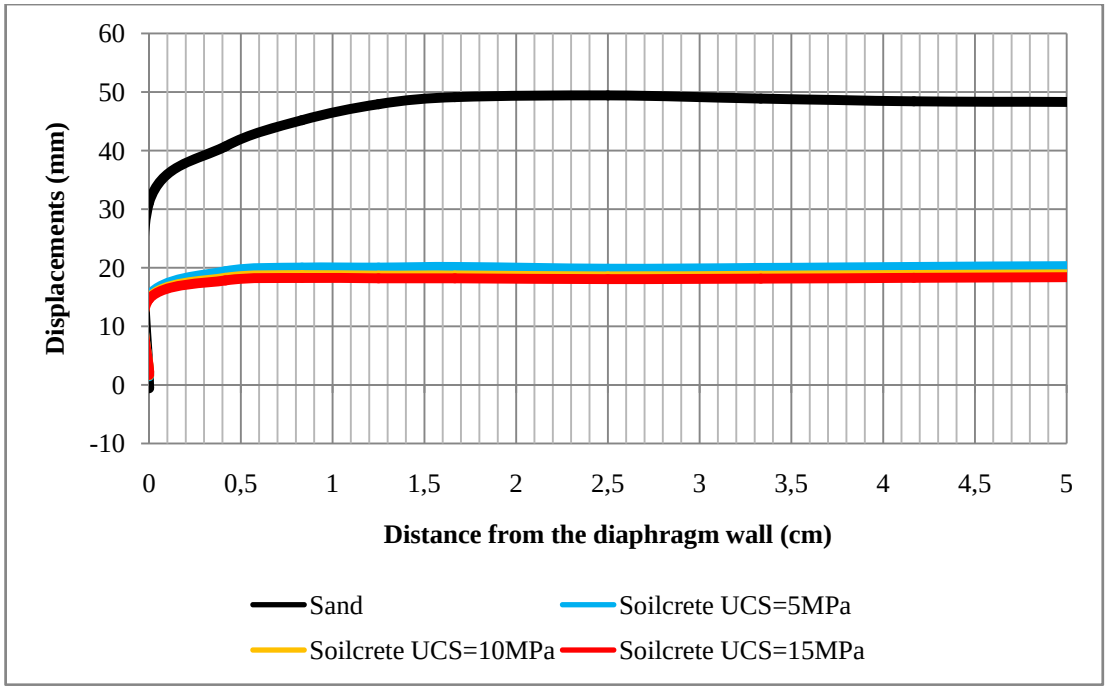

Figure A-14 Vertical displacements on the excavation level according to UCS for location IV, sand profile

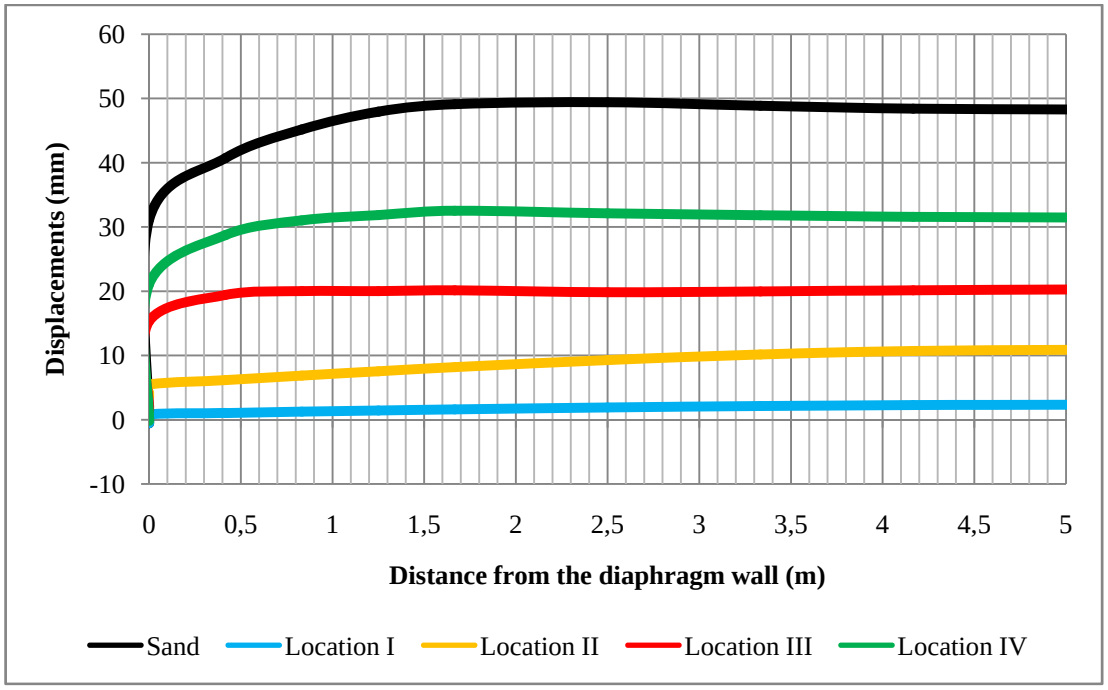

Figure A-15 Vertical displacements on the excavation level according to location types for UCS=5 MPa, sand profile

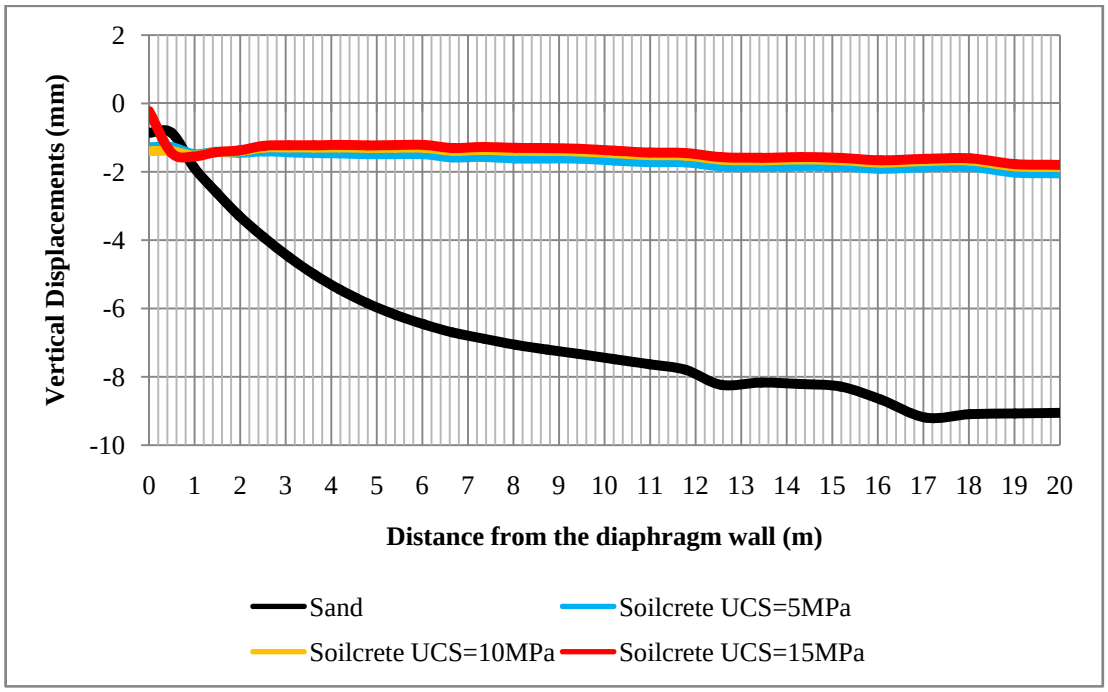

Figure A-16 Vertical displacements behind the diaphragm wall according to UCS for the location I, sand profile

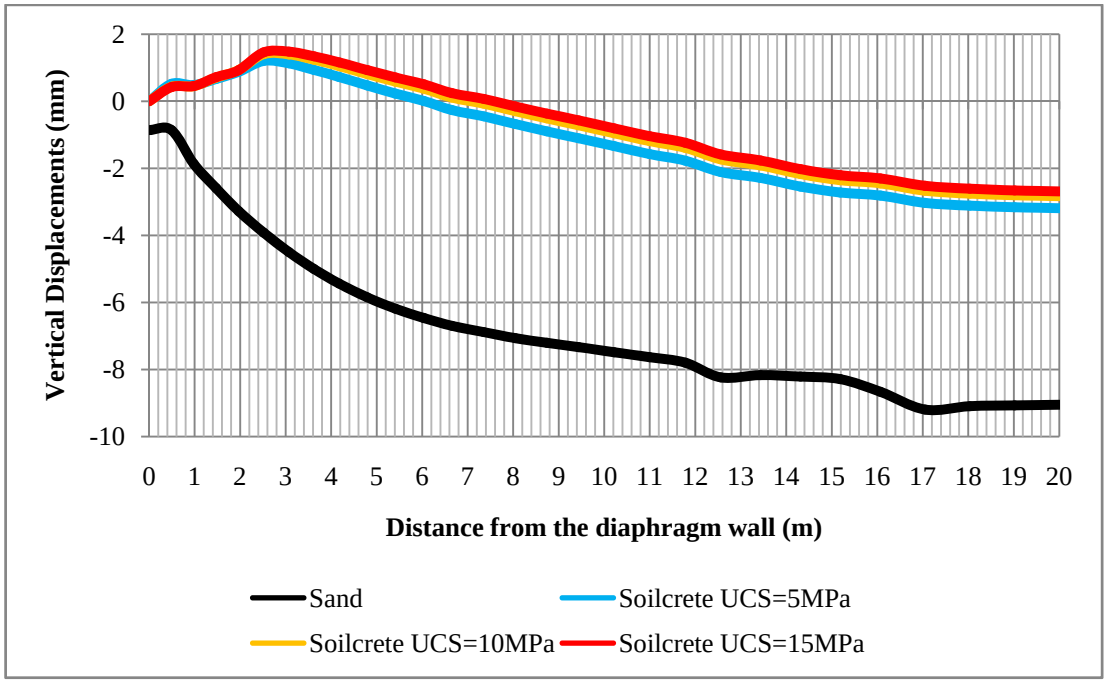

Figure A-17 Vertical displacements behind the diaphragm wall according to UCS for the location II, sand profile

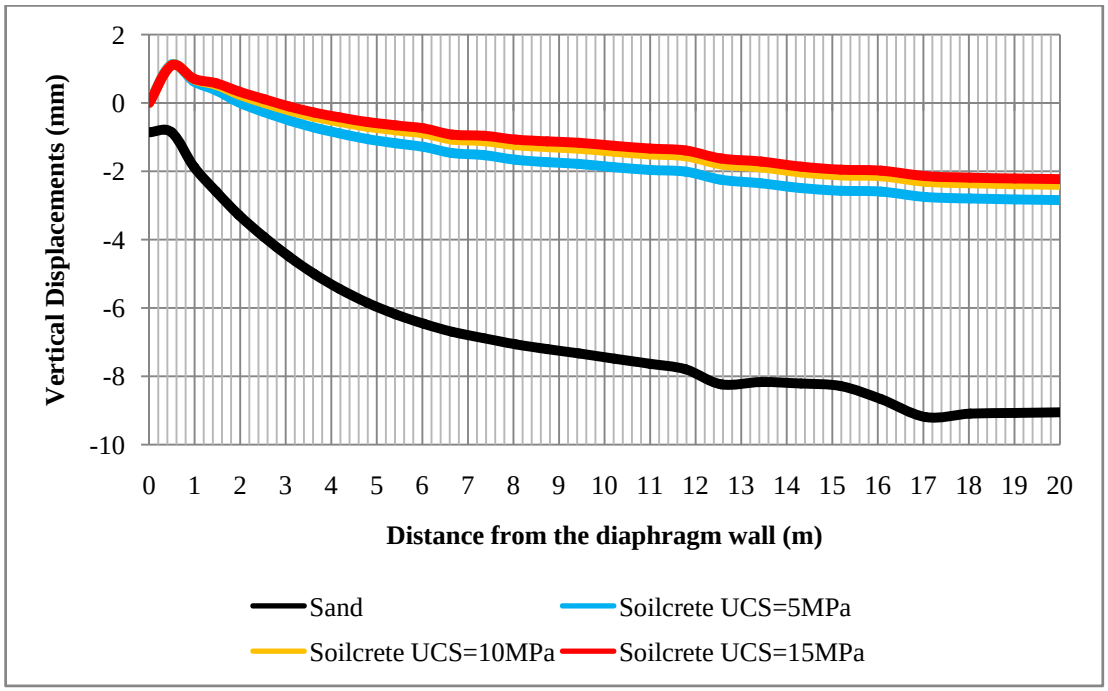

Figure A-18 Vertical displacements behind the diaphragm wall according to UCS for the location III, sand profile

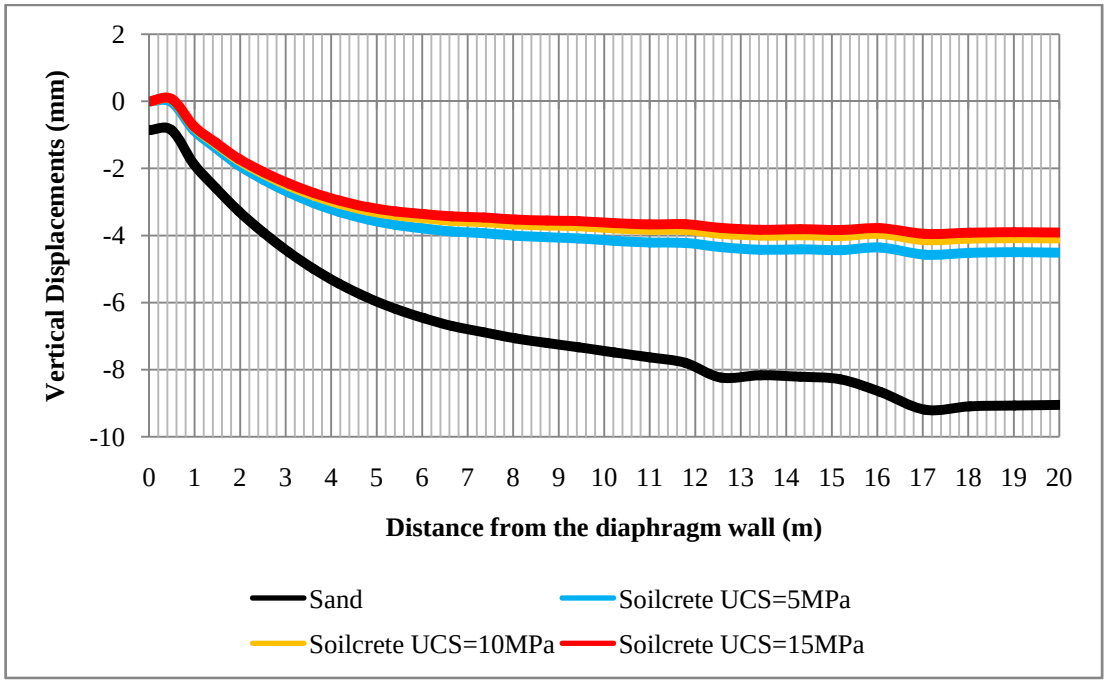

Figure A-19 Vertical displacements behind the diaphragm wall according to UCS for the location IV, sand profile

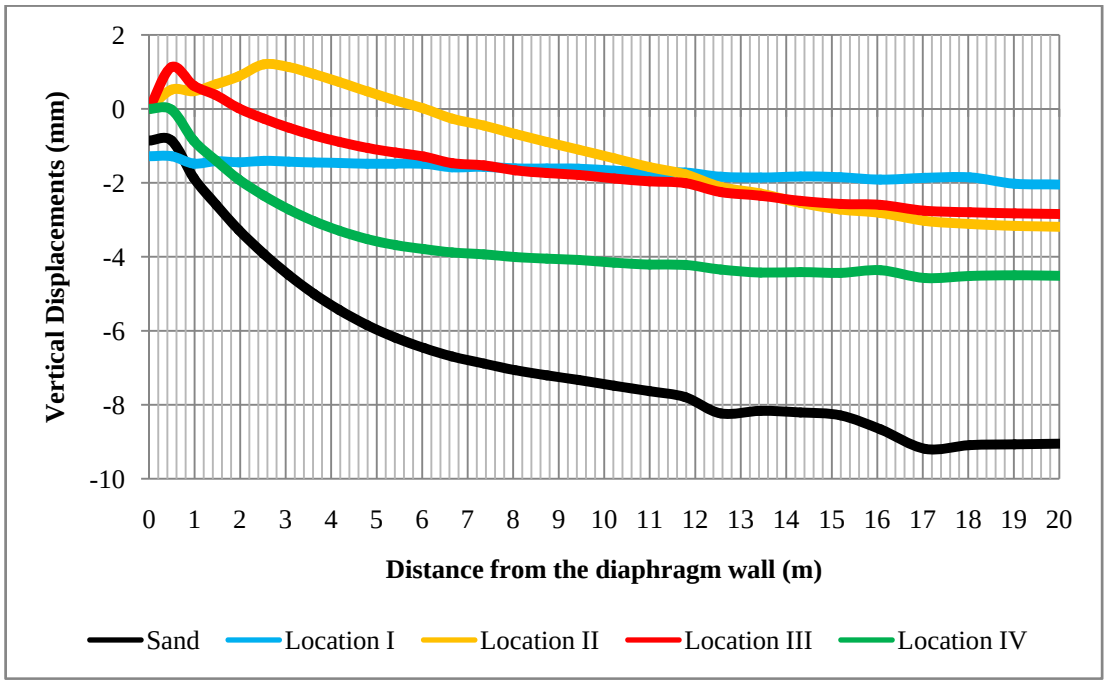

Figure A-20 Vertical displacements behind the diaphragm wall on the ground surface according to location types for UCS=5 MPa, sand profile

APPENDIX B

DISPLACEMENTS AND MOMENTS CURVES

FOR THE CLAY PROFILE

(PLAXIS 3D, MOHR COULOMB SOIL MODEL)

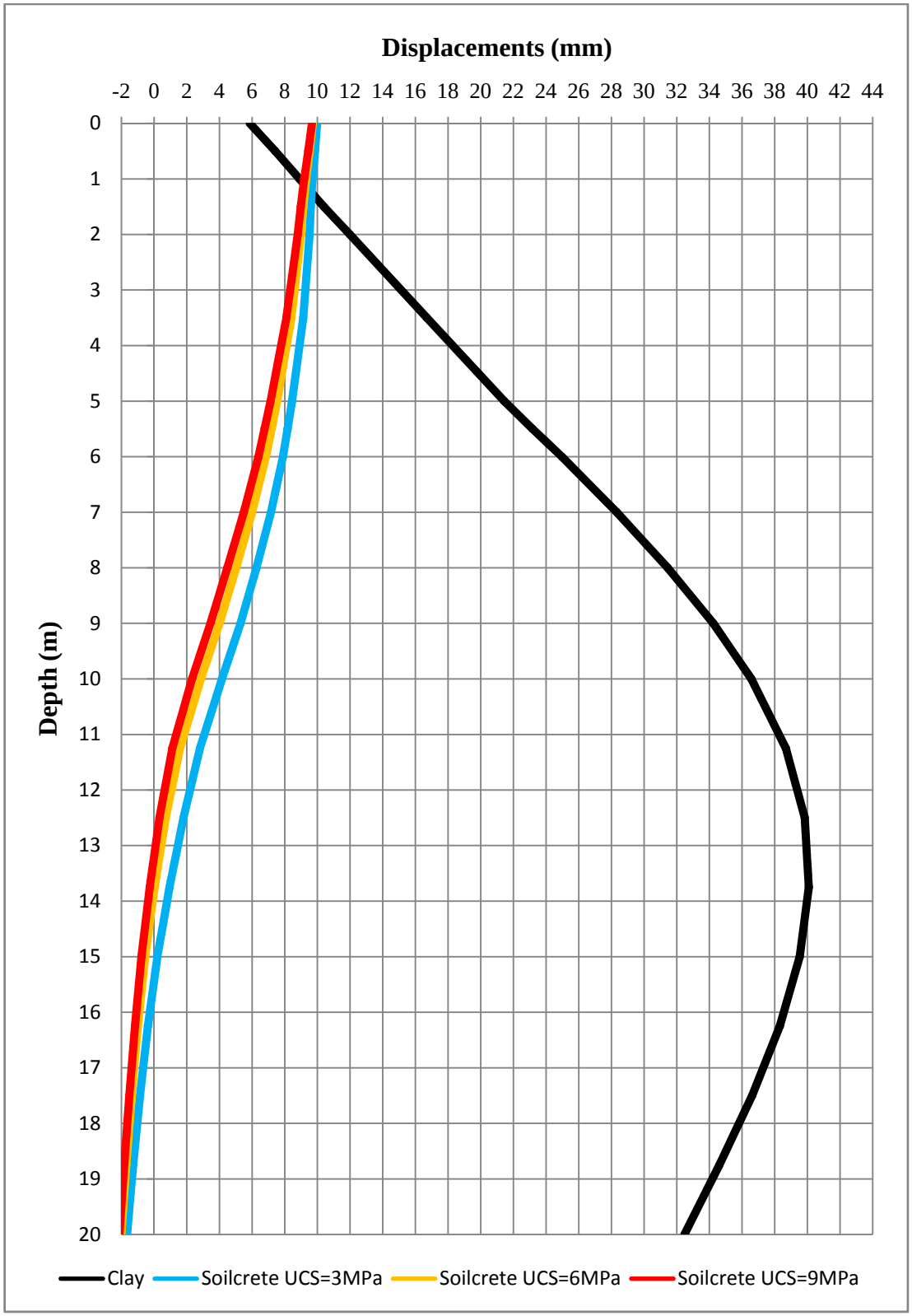

Figure B-1 Diaphragm wall displacements according to USC on the clay profile (Location I)

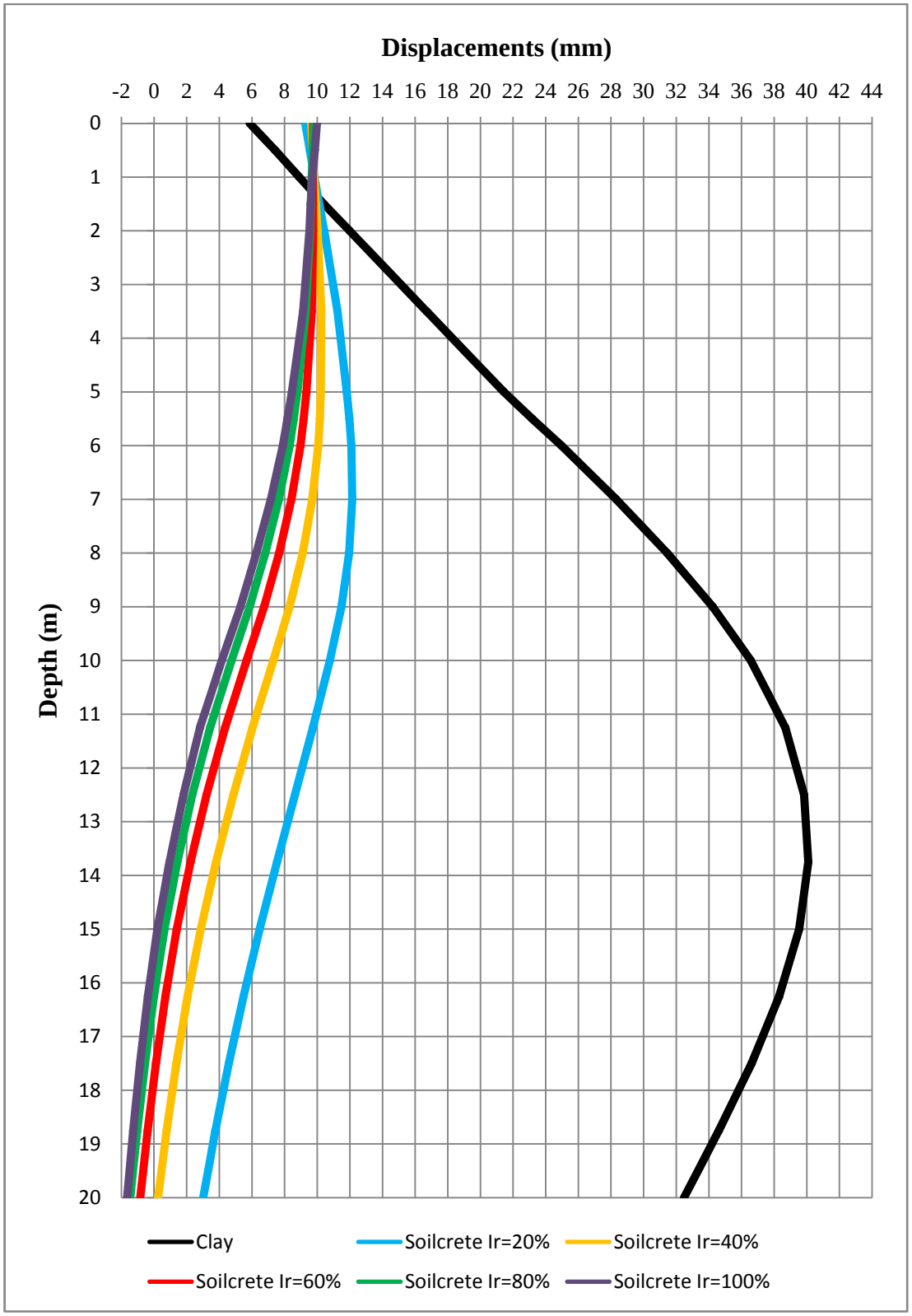

Figure B-2 Diaphragm wall displacements according to treated soil area ratio (I_r) for pattern I and USC= 3MPa, clay profile, Location I.

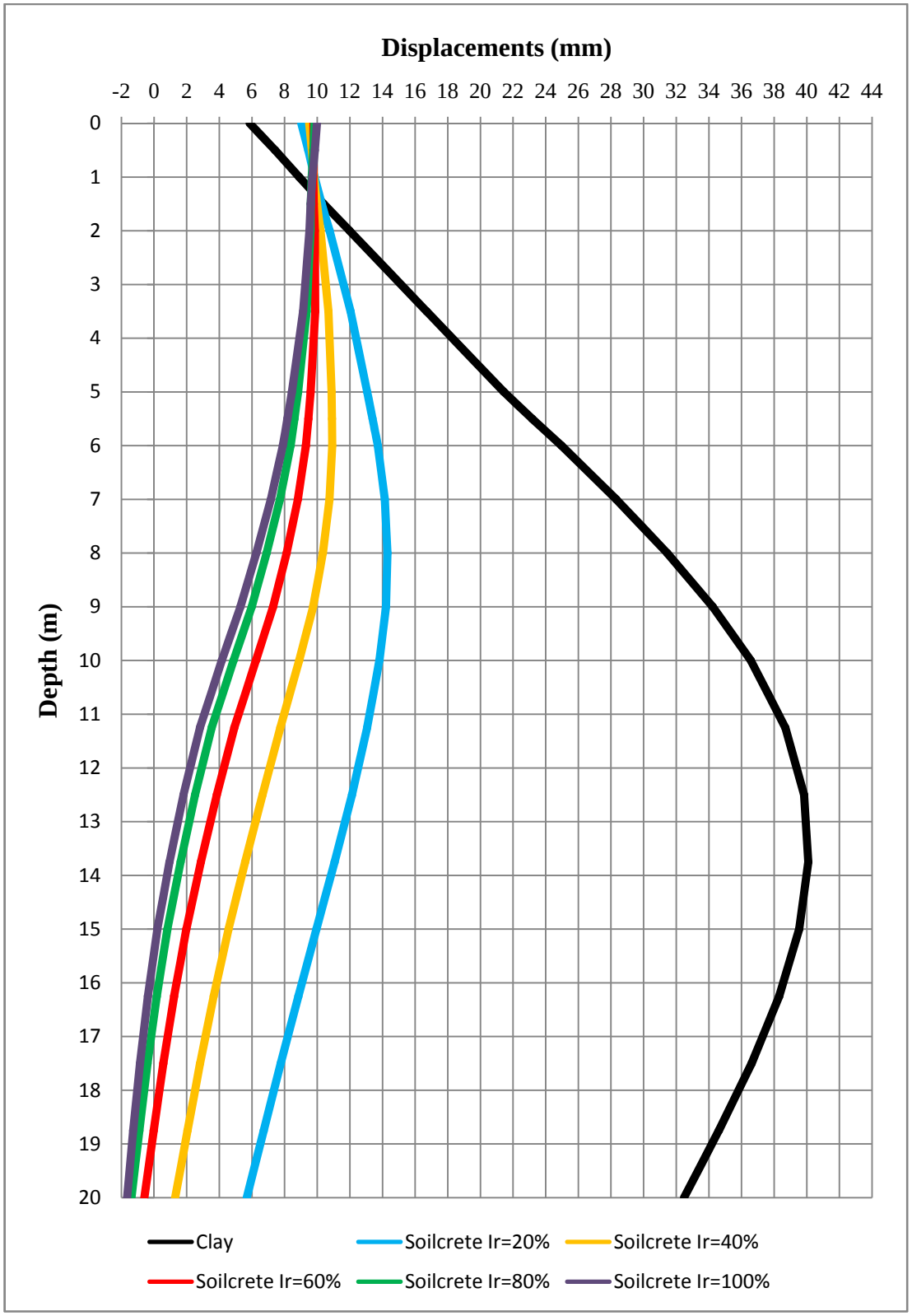

Figure B-3 Diaphragm wall displacements according to treated soil area ratio (I_r) for pattern II and USC= 3MPa, clay profile, Location I.

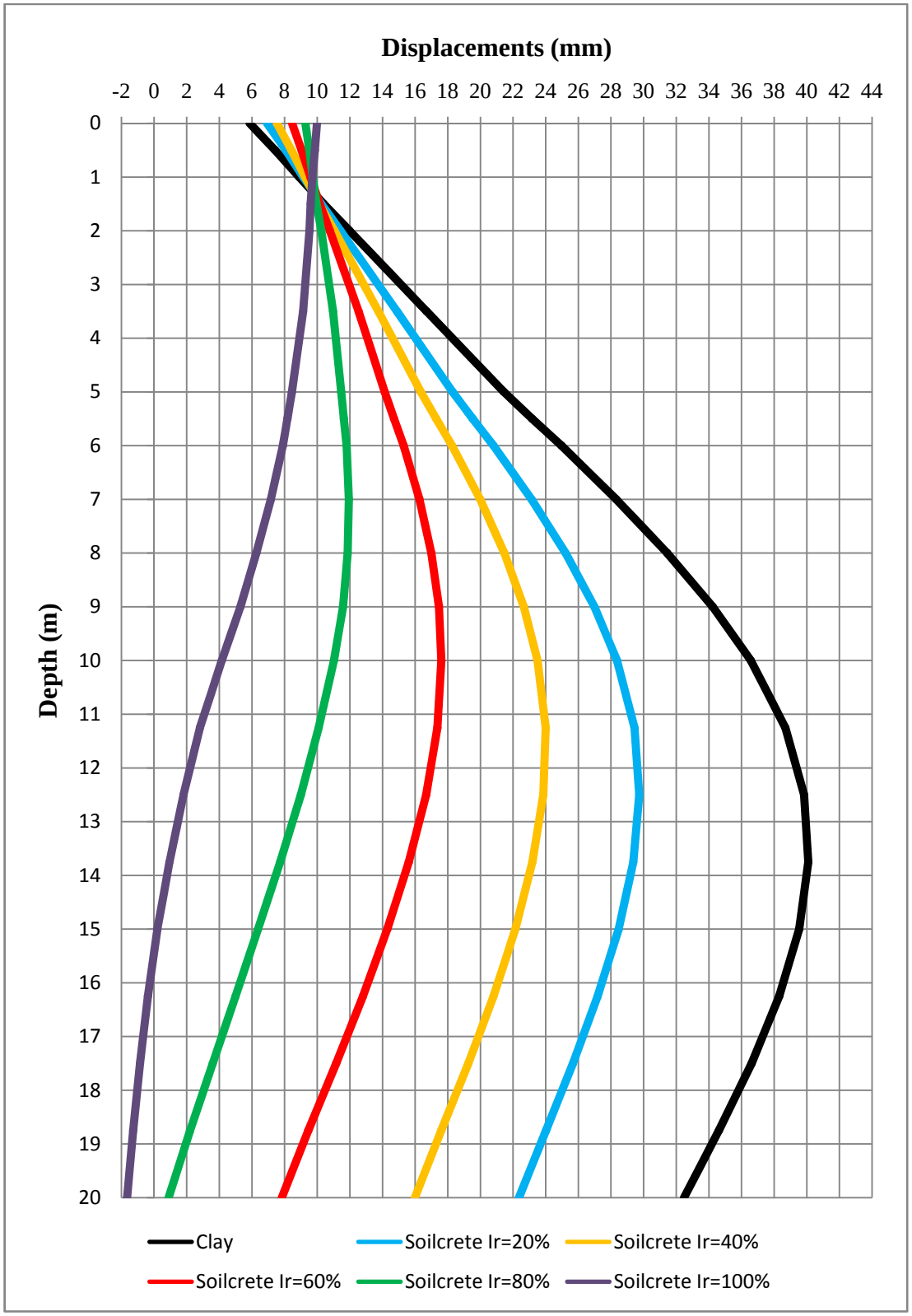

Figure B-4 Diaphragm wall displacements according to treated soil area ratio (I_r) for pattern III and USC= 3MPa, clay profile, Location I.

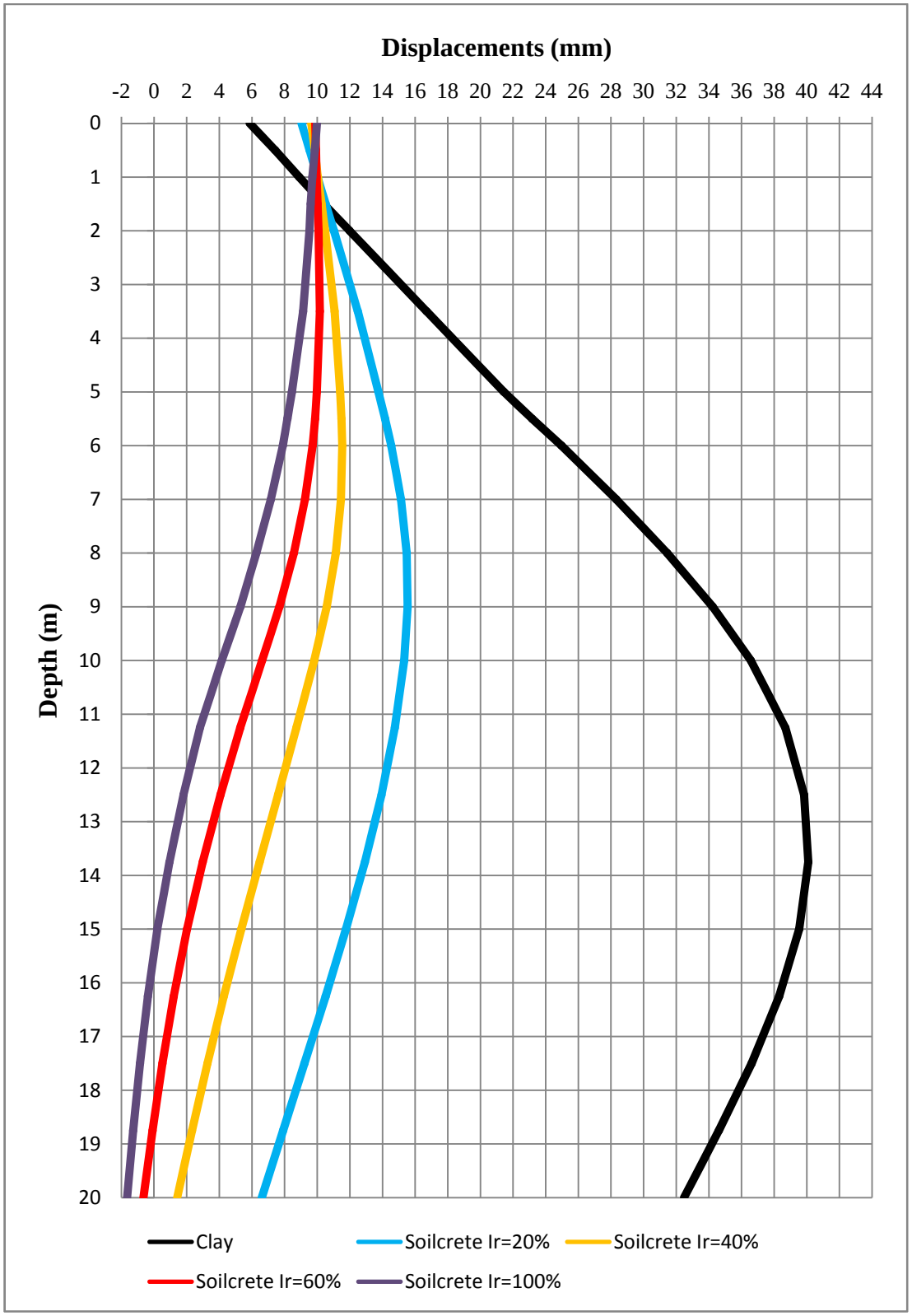

Figure B-5 Diaphragm wall displacements according to treated soil area ratio (I_r) for pattern IV and USC= 3MPa, clay profile, Location I.

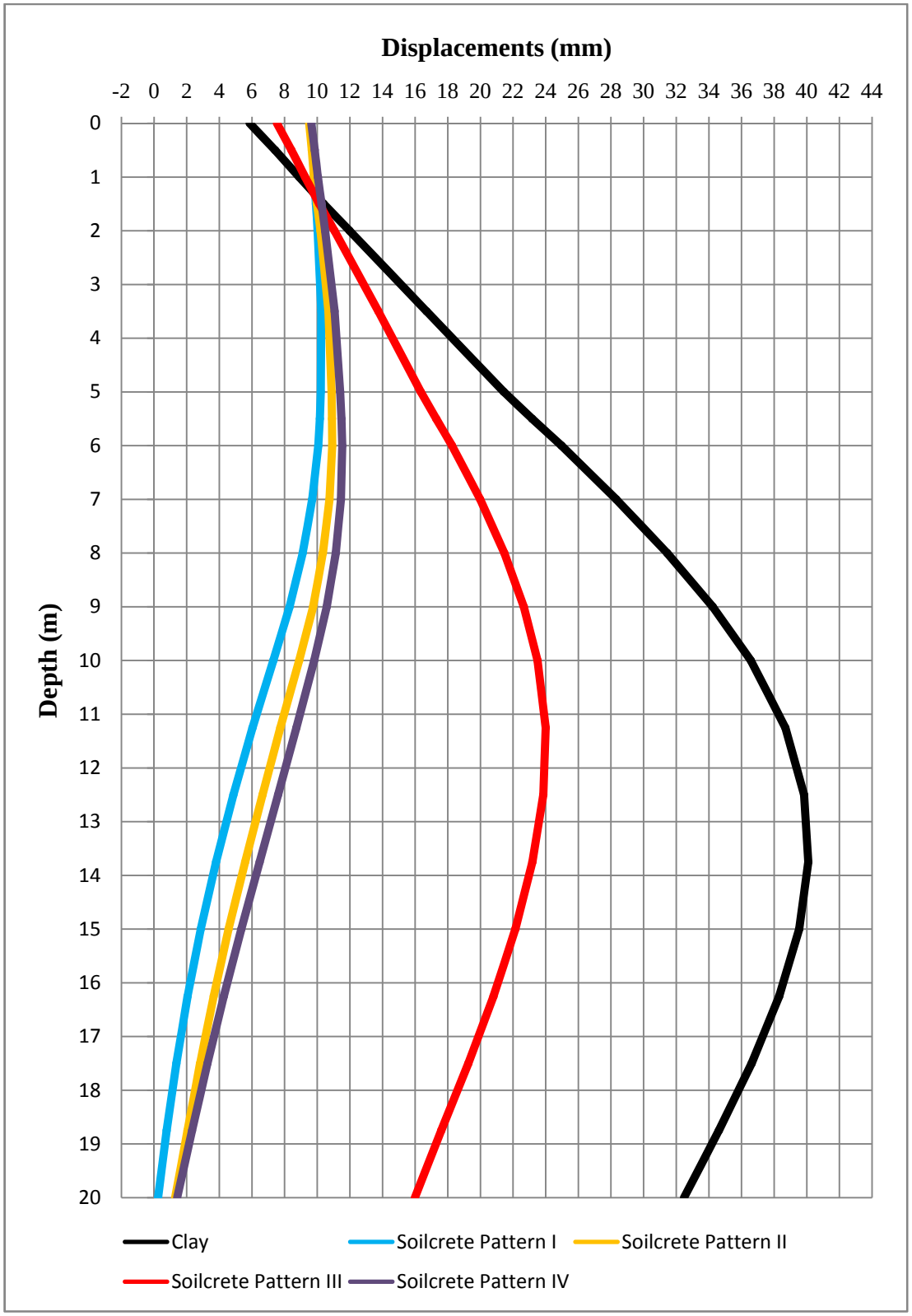

Figure B-6 Diaphragm wall lateral displacements according to pattern types for UCS= 3MPa, clay profile, Location I, I_r=40%

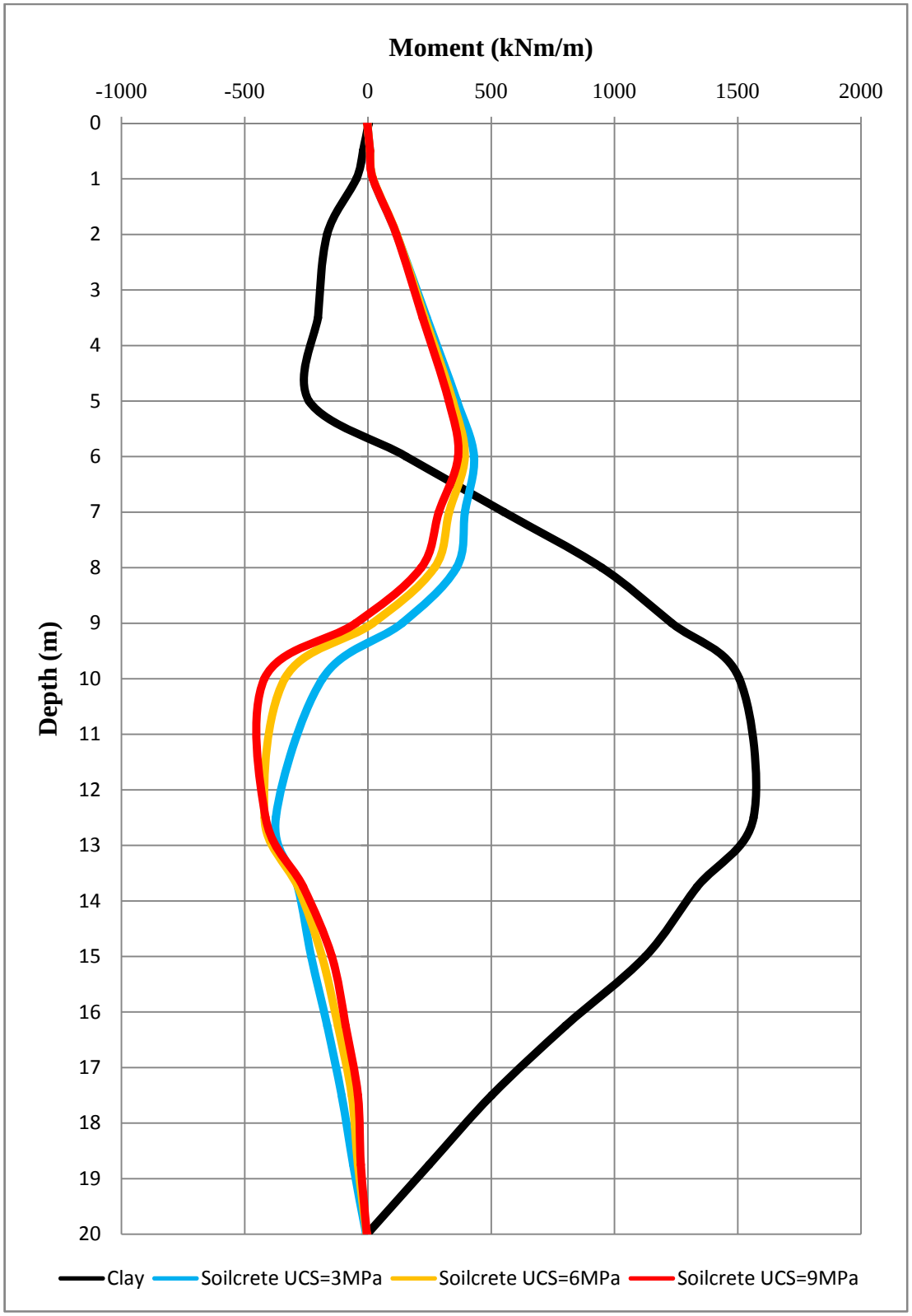

Figure B-7 Diaphragm wall moments displacements according to UCS, clay profile, Location I, I_r=100%

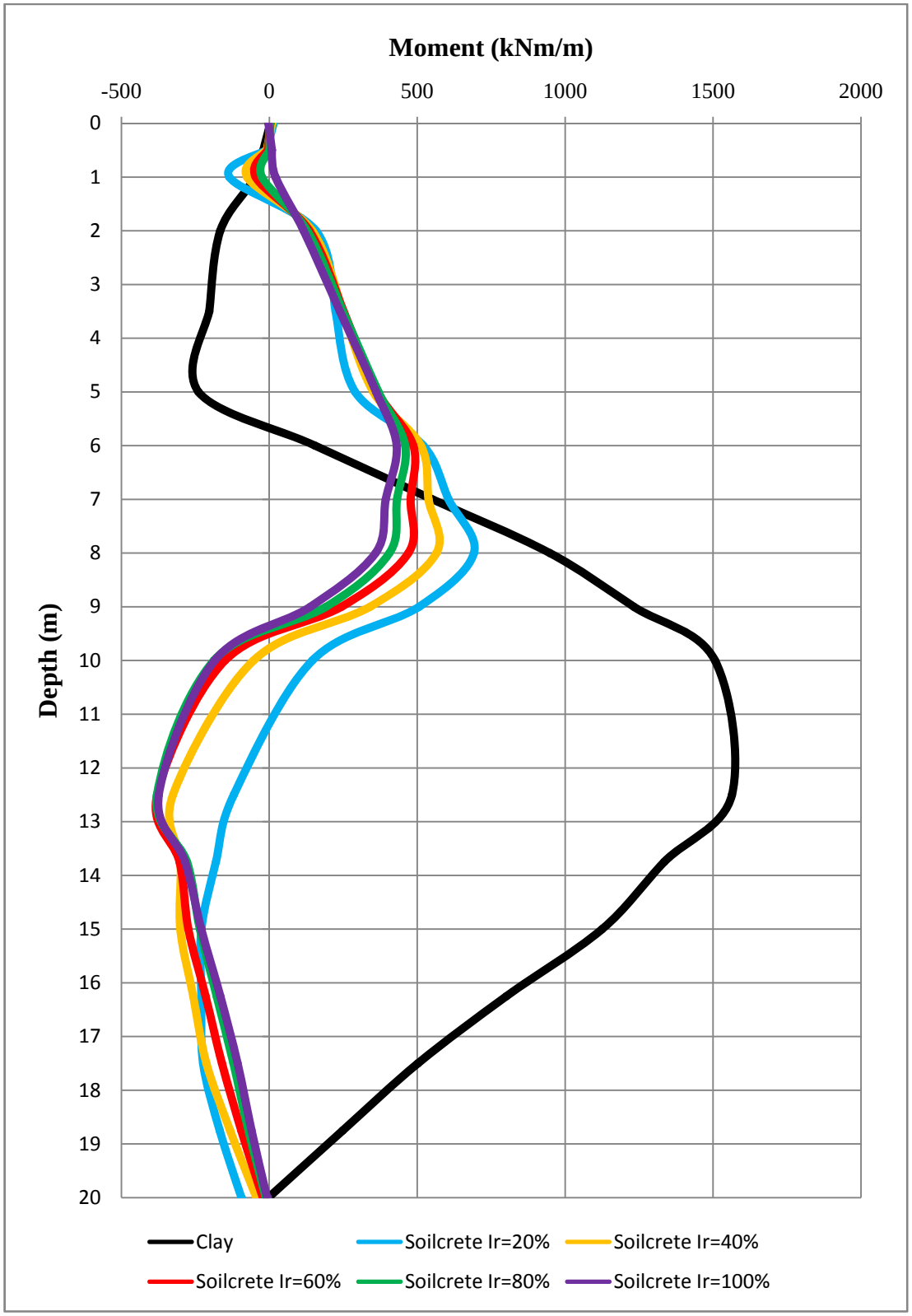

Figure B-8 Diaphragm wall moments according to treated soil area ratio (I_r) for pattern I and UCS= 3 MPa, clay profile, Location I

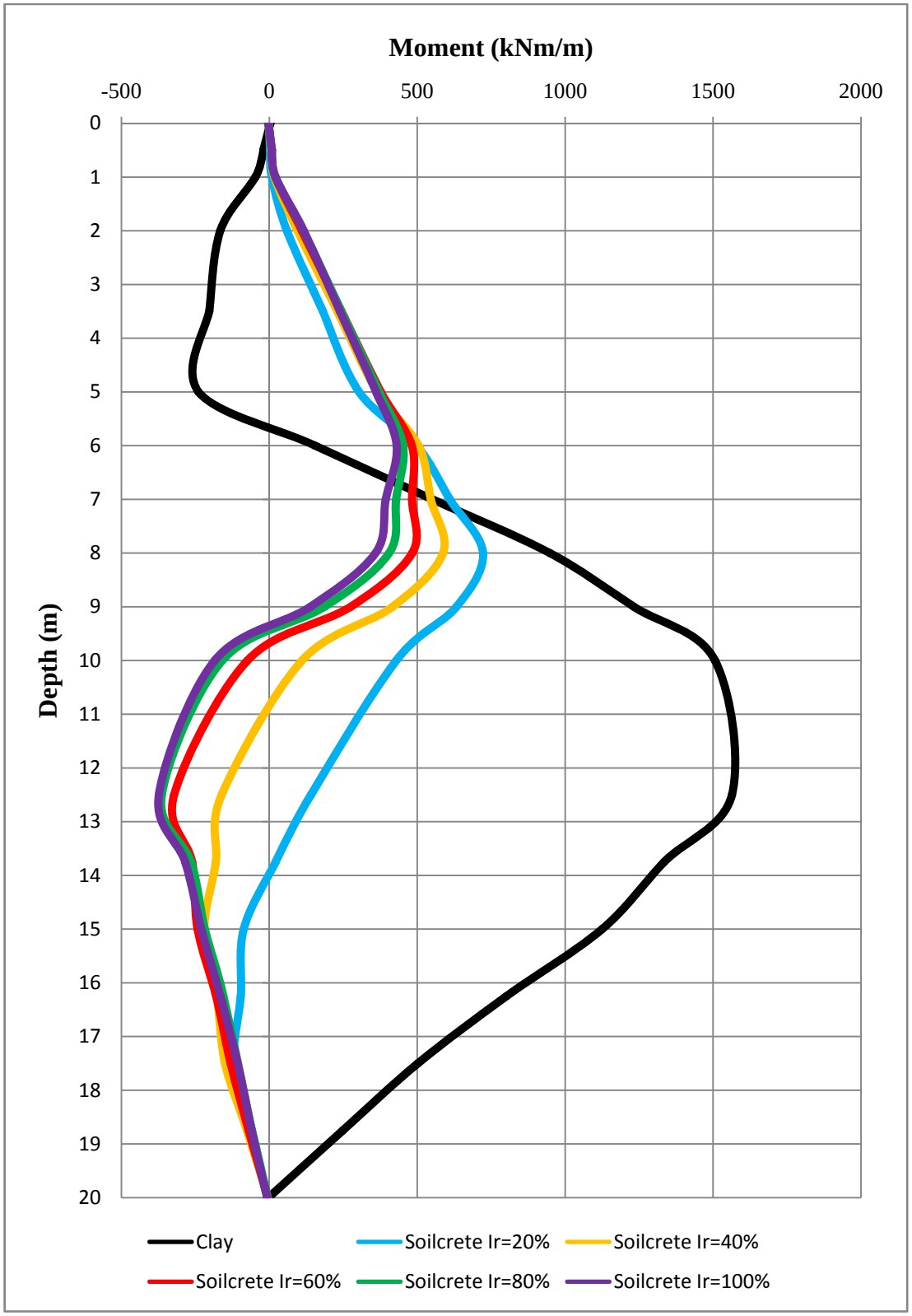

Figure B-9 Diaphragm wall moments according to treated soil area ratio (I_r) for pattern II and UCS= 3 MPa, clay profile, Location I

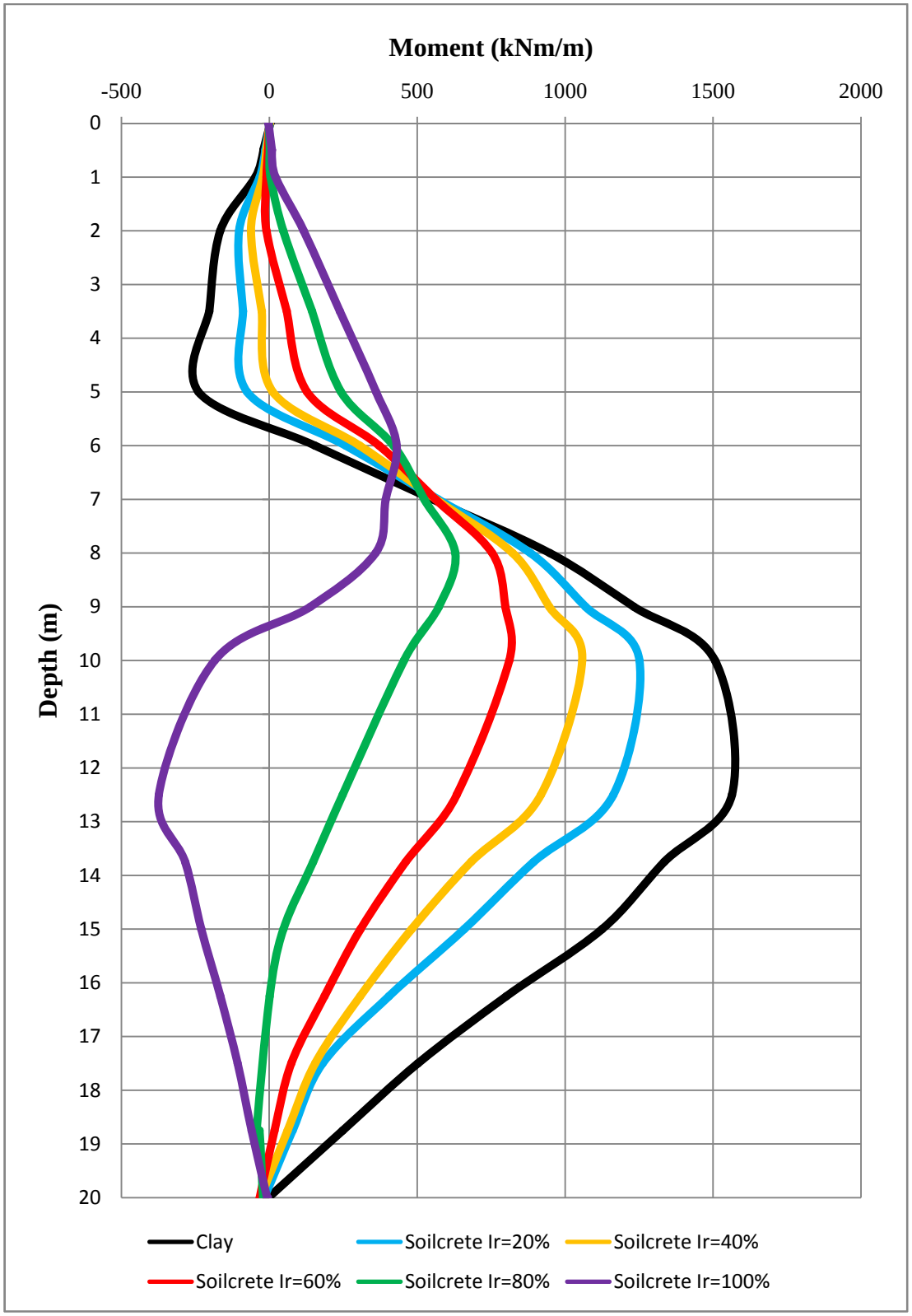

Figure B-10 Diaphragm wall moments according to treated soil area ratio (I_r) for pattern III and UCS= 3 MPa, clay profile, Location I

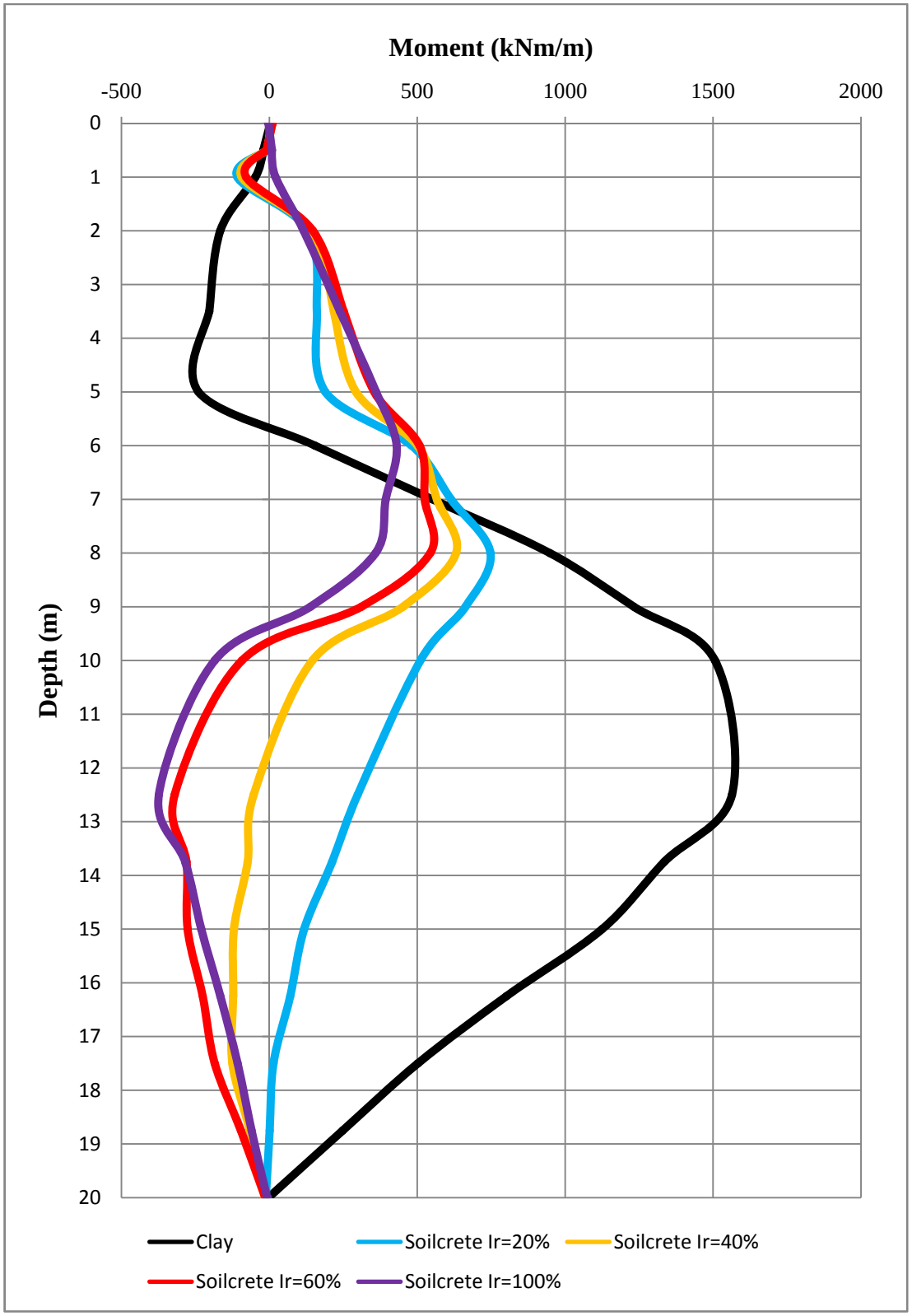

Figure B-11 Diaphragm wall moments according to treated soil area ratio (I_r) for pattern IV and UCS= 3 MPa, clay profile, Location I

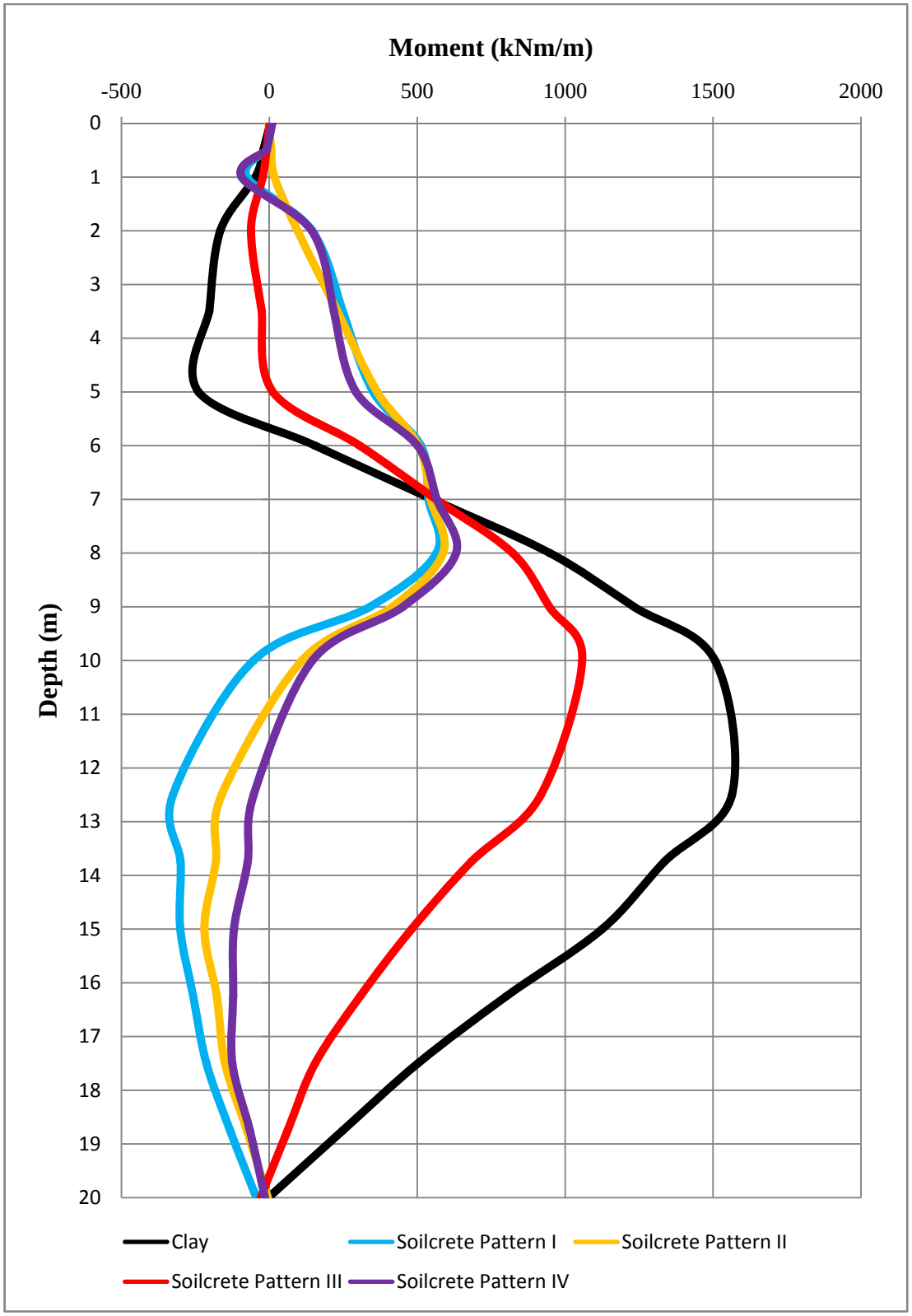

Figure B-12 Diaphragm wall moments according to pattern types for UCS= 3MPa, clay profile, Location I, I_r=40%

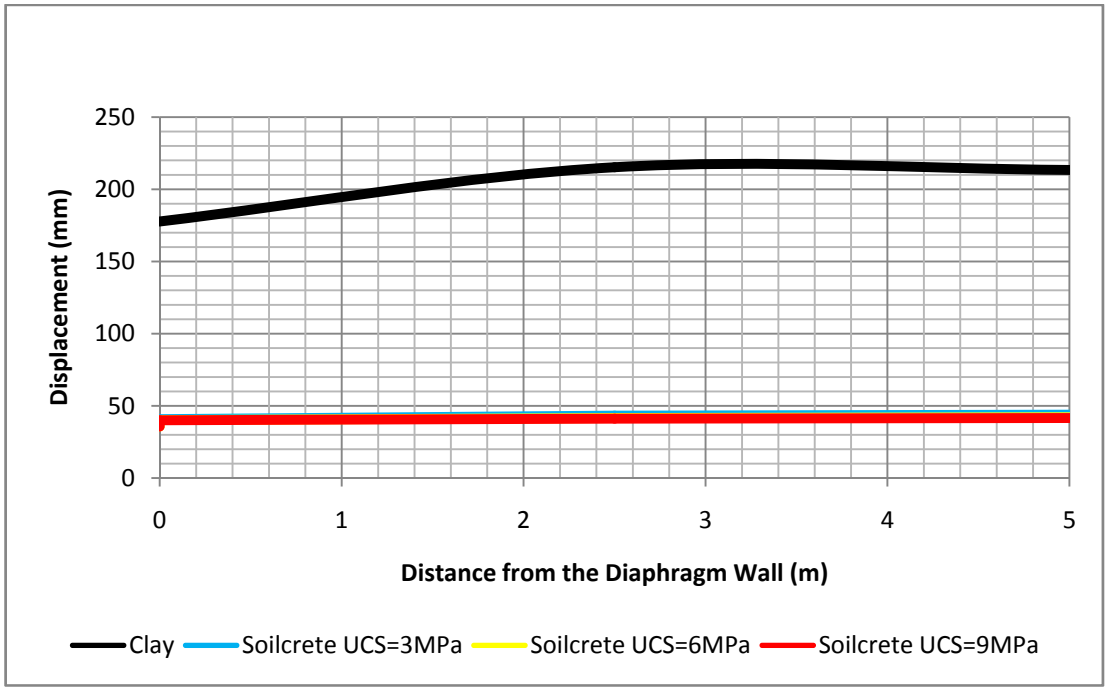

Figure B-13 Vertical displacements on the excavation level according to USC on the clay profile (Location I)

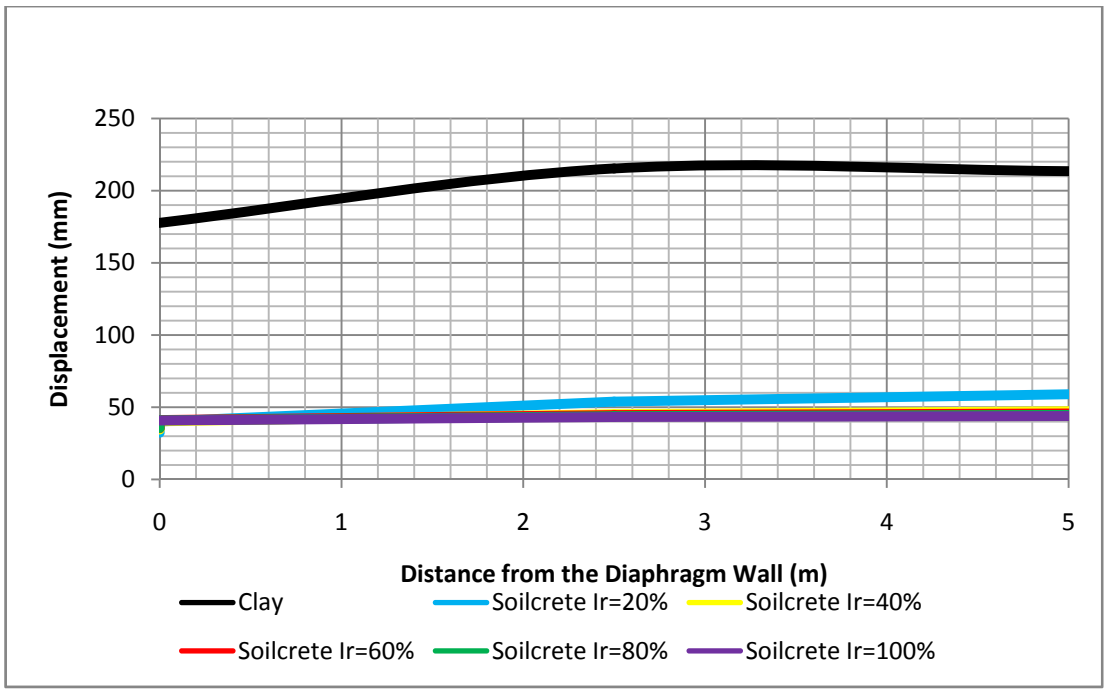

Figure B-14 Vertical displacements on the excavation level according to treated soil area ratio (I_r) for pattern I and UCS=3 MPa, clay profile, Location I

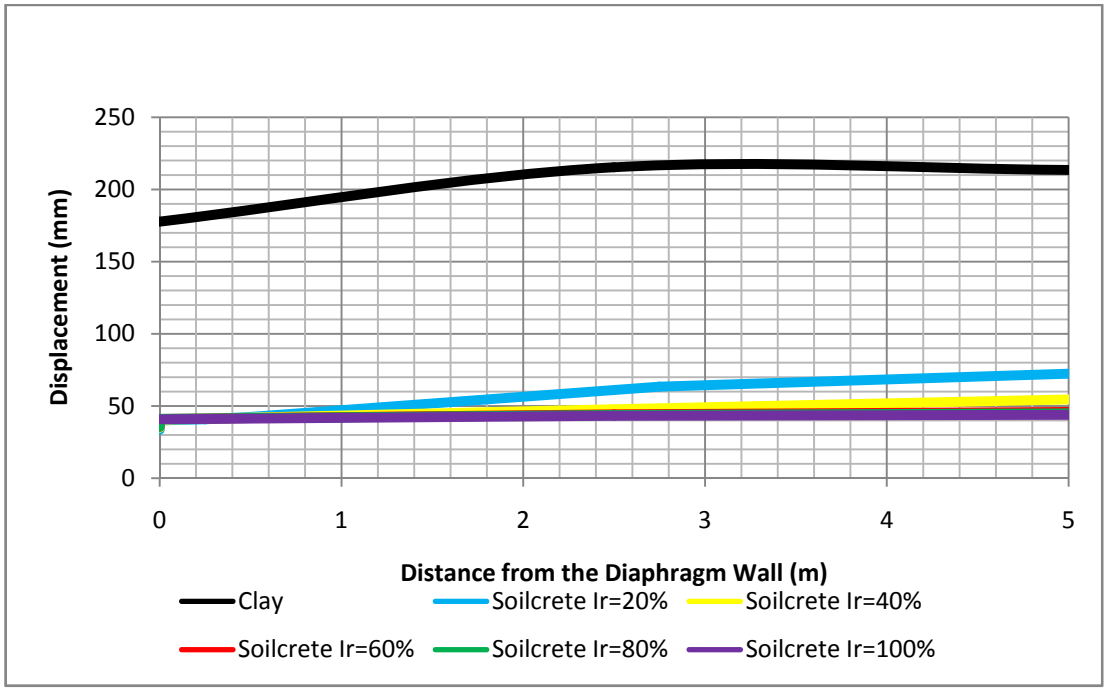

Figure B-15 Vertical displacements on the excavation level according to treated soil area ratio (I_r) for pattern II and UCS=3 MPa, clay profile, Location I

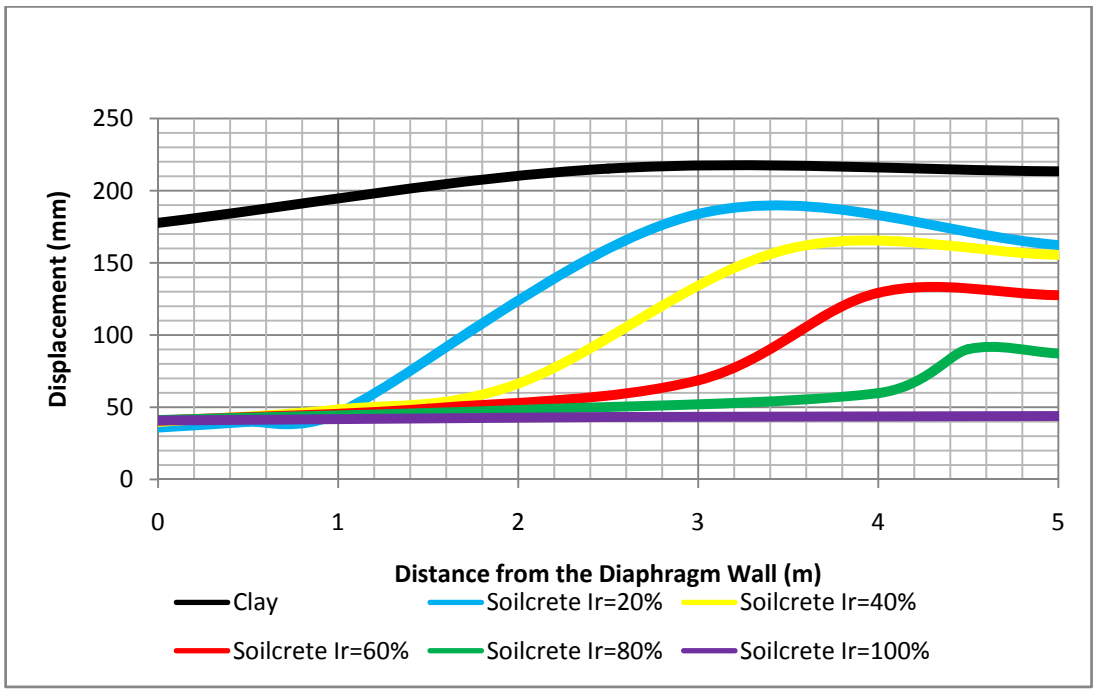

Figure B-16 Vertical displacements on the excavation level according to treated soil area ratio (I_r) for pattern III and UCS=3 MPa, clay profile, Location I

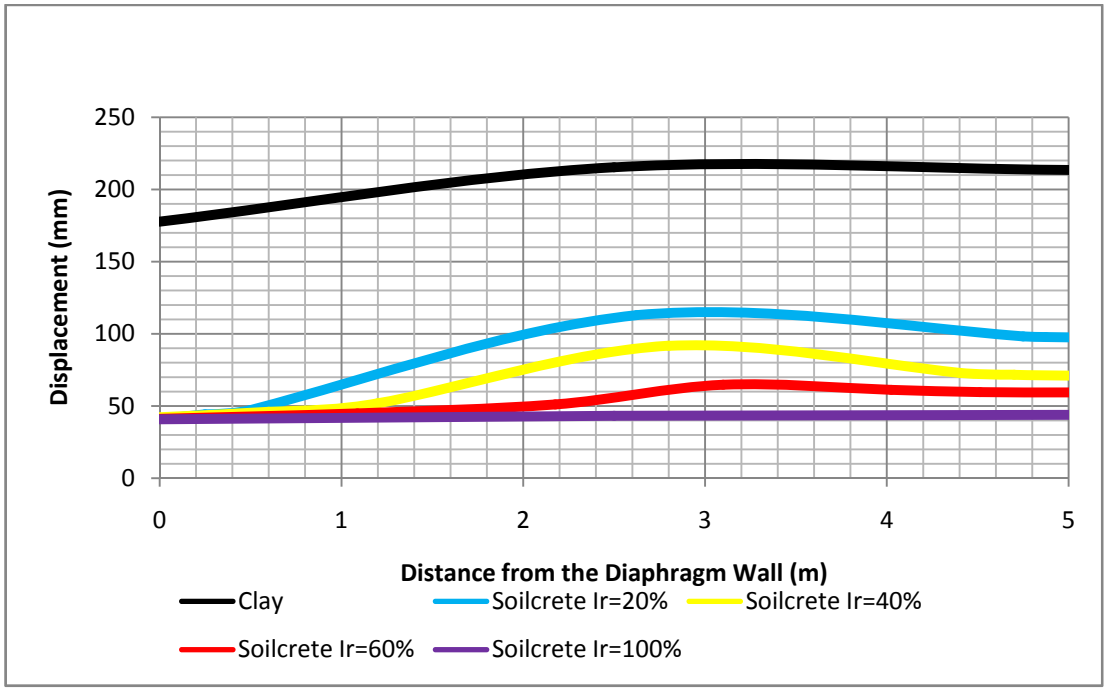

Figure B-17 Vertical displacements on the excavation level according to treated soil area ratio (I_r) for pattern IV and UCS=3 MPa, clay profile, Location I

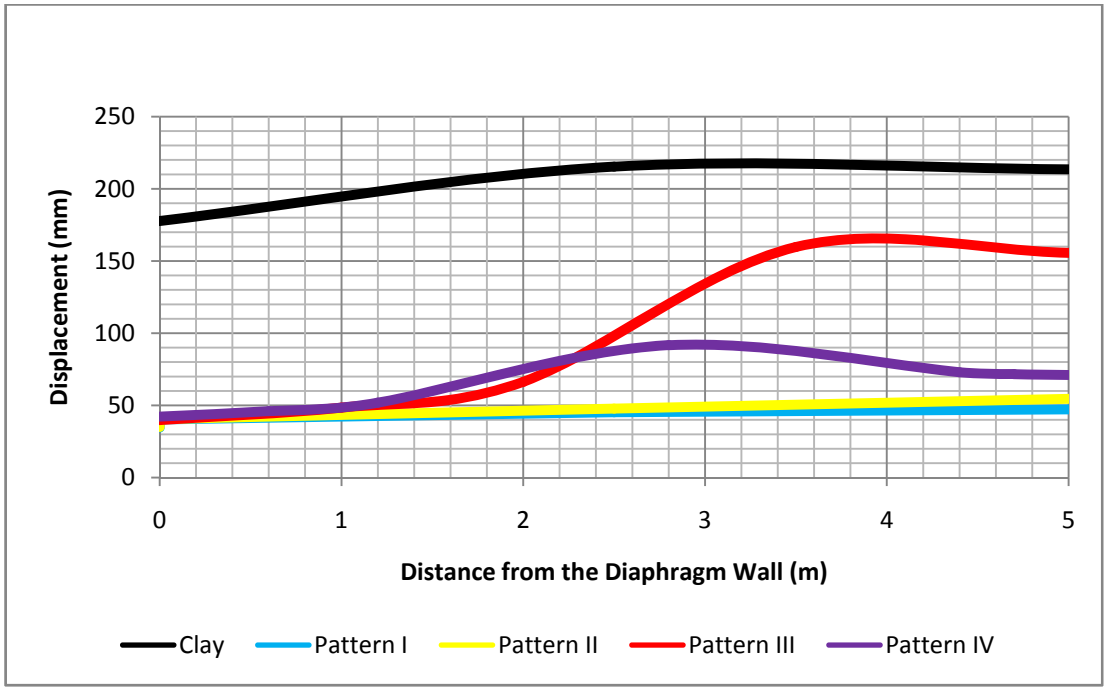

Figure B-18 Vertical displacements on the excavation level according to pattern types for UCS= 3 MPa, clay profile, Location I, Ir=40%

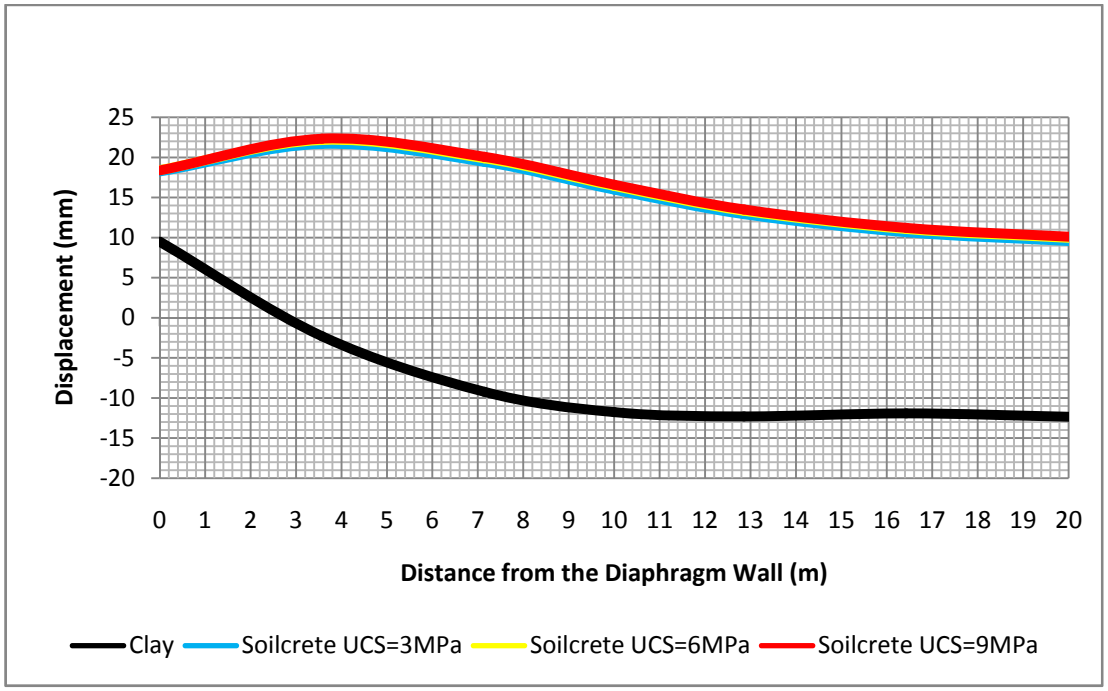

Figure B-19 Vertical displacements behind the diaphragm wall on the ground surface according to UCS, clay profile, Location I, Ir=100%

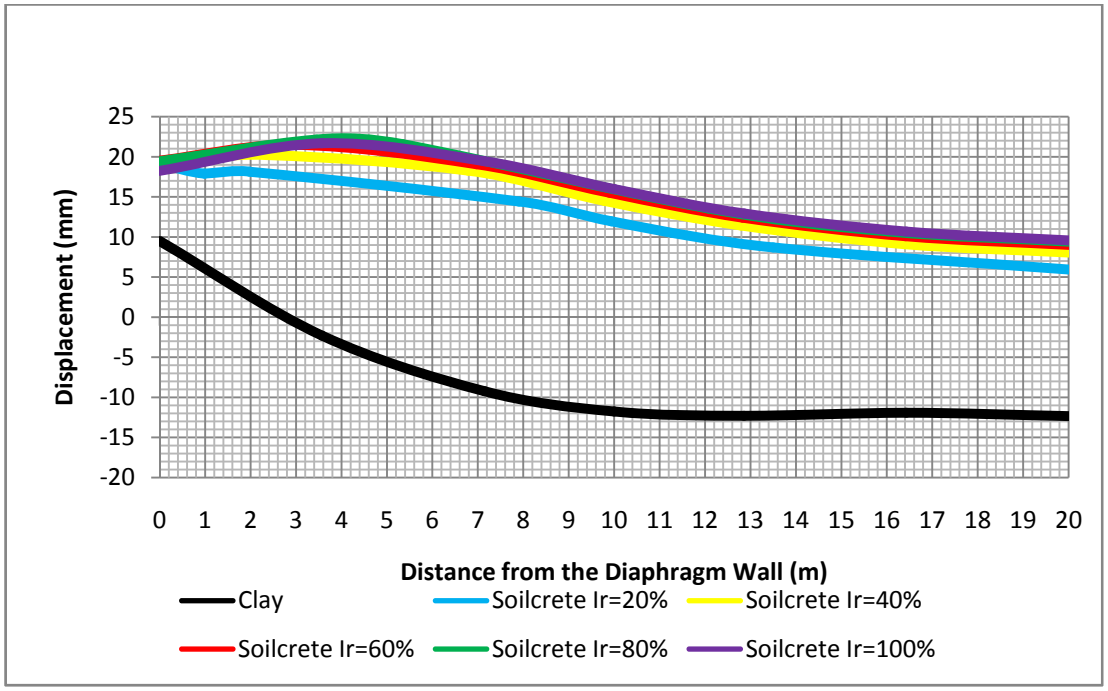

Figure B-20 Vertical displacements behind the diaphragm wall according to treated soil area ratio (I_r) for pattern I and UCS= 3 MPa, clay profile, Location I

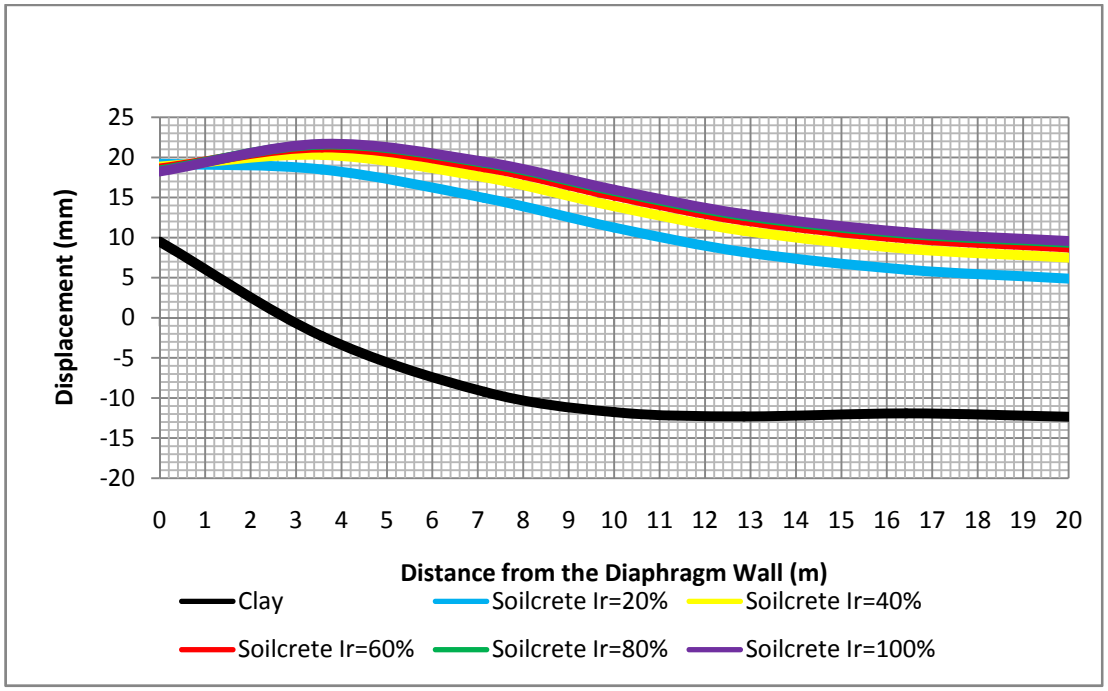

Figure B-21 Vertical displacements behind the diaphragm wall according to treated soil area ratio (I_r) for pattern II and UCS= 3 MPa, clay profile, Location I

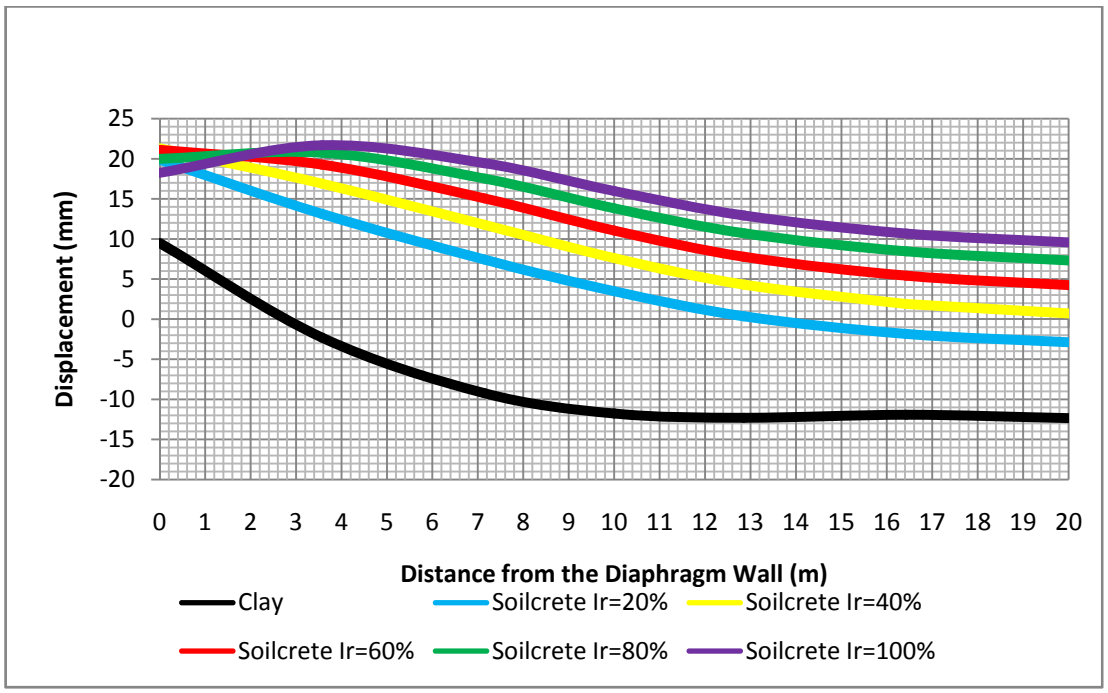

Figure B-22 Vertical displacements behind the diaphragm wall according to treated soil area ratio (I_r) for pattern III and UCS= 3 MPa, clay profile, Location I

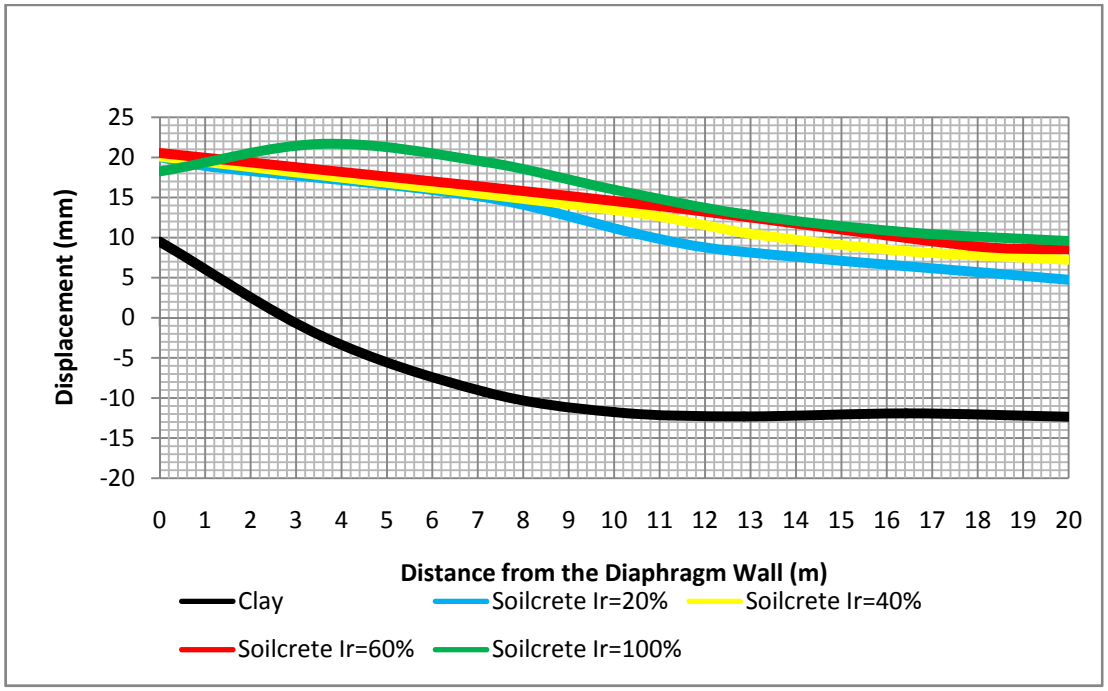

Figure B-23 Vertical displacements behind the diaphragm wall according to treated soil area ratio (I_r) for pattern IV and UCS= 3 MPa, clay profile, Location I

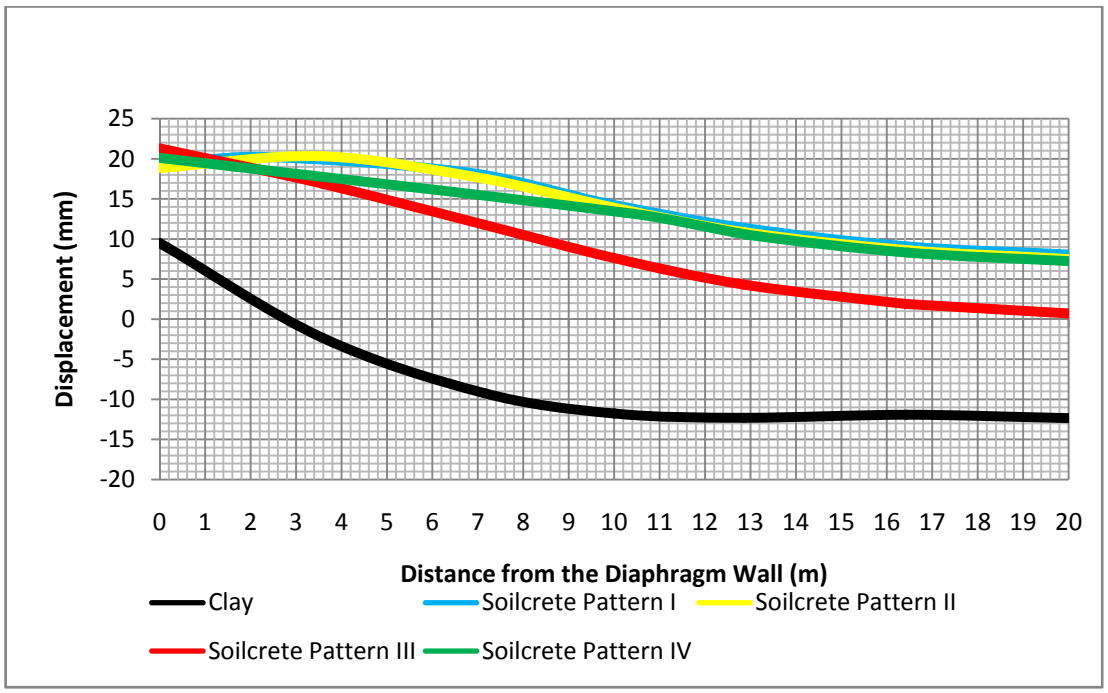

Figure B-24 Vertical displacements behind the diaphragm wall according to pattern types for UCS = 3 MPa , clay profile, Location I, Ir=40%

APPENDIX C

DISPLACEMENTS AND MOMENTS CURVES

FOR THE CLAY PROFILE

(PLAXIS 2D, MOHR COULOMB SOIL MODEL)

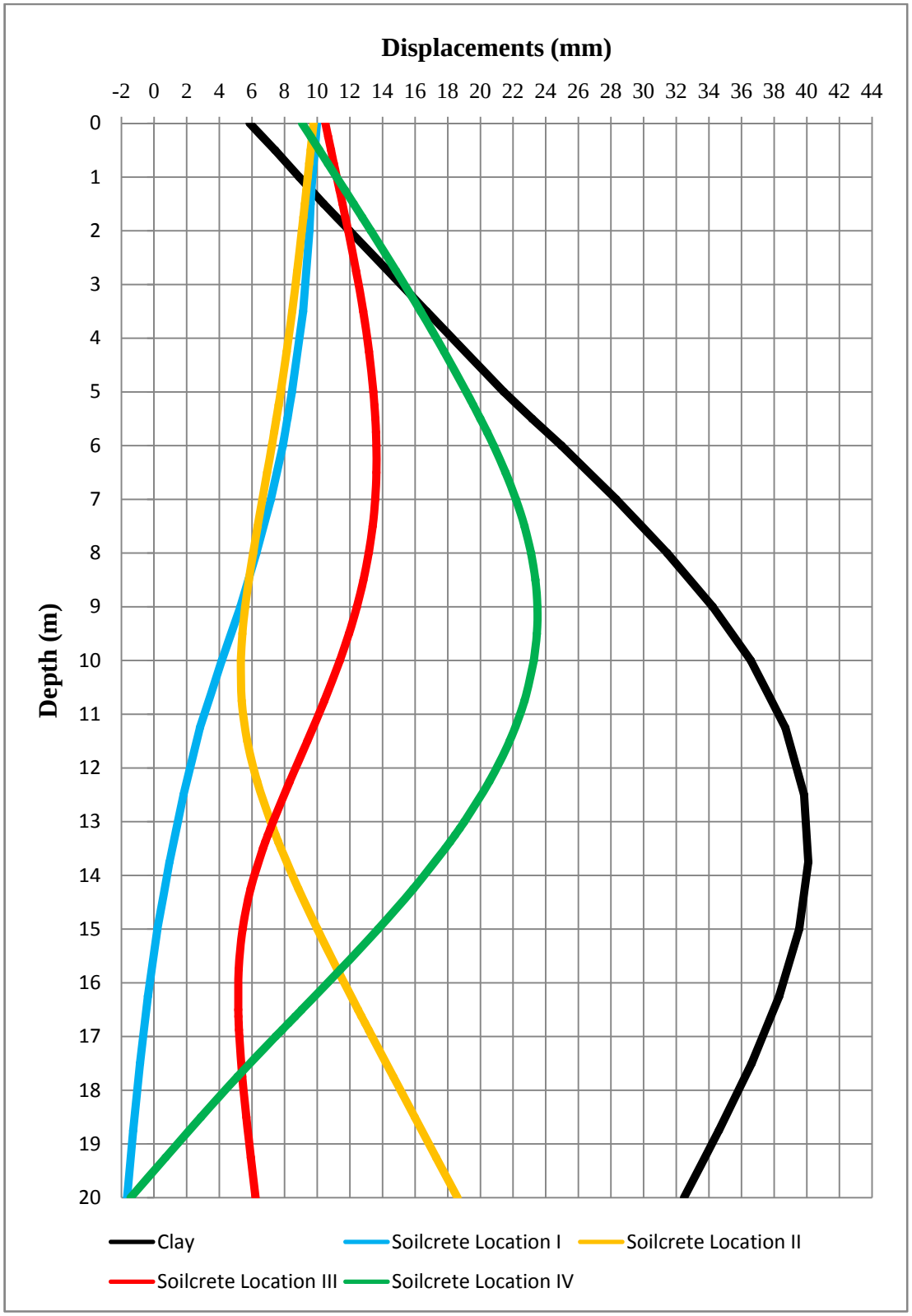

Figure C-1 Diaphragm wall displacements according to location types for UCS= 3 MPa and I_r=100%, clay profile

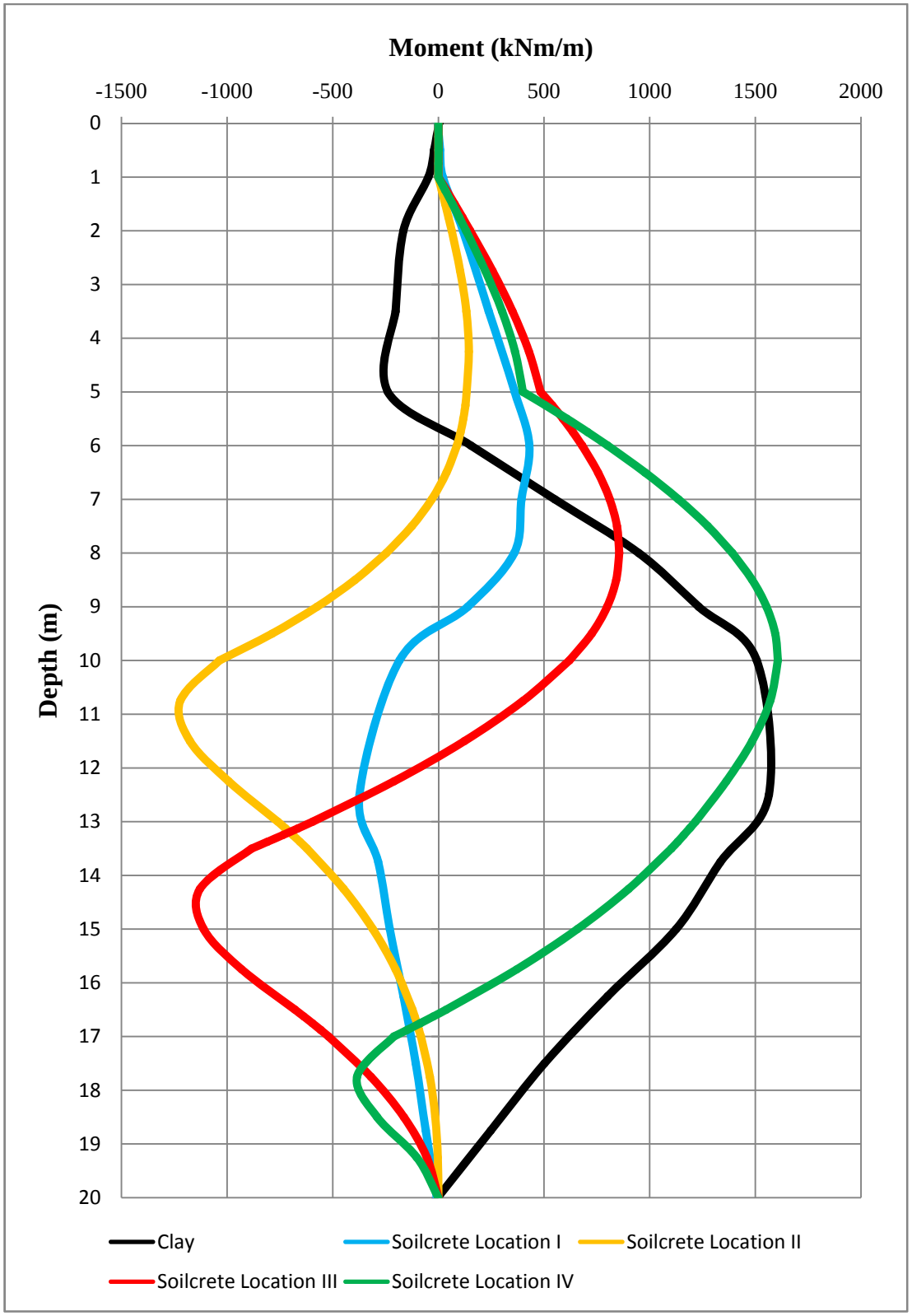

Figure C-2 Diaphragm wall moments according to location types for UCS=3 MPa and I_r =100%, clay profile

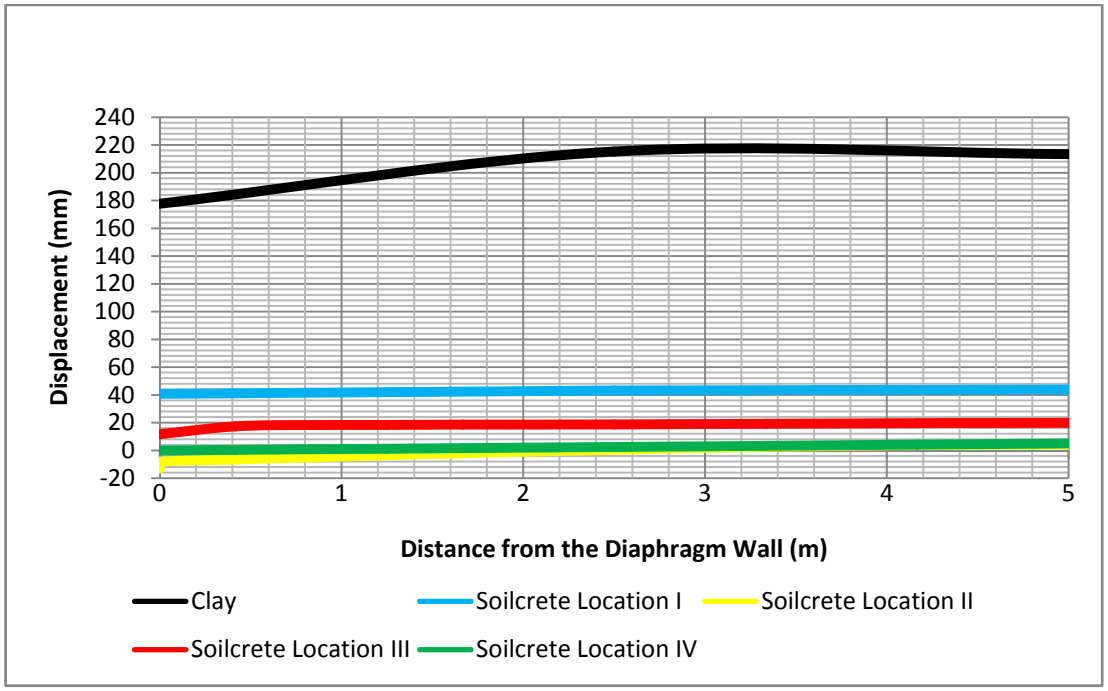

Figure C-3 Vertical displacements on the excavation level according to location types for UCS=3 MPa and I_r =100%, clay profile

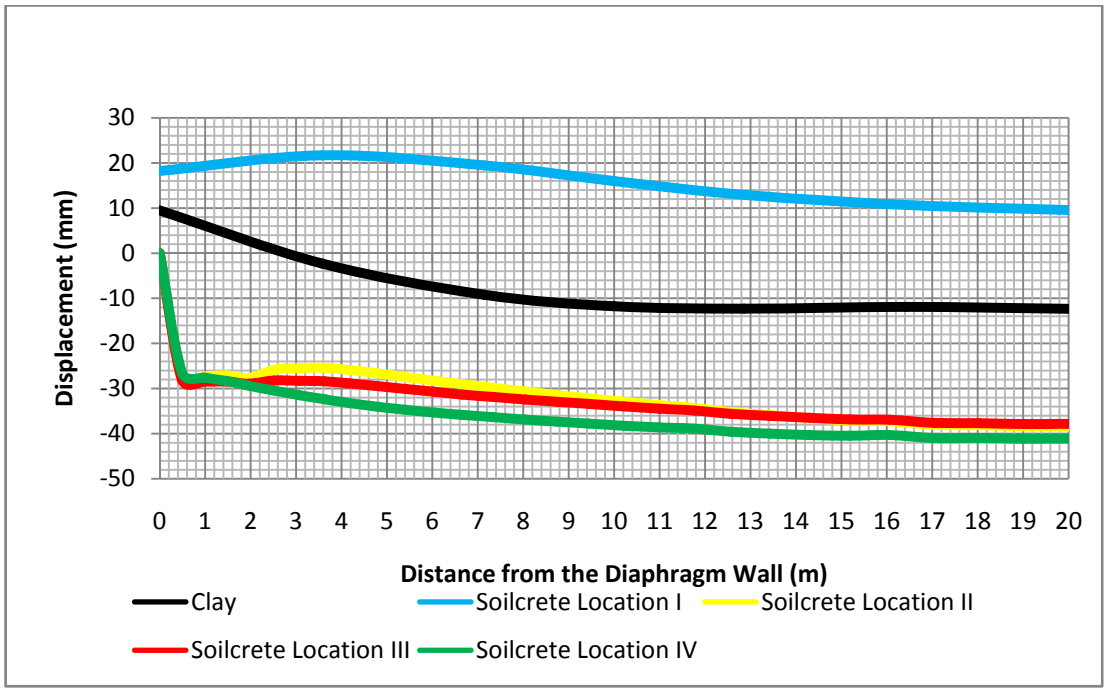

Figure C-4 Vertical displacements behind the diaphragm wall according to location types for UCS=3 MPa I_r =100%, clay profile